UNIVERSITÄT ZU LÜBECK

From Lübeck Institute of Experimental Dermatology
of the University of Lübeck
Managing Director: Prof. Dr. med. Dr. rer. nat. Enno Schmidt

Drug repurposing for epidermolysis bullosa acquisita

Dissertation for Fulfilment of Requirements
for the Doctoral Degree
of the University of Lübeck

from the Department of Natural Sciences

Submitted by

Saeedeh Ghorbanalipoor, M.Sc.
from Tehran, Iran

Lübeck 2019

First referee: Prof. Dr. med. Ralf J. Ludwig
Second referee: Prof. Dr. rer. nat. Rudolf Manz
Chairman: Prof. Dr. rer. nat. Norbert Tautz
Date of oral examination:18.10.2019
Approved for printing: Lübeck, 21.10.2019

Dedicated to my parents and my husband

Table of Contents

Abstract

Immunosuppressive agents are currently used in treatment of epidermolysis bullosa acquisita (EBA). Despite this, EBA still remains a difficult to treat autoimmune disease for most patients. Hence, there is a high medical need to develop new drugs for EBA treatment. Drug repurposing, application of the existing drugs for a new indication, shortens the drug development process. In the present study, utilizing a polymorphonuclear leukocyte (PMN)-based screening platform (reactive oxygen species (ROS) release assay), the Prestwick chemical library (PCL) was screened for identification of the drugs with inhibitory impact on PMNs as one of the crucial immune cell types implicated in effector phase of EBA pathogenesis. Through this process, 33 promising drugs were detected which were further filtered for their cytotoxicity and dose response. This *in vitro* screen and validation ultimately led to the identification of six candidate drugs namely amodiaquine (Amo), apomorphine (Apo), auranofin (Au), dobutamin (Dob), niclosamide (Nic) and tamoxifen (Tam). Furthermore, conserved activity of three compounds (Amo, Apo and Tam) was demonstrated in experimental EBA utilizing the Ab-transfer-induced model. Of those, Apo and Tam exhibited more alleviating potency in both the clinical and the histological disease and were thus opted for further *in vivo* interrogation. Application of their combined treatment potentiated their effectiveness rendering a synergistic/additive effect of Apo and Tam on disease attenuation. Tam, a selective estrogen receptor modulator (SERM), sustained its effectiveness in reduction of the disease severity at all tested doses. Hence, this validation increased the confidence for further elucidation of its underlying mechanism of action in relieving EBA symptoms. Use of estrogen-receptor knockout mice (αERKO and βERKO) enabled to reveal that Tam's efficacy is exerted through an estrogen receptor (ER)-dependent pathway. Besides, RNA-Seq results and further pathway analysis suggested that PI3K/Akt signaling pathway, whose activation in PMNs is of significant importance in EBA pathogenesis, was among the mostly affected signaling pathways by Tam treatment. Suppression of PKC/MEK/ERK and PKC/PI3K/Akt pathways along with the induction of a Th2-polarized immune response by Tam on the other hand has been argued to mediate immune-modulatory effects of Tam. More importantly,

results obtained from RNA-Seq revealed that Tam induced a considerable down-regulation of *S100a7a*. *S100a7a* is a gene whose expression is regulated by pro-inflammatory cytokines and its overexpression is reported in several inflammatory skin diseases which are associated with high infiltration of immune cells. In view of all that has been mentioned so far, it can be assumed that Tam exerts its alleviating activity in the experimental EBA by abrogation of pro-inflammatory milieu leading to a down-regulation of *S100a7a* followed by a diminished migration as well as activation of immune cells in particular PMNs. In conclusion, drug repurposing enabled to identify immunomodulatory impact of tamoxifen, a well-known SERM, on treatment of experimental EBA. Hence, it can be considered as a potential therapeutic option for treatment of EBA or in general all inflammatory autoimmune diseases such as pemphigoid diseases.

Zusammenfassung

Trotz neuer Erkenntnisse in der Pathogenese der Epidermolysis bullosa acquisita (EBA) ist die unspezifische Immunsuppression weiterhin der Therapiestandard. Auch unter langandauernder Immunsuppression kann erst nach mehreren Monaten eine Remission induziert werden. Darüber hinaus tragen Nebenwirkungen dieser Therapie zur hohen Morbidität und Mortalität der EBA bei. Daher besteht ein hoher Bedarf neue Medikamente zur Behandlung der EBA zu entwickeln. Die Verwendung bereits zugelassener Arzneimittel in anderen Indikationen („Repurposing“), verkürzt den Arzneimittelentwicklungsprozess. In einem Screening Verfahren an einem komplexen biologischen Prozess, der eine zentrale Rolle in der EBA Pathogenese spielt, der Aktivierung neutrophiler Granulozyten (PMN) durch Immunkomplexe, untersuchte ich den Einfluss von 1.200 zugelassenen Medikamenten, die Teil der Prestwick Chemical Libayr (PCL) sind. Hierdurch wurden insgesamt 33 potentielle Medikamente identifiziert, die weiter *in vitro* validiert (Reproduzierbarkeit, Toxizität) wurden. Dieses führte schließlich zur Identifizierung von sechs potentiellen Arzneimitteln, die die PMN Aktivierung inhibieren: Amodiaquin (Amo), Apomorphin (Apo), Auranofin (Au), Dobutamin (Dob), Niclosamid (Nic) und Tamoxifen (Tam). In der drauf folgenden *in vivo* Testung in einem Antikörpertransfer-induzierten Mausmodell der EBA reduzierten 3 (Amo, Apo und Tam) der 6 Medikament die Krankheitsaktivität an Tag 16 (primärer Endpunkt). Darüber hinaus war die Kombinationstherapie von Tam und Apo effektiver als die jeweilige Monotherapie. Zur weiteren Aufklärung des Wirkmechanismus wurde Tam gewählt, da Tam über ein breites Dosisspektum *in vivo* wirksam war. In Östrogenrezeptor Knockout-Mäusen (αERKO und βERKO) war die Wirkung des Östrogenrezeptor (ER) modulierenden Tam aufgehoben. Daher schient Tam über eine Modulation des ER-Signalrings zu wirken. Die Kontrastierung der RNA Expression in erkrankter Haut von Tam pder Lösungsmittel behandelten zeigte, dass der PI3K / Akt-Signalweg, dessen Aktivierung in PMNs für die EBA-Pathogenese von erheblicher Bedeutung ist, zu den am häufigsten von der Tam-Behandlung betroffenen Signalwegen gehört. Auf Einzelgenebene zeigte sich, dass Tam Behandlung mit eine erhebliche Herunterregulierung des *S100a7a* assoziiert ist. *S100a7a* ist ein Gen, dessen

Expression durch entzündungsfördernde Zytokine reguliert wird und dessen Überexpression bei mehreren entzündlichen Hauterkrankungen berichtet wird, die mit einer hohen Infiltration von Immunzellen verbunden sind. Daher können die hier in einem iermodell der EBA validierten 3 Medikamente, insbesondere Tam, mögliche therapeutische Option für die Behandlung von EBA oder anderer entzündlichen Autoimmunerkrankungen wie Pemphigoid-Erkrankungen angesehen werden.

1 Introduction

1.1 Skin

1.1.1 Skin structure and function

The skin, the largest organ of the human body, is a life-sustaining interface between the body and the external environment. It comprises a multi-laminate cellular epidermis and an underlying dermis of connective tissue separated by a dermal–epidermal basement membrane zone (BMZ). A layer of subcutaneous fat lies below the dermis, which is separated from the rest of the body by a layer of striated muscle [1, 2].

The **epidermis** is composed of terminally differentiated, stratified, squamous epithelial cells. It predominantly consists of keratinocytes which move progressively from the basement membrane towards the skin surface, forming four morphological well-defined strata [1] (Figure 1.1). The bottom layer of the epidermis, the basal layer is responsible for continuously renewing the cells of the epidermis. In the subsequent layer, spinous layer, basal keratinocytes differentiate and begin a maturation process, but also divide to restore the basal layer. Cells that move into the spinous layer change from being columnar to being polygonal in shape and start to synthesize keratins that are distinct from the basal layer keratins. The spinous layer is followed by the granular layer in which cells encompass numerous intracellular keratohyalin granules [1, 3]. The skin’s barrier properties are mainly due to the stratum corneum, the outermost layer of epidermis. Cells in this layer, known as corneocytes, are keratinocyte-derived cells that have become flattened and have undergone cornification. During cornification, epidermal keratinocytes undergo a unique form of terminal differentiation and programmed cell death [1, 4].

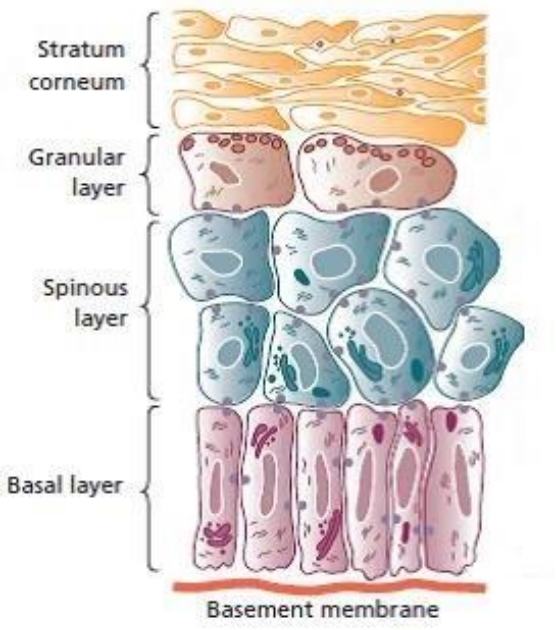

Figure 1. 1: Strata of the epidermis.
In humans, the epidermis is composed of four (or five) layers of epithelial cells. From deep to superficial, these layers are the basal layer, the spinous layer, the granular layer, and the stratum corneum. Only on the palms of the hands and the soles of the feet there is a fifth layer, called the stratum lucidum, situated between the stratum corneum and the granular layer. (From [1])

The functions and homeostasis of the skin critically depend on integrated organization and cohesion between the cells of the epidermis and the dermis. The **BMZ** is a highly specialized structure located at the interface between the epidermis and the dermis [5-8]. The BMZ is supra-structurally an anchoring complex which consecutively includes the hemidesmosomes at the basal surface of the keratinocytes, the anchoring filaments extruding from the hemidesmosomes through the lamina lucida, and the anchoring fibrils expanding from the lamina densa into the dermis [7, 8] (Figure 1.2).

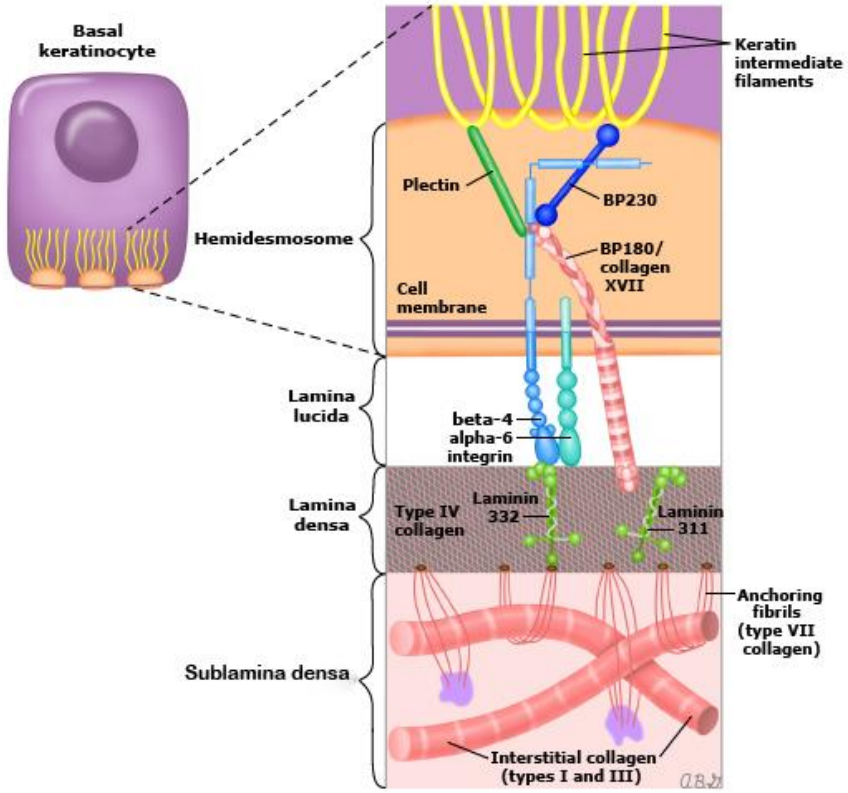

Figure 1. 2: Ultrastructural features of the BMZ.
From the most superficial to the deepest, the BMZ consists of four layers of basal keratinocytes layer, the lamina lucida layer, the lamina densa layer, and the sublamina densa layer. Keratin intermediate filaments and hemidesmosomes are situated within the basal keratinocytes. There are anchoring filaments within the lamina lucida. Type IV collagen, laminin 332, 311, and 511 are located within the lamina densa. There are anchoring fibrils, composed of type VII collagen, within the sublamina densa [1]. (Figure modified from [9])

The major component of the human skin is the **dermis**. It provides the flexibility, elasticity and tensile properties of the skin. It preserves the body from mechanical injury, helps in temperature regulation and comprises receptors of sensory stimuli. The dermis is less cellular than the epidermis and primarily includes the extracellular matrix (ECM) of connective tissue, a complex meshwork of various macromolecules. There are four major classes of ECM components: (i) collagen fibers, which provide tensile strength to allow the skin to serve as a protective organ against external trauma; (ii) elastic tissues, which provide elasticity and resilience to normal skin; (iii) non-collagenous glycoproteins, such as fibrillins, fibulins and integrins, which often serve as organizers of the matrix and facilitate cell–matrix interactions; and (iv) proteoglycan/glycosaminoglycan

macromolecules, which provide hydration to the skin. The maintenance of proper quantities and appropriate interactions between the ECM components is a requirement for the physiological homeostasis of the dermis [1, 10].

1.1.2 Skin immune system

Although it has been a long time since non-immune functions of skin have been appreciated, its immune properties was not “officially” investigated until 1978, when Streilein [11] coined the term skin-associated lymphoid tissue (SALT) to delineate the continuous trafficking of immune cells between the skin, draining lymph nodes (dLNs), and the peripheral circulation [12]. Immune response in the skin is critical for host defense against pathogenic microorganisms. However, immune dysregulation may result in chronic inflammatory or autoimmune skin diseases. Extensive crosstalk between the various cellular and microbial constituents of the skin regulates immune reactions to ensure effective host defense to maintain and restore homeostasis, and to inhibit chronic diseases [2]. Besides the Langerhans cells (LCs), antigen detecting and processing cells, some subtypes of T cells (mainly CD8+ T cells) reside in the epidermis as well. Cutaneous immune surveillance is also carried out in the dermis by an array of tissue-resident T cells, macrophages, and dendritic cells (DCs) [1] (Figure 1.3).

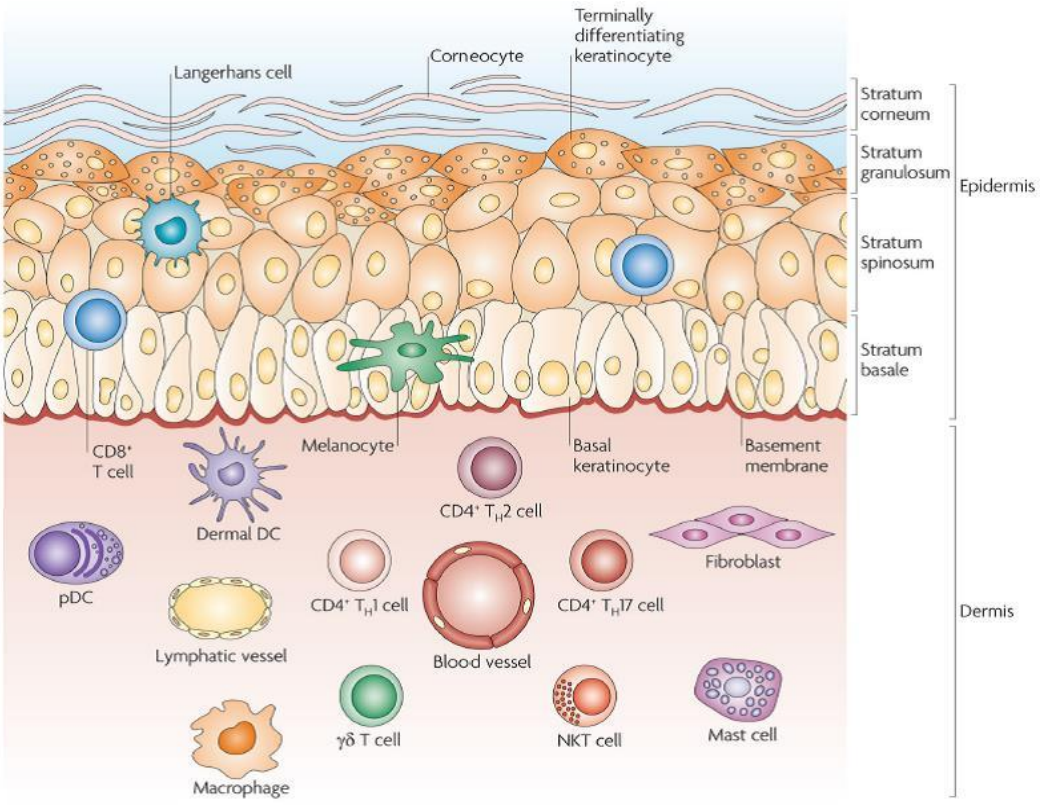

Figure 1. 3: Immune cell component of the skin.
The epidermis does not only comprise keratinocytes, but also melanocytes and immune cells such as LCs and T lymphocytes (primarily CD8+ T cells) which are present in the basal layer (stratum basale) and spinous layer (stratum spinosum). The underlying dermis is consisting of larger immune cell diversity. It encompasses many specialized cells, such as DC subsets, including dermal DCs and plasmacytoid DCs (pDCs), and T cell subsets, including CD4+ T helper 1 (TH1), TH2 and TH17 cells, γδ T cells and natural killer T (NKT) cells. Moreover, macrophages, mast cells and fibroblasts are also present. The dermis is drained by lymphatic and vascular conduits, through which migrating cells can traffic. (From [3])

1.2 Autoimmune bullous diseases (AIBDs)

AIBDs are prototypical autoantibody (aAb)-mediated organ-specific autoimmune diseases and are clinically characterized by formation of blisters and erosions on the skin and/or on mucous membranes, and are overall difficult to treat [13-16]. Their incidence and prevalence has steadily increased over the past decades [13, 17]. AIBDs meet all required criteria to be classified as autoimmune diseases. These criteria were primarily modelled on Koch's postulates by Witebsky in 1957 and were further refined by Rose and Bona in 1993 [18, 19]. Koch's postulates comprise three principles:

(i) Direct evidence from transfer of pathogenic autoantibodies or pathogenic T cells; in AIBDs proved by a large body of evidence by disease induction through injecting patient-derived autoantibodies into mice [20-28].

(ii) Indirect evidence based on reproduction of the autoimmune disease in experimental animal models; corroborated by disease induction by immunizing the mice with determined autoantigen in immunization induced mouse models of AIBDs [29-31].

(iii) Incidental evidence from clinical clues; exemplified by demonstration of aAb deposition in the affected tissue.

AIBDs are mediated by aAbs targeting adhesion junctions that mediate cell-cell or cell-matrix interactions in the skin [32]. Dysregulated skin immune response, a break of self-tolerance, and the generation of aAbs to structural proteins of the skin underpin the disease pathology in AIBDs. AIBDs can be categorized into three different groups, namely pemphigus diseases, pemphigoid diseases, and dermatitis herpetiformis [33]. In pemphigus diseases (e.g., pemphigus vulgaris (PV), and pemphigus foliaceus (PF)), a family of intra-epidermal AIBDs, the aAbs are directed against cadherins (specifically, desmogleins), which are an integral part of desmosomes. Desmosomes are adhesion junctions that anchor the intermediate filament cytoskeleton to keratinocyte plasma membranes at cell-cell borders. In sub-epidermal AIBDs or pemphigoid diseases (e.g., bullous pemphigoid (BP), mucous membrane pemphigoid (MMP) and epidermolysis bullosa acquisita (EBA)), aAbs are directed against structural proteins of the dermal-epidermal junction (DEJ), and the result is cleavage between the epidermis and the dermis [13, 14, 32] (Figure 1.4). Dermatitis herpetiformis is associated with celiac disease and characterized by aAbs against transglutaminase 2 and 3 [33].

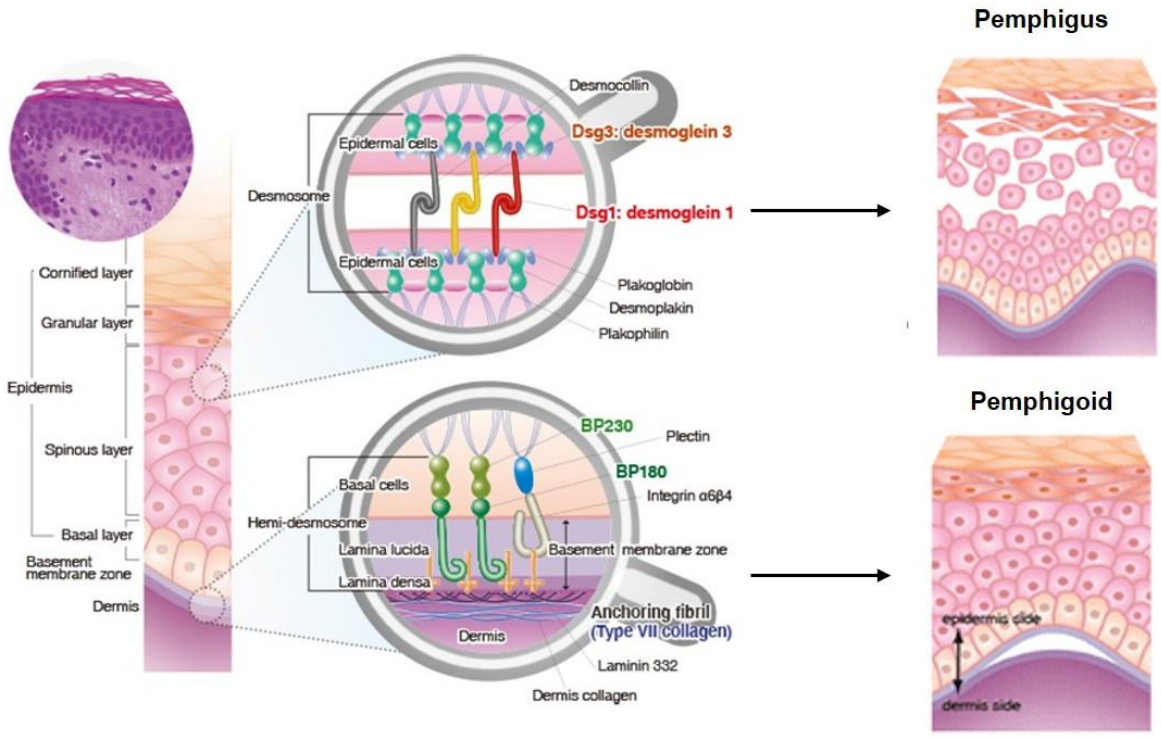

Figure 1. 4: Schematic presentation of desmosomal and hemidesmosomal target antigens in AIBDs.
On left side, a histological section of normal human skin and its constituent layers are shown. Magnified section on top exhibits two neighboring epidermal keratinocytes. Pemphigus diseases are histologically characterized by intra-epidermal split formation (on top right). The desmosomal target antigens of the pemphigus diseases encompass desmosomal plaque proteins (e.g., desmoplakin, etc.) and transmembrane proteins of the cadherin group (desmoglein 1 and 3, desmocollin 1). Hemidesmosomal target antigens of pemphigoid diseases are depicted in lower magnified section. In these diseases, split occurs at the DEJ (bottom right). Hemidesmosomal plaque proteins (e.g., BP230, plectin) interact with the transmembrane proteins BP180 and α6β4-integrin, which, in turn, are connected by mean of laminin 332 to type VII collagen (COL7). COL7 establishes a connection to dermal collagens [13]. (Figure modified from [34])

1.3 Epidermolysis bullosa acquisita (EBA)

1.3.1 Background

The supra-structural elements of the BMZ form a highly organized structure from the inside the basal epidermal keratinocyte into the dermal ECM. The epidermis and its underlying BMZ are attached to the dermis via the anchoring fibrils (AFs) [6]. Any condition such as hereditary defect in the gene coding AFs and an acquired sub-epidermal bullous disease leading to the reduced or a complete absence of normal functioning AFs result in the same clinical consequences.

These disorders are collectively called epidermolysis bullosa (EB) [35]. Inherited EB is a clinically and genetically heterogeneous group of disorders characterized by skin fragility, blister formation and erosions of the skin and mucous membrane [6].

Eliot initially reported a patient with a non-hereditary variant of EB in 1895 [36], and the term “epidermolysis bullosa acquisita” was first coined by Kablitz in 1904 [37]. EBA is an acquired chronic sub-epidermal bullous disease with clinical manifestation resembling the inherited form of dystrophic epidermolysis bullosa (DEB). In DEB, there is a hereditary deficiency in the gene encoding COL7, the major component of AFs. In EBA, there is also a paucity of AFs, but this reduction is due to the presence of aAbs directed against COL7 within AFs [38]. EBA is classified into two major clinical subtypes: (i) A non-inflammatory mechano-bullous variant of EBA, afflicting approximately 1/3 of the patients. It is associated with blisters and erosions at mechanically exposed sites with minimal clinical or histologic inflammation. (ii) An inflammatory variant, observed in approximately 2/3 of the cases. Both forms are characterized by tissue-bound as well as circulating aAbs against COL7 in AFs of the BMZ resulting in recalcitrant blisters on the skin and mucous membranes [33, 38-40]. Inflammatory EBA clinically resembles other AIBDs for instance BP, linear IgA disease (LAD), MMPs or Brunsting-Perry pemphigoid. In 1971, Roenigk *et al.* first established the diagnostic criteria for EBA including (i) onset of the disease in adulthood, (ii) lack of familial history for hereditary skin blistering diseases, (iii) trauma-induced or spontaneous formation of blisters mimicking DEB, (iv) exclusion of other blistering skin conditions. EBA is a rare AIBD with a worldwide incidence ranging from 0.2 to 0.5 /million inhabitants/year [33, 40]. In Germany, the prevalence of EBA has been reported 2.84/million inhabitants, i.e. about 230 EBA patients according to an analysis conducted on database of the largest German insurance company from 2014 [41]. There is a wide range of age at onset of the disease from early childhood to elderly adulthood with an average age of 50 years [40, 42]. No gender predilection has been reported [38, 40].

1.3.2 Targeted autoantigen in EBA

In 1984 Woodley *et al*. detected a 290-kDa protein within the DEJ of human skin, and identified it as the target autoantigen of EBA aAbs and later demonstrated that this protein was the carboxyl terminus of COL7 within AFs [43, 44]. COL7, encoded by the COL7A1 gene, is a major component of AFs of the DEJ on the dermal side at the lamina densa/papillary dermis interface [45]. COL7 exists in the basement membrane of the skin, cornea, oral mucosa, cervix, oesophagus, colon, anus, and chorioamnion [46]. It is basically synthesized by epidermal keratinocytes and, to a lesser extent, dermal fibroblasts express the gene in culture [47]. Similar to other collagen molecules, COL7 also consists of three α-chains, each composing of a 145-kDa triple-helical collagenous segment characterized by repeating Gly-X-Y amino acid sequences and a 39-amino acid non-collagenous (NC) hinge region, flanked by a 145-kDa amino-terminal NC1 domain and a small 34-kDa carboxyl-terminal NC2 domain [48]. NC1 domain consists of several subdomains with homology to adhesive proteins such as a cartilage matrix protein (CMP) domain, nine fibronectin III-like (FNIII) domains, a von Willebrand factor A-like (vWFA) domain and a cysteine and proline-rich domain (Figure 1.5). NC1 domain may mediate binding of COL7 to other BMZ and matrix constituents stabilizing the adhesion of the BMZ to the beneath dermis. Using a recombinant NC1, its interactions with various ECM components namely fibronectin, laminin 5, type I collagen (COL1), and type IV collagen (COL4) have been shown. NC2 domain is structurally similar to the Kunitz protease inhibitor molecule. A portion of the NC2 domain is removed by proteolytic cleavage and then two identical COL7 molecules aggregate tail-to-tail to construct a dimer linked by disulphide bonds [49, 50]. The NC1 domain has been detected as a major antigenic epitope in EBA patients [51], while in very few number of patients the NC2 and collagenous domains show minor antigenic activity [52-54]. AAbs against COL7 were also detected in a bullous variant of systemic lupus erythematosus (BSLE) [55, 56].

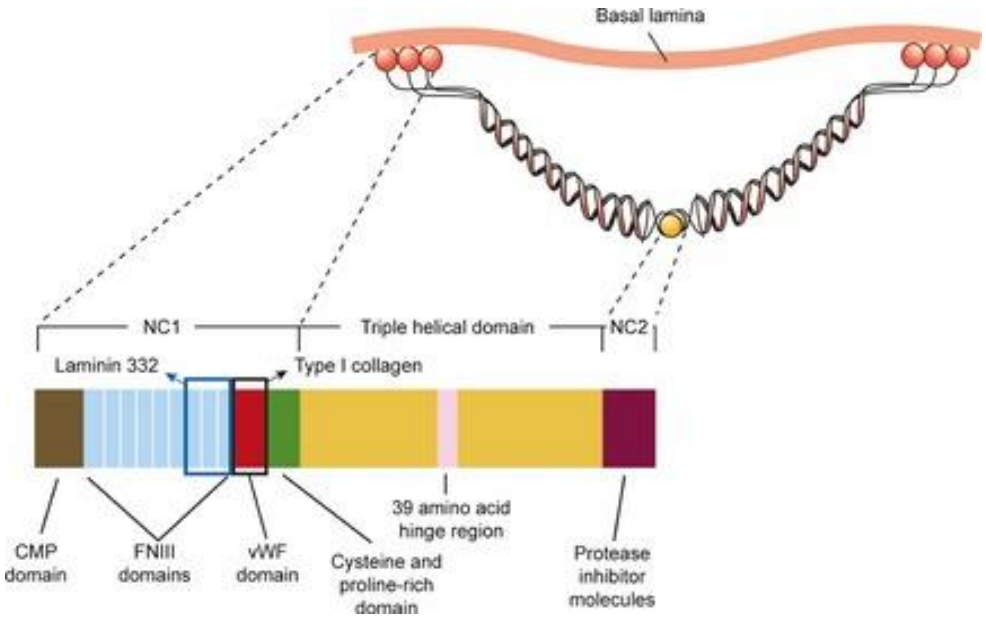

Figure 1. 5: Schematic demonstration of human COL7 components.
COL7 has three identical α chains consisting of the 145-kDa triple helical domain flanked by two NC domains; a 145-kDa NC1 domain and a 34-kDa NC2 domain. The NC1 domain comprises a CMP, FNIII subdomains, a vWFA and a cysteine and proline-rich subdomain. The NC2 domain is structurally similar to protease inhibitors. The triple helical domain contains a 39-amino acid hinge region. The AF structure contains two COL7s that form an antiparallel dimer. The NC2 domain at the C-terminus undergoes partial proteolytic processing before forming a disulphide bond with another NC2 domain. The NC1 domain at the N-terminus interacts with the basal lamina (laminin-332 and COL4), or COL1 to a lesser extent. (From [57])

1.3.3 Pathophysiology

Pathogenesis of all autoimmune diseases includes a breach of the immune tolerance leading to an abnormal immune response and characterized by aAbs and autoreactive T-cell responses to self-molecules [58]. Like many other disorders, autoimmune diseases result from a combination of genetic and environmental factors [59]. Similarly, in EBA, pathogenesis is briefly divided into three distinct phases: (i) Afferent/induction phase: break of tolerance to COL7, (ii) Presence of aAbs in the bloodstream, (iii) Efferent phase: aAb-mediated inflammation and sub-epidermal blister formation, and resolution of the disease [40, 60].

1.3.3.1 Afferent/induction phase: break of tolerance to COL7

1.3.3.1.1 Genetic factors and microbiota

Even though, EBA is not a genetic disease, some patients with EBA may have a genetic susceptibility to the disease. An association of EBA with the major histocompatibility complex (MHC) haplotype, specifically HLA-DR2 [61] and HLA-DRB1 ∗15:03 [62] has been reported. In the same line, it has been reported that black-skinned people seem to be more susceptible to develop EBA, demonstrating a genetic predilection outside the MHC locus [62]. Furthermore, identification of coincident EBA cases in the members of a family provided further support for the genetic association of EBA [63]. MHC-restriction is also present in the immunization-induced model of EBA in mice. A strong association has been revealed between the disease induction with the MHC haplotype H2s. After immunization of the mice from various inbred strains with recombinant murine COL7, different responses were observed. SJL/J mice (H2s), B6.SJL-H2s (H2s) and female MRL/MpJ (H2k) developed severe disease. However, in MRL/MpJ males, diseased phenotype started with a 4-week delay. C57Bl/10.s (H2s) showed a mild and transient disease. All other strains, including DBA/1J (H2q), NZM2410/J (H2z), NOD/ShiLtJ (H2g7), C57Bl/10.q (H2q), BXBD/TyJ (H2b), and C57Bl/6J (H2b) mice, were resistant to EBA induction. This finding pinpoints the pivotal role of MHC locus in disease pathogenesis. [64]. Interestingly, several non-MHC quantitative trait loci (QTL) linked to specific chromosomes that restrict susceptibility to EBA, were also identified in experimental EBA [65]. In addition to genetic factors, gene-microbiota interactions have been described to impact disease development in immunization-induced EBA [66, 67].

1.3.3.1.2 T- and B- cells in the induction phase of EBA

Autoreactive T cells recognizing the NC1 domain of COL7 have been detected in an EBA patient [68]. In mouse models of EBA, T cell requirement for disease induction has been shown using T-cell-deficient SJL^{nude} mice. These mice are protected from induction of immunization-induced EBA. However, adoptive transfer of T cells from immunized wild-type SJL mice into SJL^{nude} mice led to aAb

production and to restoration of the disease [69]. In immunization-induced EBA, it has been also shown that CD4 T cells but not CD8 T cells are the required T cell subset for induction of aAb production. Furthermore, cell-depleting methods have revealed that various antigen presenting cells (APCs) such as B cells, DCs, and macrophages are required for formation of COL7-reactive CD4 T cells in the experimental EBA [70]. Moreover, a predominant Th1-type cytokine profile is observed in dLNs of the mice that develop clinical disease, whereas a Th2-type cytokine profile is associated with resistance to disease induction in mice [71]. It has been shown that splenic regulatory B cells (Bregs) from COL7-immunized mice decreased aAb production following autoantigen-restimulation of isolated dLN cells from COL7-immunized mice. Additionally, splenic Breg number was higher in immunized mice in comparison with non-immunized control group [72]. This finding was consistent with human data demonstrating that blood Bregs from patients with autoimmune diseases, including AIBDs, were expanded compared with healthy individuals [73].

1.3.3.2 Presence of aAb in the bloodstream

Pathogenic role of aAb to COL7 in EBA is supported by multiple lines of clinical evidence. For instance, blister formation in an infant was induced by the passive transfer of aAb from an EBA-afflicted mother [74]. In addition, an intra-individual correlation between anti-COL7 aAb titers and the disease severity has been described [75, 76]. The pathogenic relevance of aAbs against COL7 is also demonstrated (i) *ex vivo* by indicating breakdown of the DEJ in skin sections in the presence of anti-COL7 IgG/IgA and neutrophils [77, 78], and (ii) *in vivo,* by development of inflammation and blister formation in mice following transfer of anti-COL7 IgG [26, 79] or by immunization [31, 70]. AAbs can be maintained either by the continuous activation of B cells resulting in the formation of short-lived plasma cells, or the persistence of long-lived plasma cells [80]. In the experimental EBA, production of the antigen-specific Abs is restricted to peripheral LNs [40]. This concept is supported by the detection of antigen-specific B cells in peripheral LNs [81]. Accordingly, COL7 aAbs are generated at these anatomical locations. COL7-specific plasma cells were also restricted to dLNs of the immunized mice [82]. After the anti-COL7 IgG is released into the bloodstream, its half-life is

controlled by neonatal Fc receptor (FcRn). The FcRn protects IgG from catabolism. FcRn shares high structural homology to MHC class I family of proteins, however it is encoded outside the MHC gene complex [83]. Decreased levels of aAb were reported in FcRn-deficient mice compared with wild type controls in both the Ab-transfer- and the immunization-induced EBA. This is accompanied by protection from tissue damage but could be abrogated by transfer of excessive amounts of anti-COL7 Abs [84].

1.3.3.3 Efferent phase: AAb-mediated inflammation and sub-epidermal blister formation

1.3.3.3.1 Complement

One of the first steps of the effector phase of the experimental EBA is represented by the aAb deposition at the DEJ, followed by generation of a pro-inflammatory milieu including complement activation. Contribution of the complement system to the autoimmune tissue injury in EBA has been previously supported by a number of observations and experimental studies. Anti-COL7 Abs are able to activate the complement system *in vitro* and *in vivo*. In the skin of patients with EBA, deposition of different complement components including complement component 3 (C3), C5b, and membrane attack complex (MAC) have been detected [85]. IgG1 and IgG3 anti-COL7 Ab subclasses are shown to activate complement and induce DEJ separation *ex vivo* [86]. In Ab-transfer-induced model of EBA, C5-deficient mice were completely protected from disease induction [26]. To determine which molecule downstream of C5 is crucial for disease induction in EBA, (C5a receptor 1-/-) C5ar1-/- and C6-/- mice were injected with anti-murine COL7 Abs. C5ar1−/− mice were significantly protected from blister formation, suggesting that C5a–C5aR1 interactions are crucial intermediates linking pathogenicity of Abs to tissue injury in this mouse model of EBA. On contrary, in C6-/- mice, disease was induced to the same extent as wild type controls, providing evidence that MAC is dispensable for blister formation in this model [87]. Depositions of complement-fixing IgG2a and IgG2b aAbs and C3 are regularly observed at the DEJ in immunization-induced EBA [31]. Furthermore, the alternative pathway of complement system has been also identified as another important contributor to

the blister formation in Ab-transfer-induced EBA. Mice deficient in alternative (factor B-/- mice) and, to a lesser extent, in the classical complement pathway (C1q-/- mice) showed an improved disease activity. By contrast, mice with deficiency in lectin pathway of complement depicted a similar disease severity to controls [88].

In order to provide a comprehensive overview on the neutrophils' contribution to the pathogenesis of inflammatory form of EBA, their role will be separately discussed later in this chapter.

1.3.3.3.2 The resolution phase of EBA

Flightless I (Flii) protein belongs to gelsolin family of actin-binding proteins. In addition to its role in the regulation of the cytoskeleton [89], Flii has been also identified as an important regulator of wound healing. It affects both epidermal keratinocytes and dermal fibroblast, cellular proliferation, motility, and matrix deposition [90]. Overexpression of Flii impairs wound healing process, increases wound area, reduces cell proliferation, and delays epithelial migration [91]. Moreover in patients with psoriasis, an overexpression of Flii has been demonstrated in psoriatic lesions compared with normal human skin [92]. Elevated expression of Flii mimics almost all features observed in EBA such as induction of thinner and more fragile skin accompanied by impaired hemidesmosome structure, reduced expression of COL7 at the BMZ, and altered arrangement of COL7 [93, 94]. Although Flii overexpressing mice per se do not develop blisters, their skin is structurally altered, which includes reduced cell adhesion, irregular hemidesmosome structure, decreased COL7 expression, altered integrin signaling and increased skin blistering in experimental models of EBA [93, 95, 96]. In the Ab-transfer-induced EBA, induction of EBA resulted in an elevated cutaneous Flii expression in mice. In Flii+/- mice, low expression of Flii significantly impaired blister formation in the experimental EBA [95]. Further studies to investigate its therapeutic relevance revealed that Flii-neutralizing Ab relieves clinical disease score in the experimental EBA [94]. These findings imply notable contribution of pathways that are involved in the resolution of cutaneous involvement. Consequently, EBA may be only developed when there is an imbalance between

pro-inflammatory, anti-inflammatory, and resolving pathways skewing towards pro-inflammatory mechanisms [40].

1.3.4 Animal models of EBA

As etiology and pathology of many autoimmune disorders remain to be fully determined, there are many methods to induce autoimmune diseases in animals. Based on their principle, those methods can be classified into three categories; (i) immunization with autoantigen, (ii) transfer of autoimmunity (i.e. autoreactive lymphocyte and/or aAbs), and (iii) induction by environmental factors [97]. Two animal models exist for induction of EBA in mouse namely immunization-induced and Ab-transfer-induced.

1.3.4.1 Immunization-induced EBA

Immunization with homologous or heterologous autoantigens can break the immune tolerance and may lead to the induction of experimental autoimmune diseases [97]. The immunization-induced model of EBA was initially established using a recombinant homologous peptide fragment from the immunogenic NC1 domain of murine COL7 (mCOL7), fibronectin-III-like domains (FNIII) 7 and 8 of COL7 (mCOL7C) supplemented with a glutathione S-transferase (GST)-tag. In this model, mice were immunized at the tail base for 4 times with 40µg of GST-mCOL7C emulsified in the non-ionic block copolymer adjuvant TiterMax. In this model, circulating aAbs directed against mouse COL7 were detected as early as 1 week after immunization. In mice genetically susceptible to develop clinical EBA manifestations (SJL/J, B6.SJL-H2s, B10.s, MRL/MpJ and to a lesser extent BALB/c and FcγRIIB-/- mice in C57BL/6 background), skin inflammation was observed 1-2 weeks after detection of circulating aAbs [31, 40]. In another immunization-induced model of EBA, mice are immunized with a different immune-dominant epitope of the murine NC1 domain. Here, mice received a single injection of 60µg recombinant mCOL7-vWFA2 emulsified in the non-ionic block copolymer adjuvant TiterMax, at their hind footpad. All EBA susceptible mice (SJL, C57BL/6 (B6), and B6.SJL-H2s C3c/1CyJ (B6.s)) produced aAbs 8 weeks after immunization, while aAb development was seen in nearly 70% of BALB/c [70]. In

both models, disease susceptibility was associated with H2s haplotype. Immunization-induced EBA is suitable to model the induction phase of the disease and to study the mechanisms involved in the break of immuno-tolerance and long-term therapeutic intervention [98].

1.3.4.2 Ab-transfer-induced EBA

The transfer of serum or aAbs is a broadly applied method to model autoimmune diseases. The donor and the recipient animals may belong to identical or different species [97]. In Ab-transfer induced EBA, IgG, purified from immunized rabbits with recombinant mCOL7, is transferred into the mice in order to induce the experimental EBA [26]. In the first animal model of EBA, polyclonal rabbit Abs were generated following immunization of rabbits with 3 fragments located within the NC1 domain of mCOL7, termed mCOL7A, mCOL7B and mCOL7C. Mice were repeatedly (every second day) subcutaneously injected with total rabbit immune IgG at doses of 3.5, 7.5, and 15 mg/ml over a period of 12 days. Widespread lesions were observed 4-7 days after the first injection, and the magnitude of the disease was correlated with the amount of injected IgG [26]. In order to prevent non-specific effects of high concentrations of rabbit IgG, this model was modified using affinity (against mCOL7C) purified IgG. In this procedure, the injection of only 10µg/g BW of affinity purified rabbit anti-mCOL7C IgG was sufficient to induce skin inflammation, blisters and erosions [99]. Following a similar approach, an additional Ab-transfer induced model of EBA was developed in which affinity purified rabbit IgG against NC1 fragment of human COL7 (hCOL7) was injected to mice. In this model, SKH1 mice received daily intra-dermal injections of purified IgG fractions from 0.1 to 1 mg/g BW. Mice showed numerous erosions and crusts at day 4 after initial injection [79]. Moreover, affinity purified IgG from EBA patient was capable of disease induction in SKH1 mice [27]. A similar approach succeeded to induce experimental EBA in mice using affinity purified IgG against different epitopes of hCOL7 [100, 101]. It has also been shown that rabbit Abs against recombinant proteins containing several fragments of the NC1 domain of hCOL7 can induce blisters and lesions in COL7-humanized mice. These mice carry null mutations of mCOL7 and the hCOL7 transgene (COL7 m–/–, h+). The Abs including anti- FNIII4- FNIII5 or anti- FNIII7- FNIII8 directed to hCOL7 caused

blisters both *ex vivo* and *in vivo* [102]. Albeit several in- and outbred mouse strains develop clinical lesions in these antibody transfer models, induction of clinically manifest disease in Ab-transfer induced EBA is genetically restricted, as different inbred mouse strains show varying extent of susceptibility to blister formation, including strains that are completely resistant to disease induction [26, 103]. Overall, the Ab-transfer model of EBA is a valuable tool to delineate the effector phase of the disease. It is a swift model to investigate the therapeutic effect of treatments compared with immunization induced model because the clinical manifestations of the disease are detectable shortly (days) after the IgG transfer [98].

1.3.5 Diagnosis

Since prognosis and treatments considerably vary between the different pemphigoid diseases, accurate diagnosis of EBA is essential for a reliable prognosis, thus an efficient treatment [13]. Due to the shared clinical, pathologic, and immuno-histological features with other pemphigoid diseases (PDs), diagnosis of EBA can be challenging [9]. There is a high variability in clinical presentations of EBA, i.e. classical mechano-bullous form and inflammatory variants resembling BP, MMP, linear IgA-like disease, and Brunsting-Perry pemphigoid. Due to the high variety of clinical demonstration, exact diagnosis of EBA based solely on clinical features is not feasible [33]. In case of clinical suspicion of EBA, different diagnostic approaches are required. Tissue-bound and circulating aAbs in EBA do not only have the clinical relevance in pathogenesis of the disease but also have diagnostic values. Conventionally, immune-gold electron microscopy was the gold standard for diagnosis of EBA [104]. Currently, the diagnostic gold standard is the direct immunofluorescence (DIF) microscopy of the perilesional skin sections. In EBA, DIF microscopy represents a linear deposition of IgG, IgA and/or C3 at the DEJ. A u-serrated pattern in DIF is a diagnostic criterion for EBA or BSLE [33]. Indirect immunofluorescence (IIF) microscopy on human salt-split skin demonstrates binding of autoreactive IgG or IgA to the dermal side of the DEJ. Immunoblotting using dermal recombinant proteins or dermal extract shows existence of aAbs directed to COL7 in serum of the EBA patients. Detection of

COL7-specific aAbs may be assessed by enzyme-linked immunosorbent assay (ELISA), using various recombinant forms of the autoantigen [105].

1.3.6 Treatment

Therapy of AIBDs generally consists of suppression of the immune system, modulation of inflammation and ameliorating healing of erosions. Commonly used therapeutic agents for treatment of AIBDs may be associated with high morbidity and occasional mortality [106]. In the case of EBA, favored first-line treatments include agents that are both effective and well tolerated [9]. colchicine is recommended as a first line treatment by many experts, because its side effects are less than most of the other therapies utilized for EBA treatment [40]. However, most commonly, first line treatment for EBA comprises prednisolone (1.0-2.0 mg/kg/d) tapering + azathioprine or mycophenolate mofetil [107]. Yet, treatment of EBA is difficult, which is reflected by the long time (9 months) needed to induce remission with this or similar immunosuppressive treatments [108] .

1.3.6.1 Corticosteroids

Corticosteroid therapy for treatment of EBA is mostly combined with other immunosuppressant/modulatory agents to reduce the corticosteroid dose. Although corticosteroids are relatively effective drugs for EBA, they have so many adverse effects. Therefore, before systemic corticosteroid therapy, other treatment approaches should be taken into consideration [40]. Even though systemic corticosteroids are usually used in EBA, mechano-bullous EBA may be less responsive to corticosteroid than inflammatory variants. In general, compared with other PDs, systemic corticosteroids are less effective in EBA [35, 109].

1.3.6.2 Methotrexate and Azathioprine

Both drugs are utilized as steroid-sparing agents. These compounds are always used in combination for treatment of refractory forms of EBA [40].

1.3.6.3 Cyclosporine

Cyclosporine is a very strong steroid-sparing agent that may be used in EBA patients who have refractory disease or who develop adverse effects [106].

1.3.6.4 Colchicine

In patients who are intolerant to dapsone, colchicine may be of benefit [106]. Its use as first line treatment has been reported for patients with inflammatory type of EBA [40].

1.3.6.5 High dose Intravenous Immunoglobulin (IVIG)

IVIG containing the pooled immunoglobulin G (IgG) purified from human sera, have been utilized as replacement therapy for patients with Ab deficiencies and severe infections for decades. Later, its effective use was reported in many autoimmune diseases such as immune thrombocytopenia (ITP), Guillain-Barre syndrome, multiple sclerosis (MS), myasthenia gravis, pemphigus disease, and Kawasaki disease [40]. Treatment of the EBA patients with IVIG as monotherapy or in combination with other therapies achieved clinical improvement in case reports/case report series [9].

1.3.6.6 Dapsone

Dapsone is a sulfone-derived medication that was used in humans for treatment of leprosy in the 1940s. Since then, it has been utilized as an antimicrobial agent and has been identified to have anti-inflammatory effects. Dapsone is occasionally used as an adjunctive treatment in EBA, though published reports regarding its effectiveness in adults are sparse [110].

1.3.6.7 Rituximab

Rituximab is a chimeric monoclonal antibody against CD20 which is a protein expressed by B lymphocytes. Initially developed for the treatment of B cell

malignancies, it is increasingly being used for the therapy of autoimmune diseases including autoimmune hemolytic anemia, granulomatosis with polyangiitis (GPA), rheumatoid arthritis (RA), and pemphigus [111]. In most EBA patients treated with rituximab, several previous therapies have failed. Rituximab is mostly used as adjuvant therapy [40].

1.3.6.8 Other therapies

Other treatment approaches for EBA are plasmapheresis and extracorporeal photo-chemotherapy. These are used for EBA patients with refractory disease. Their beneficial effects have been sparsely reported in EBA. Plasmapheresis and extracorporeal photo-chemotherapy have been used in addition to other treatment modalities [40, 112]. Cyclophosphamide's use for treatment of EBA patients has been rarely reported [40]. The efficacy of minocycline, a broad-spectrum tetracycline antibiotic, was also reported in treatment of a patient with inflammatory form of EBA [113]. Success of a biological agent, daclizumab, on treatment of a patient with inflammatory EBA was reported in 2001. Daclizumab is a humanized murine monoclonal antibody against the α-subunit of the high-affinity interleukin- (IL-) 2 receptor also known as Tac (T cell activation) antigen or CD25 [114].

During the last decades, increasing knowledge on the cellular and the molecular pathogenesis of EBA has revealed new therapeutic targets interfering different phases of disease development including (i) the production of aAbs, (ii) maintenance of the circulating aAbs, and (iii) aAb-mediated tissue damage. Some of these newly discovered therapies have been successfully tested in pre-clinical models and currently await confirmatory studies of clinical trials [115, 116].

1.3.7 Challenges in EBA treatment

Management of AIBDs and especially EBA is challenging. EBA is notoriously difficult to treat and the cure rate with the standard first-line regimen is unsatisfactory. There is no consensus guidelines on the treatment of EBA [107], as it is uncommon and thus no clinical trials are available. Hence, current

treatment strategy only depends on the clinical expertise [40]. Adverse effects from standard treatments arise both from their long-term use and abrupt discontinuation. Moreover, immunosuppression is accompanied by developing infections in patients [116].

1.3.8 Prognosis

Although the course of EBA varies, the disease generally has a lengthy course persisting for years. Specifically, mucosal involvement can cause longstanding consequences including blindness and esophageal constrictions. Unrestrained cutaneous involvement may lead to joint contractures [117]. The prognosis of EBA is difficult to predict [118] and the overall prognosis and response to therapy may be less favorable in adults than in children [119]. There is no cure for EBA and the principle objective of the treatment is to harness disease activity [9].

1.4 Neutrophils/ polymorphonuclear leukocytes (PMNs)

1.4.1 Background

PMNs, as the most abundant leukocytes in the human blood circulation, represent the front line of defense against bacterial and fungal pathogens [120]. They are equipped with a wide array of antimicrobial molecules. In the circulation of healthy adults, PMNs are in a resting state ensuring that their toxic granular contents are not released to injure host tissues. Resting PMNs turn to primed state by some agents including bacterial products, chemokines, and cytokines such as tumor necrosis factor-α (TNF-α), granulocyte-monocyte colony-stimulating factor (GM-CSF), interleukin-8 (IL-8), and interferon-γ (IFN-γ). Once neutrophils are primed, they are mobilized to the site of infection/inflammation. During the priming process, PMNs undergo defined changes, which promote PMNs' function and/or lifespan. These include: mobilization of the granules containing pre-formed receptors towards the plasma membrane, elevation of the number and affinity of surface receptors, and activation of some transcription factors that induces expression of cytokines [121]. Rolling of PMNs occurs via binding of expressed L-

selectin (CD62L) on the surface of primed PMNs to its ligands (sialyl 6-sulfo Lewis X on GlyCAM-1, CD34, MadCAM-1) [122] on the endothelial cells. This induces conformational changes in integrin molecules on PMNs' surface, including very late antigen-4 (VLA-4; CD49d/CD29b), lymphocyte function-associated antigen-1 (LFA-1; CD11a/CD18), and macrophage antigen-1 (MAC-1; CD11b/CD18) which interact with their ligands on the surface of endothelial cells, such as intercellular adhesion molecule (ICAM)-1 and -2, vascular cell-adhesion molecule-1 (VCAM-1) and mucosal vascular cell-adhesion molecule-1 (MAdCAM-1), inducing high-affinity ligand binding and strong adherence. Following high-affinity adherence to the endothelium, rolling arrest is facilitated by engagement of chemo-attractants including IL-8 and leukotriene B4 (LTB4) to PMNs' receptors [121, 123]. PMNs' migration into the tissues occurs via the junctions between adjacent endothelial cells (para-cellular migration) mediating by surface ligands such as ICAM-2, PECAM-1 (platelet endothelial-cell adhesion molecule-1) and proteins of the junctional adhesion molecule (JAM) family [124]. Transcellular migration may also take place under certain circumstances like high ICAM-1 expression, and when few number of PMNs permeating and passing through pores in the cytoplasm of endothelial cells [125]. As soon as, they left the circulation and crossed the endothelium, they migrate towards site of inflammation along the chemo-attractant gradient. At the site of inflammation PMN membrane receptors for complement fragments and immunoglobulins (Ig) recognize their ligands. This leads to activation of PMNs, characterized by release of proteases (e.g., gelatinase B / matrix metalloproteinase (MMP-9)) and reactive oxygen species (ROS) which can be also toxic and cause damage to host tissue following their release from aberrantly activated PMNs in autoimmune diseases (in effector phase) [121]. Moreover, recent studies revealed that besides the contribution to the effector phase, PMNs are also capable of executing some crucial functions in the induction and transition phases of autoimmune diseases including antigen presentation, and modulation of the activity of other cell types (Figure 1.6) [120].

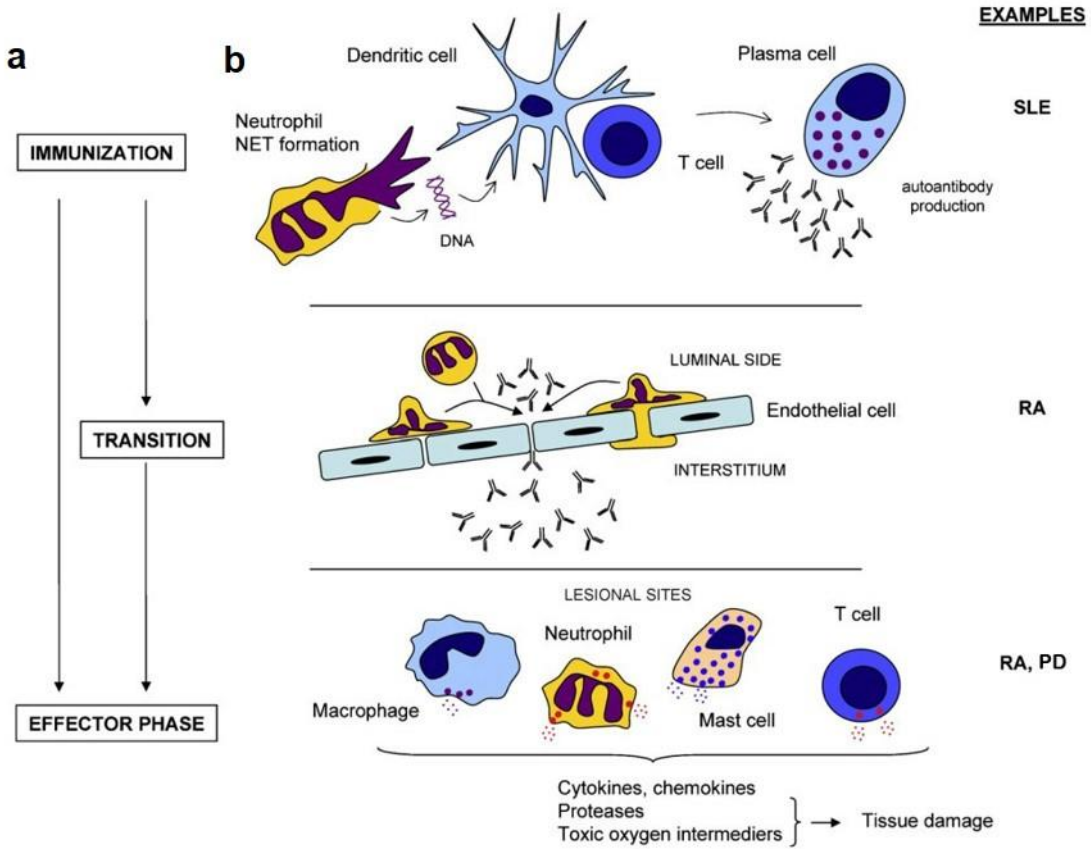

Figure 1. 6: PMNs' involvement in different phases of autoimmune diseases.
(a) Different phases of autoimmune diseases. (b) PMNs are involved in several phases of autoimmune diseases in many ways. For instance, in SLE they contribute to the induction phase of the disease by exposing the autoantigen (DNA) through NET formation. In RA, PMNs seem to drive the initiation of aAb deposition to the joints (transition phase). They are a crucial effector cell type at the lesions in PDs and RA (effector cells). Abbreviations: SLE; Systemic lupus erythematosus, RA; Rheumatoid arthritis, PD; Pemphigoid diseases [120]. (Figure modified from [120])

1.4.2 PMNs in EBA pathogenesis

1.4.2.1 PMNs' role in induction phase of EBA

Although role of PMNs as potential drivers of autoimmunity in EBA has been relatively neglected, their contribution to the induction phase of the disease has been demonstrated using GM-CSF-/- mice in the immunization-induced model of EBA. GM-CSF stimulates hematopoietic cells and induces macrophage and PMN recruitments to sites of inflammation and its effect is mainly targeted on PMNs. In GM-CSF-/- mice the titer of the aAb in sera was significantly lower compared with wild-type, associated with fewer PMN number in dLNs. A similar effect was noticed

on aAb production level in PMN-depleted wild-type mice. PMN depletion accompanied by GM-CSF deficiency (PMN depletion in GM-CSF-/-mice) led to a stronger inhibitory effect on aAb production. Furthermore, PMNs' co-localization with B cell activating factor (BAFF) in dLNs was demonstrated after immunization [126]. This was in accordance with previous findings that BAFF produced by PMNs stimulate autoreactive B cells [127, 128]. Based on these findings, the likely scenario for the role of PMNs in induction phase of EBA was that both GM-CSF and PMNs are involved in production of anti-COL7 Ab by facilitating the influx of APCs and more PMNs into peripheral LN [126].

1.4.2.2 PMNs' role in effector phase of EBA

According to a classification in which aAb-mediated diseases are categorized by the major pathologic characteristics of aAb, EBA is classified as an aAb-induced inflammatory autoimmune disease [129]. In EBA, binding of anti-COL7 Ab to their target at the DEJ, elicits the production and release of a number of inflammatory mediators such as cytokines and anaphylatoxins, predominantly C5a. This milieu leads to PMN recruitment and their subsequent activation [130] in an FcγR-dependent fashion [131] resulting in release of ROS and proteolytic enzymes, which subsequently causes sub-epidermal blister formation [130]. The Ab-transfer induced EBA model provides an opportunity to thoroughly study the PMNs' contribution to the effector/inflammatory phase of EBA. PMNs' depletion using anti-granulocyte receptor-1 antigen (Gr-1) antibody and the deficiency in CD18-common β2 subunit of all β2 integrins which is prerequisite for PMN extravasation-led to a complete protection of mice from development of disease in the Ab-transfer-induced EBA [130]. Moreover, CD18 was recently described as an essential component for PMN adhesion in the process of tissue damage in the *in vitro* and the *ex vivo* models of EBA [132]. C5a, GM-CSF, CXCL1/2, TNF-α, IL-1β, and LTB4 have been demonstrated to have pro-inflammatory functions in pathogenesis of experimental EBA [26, 126, 133-137], whereas IL-6 and IL1ra have anti-inflammatory effects [138]. In other words, functional blockade of the mediators involved in PMN recruitment, such as C5a, GM-CSF, CXCL1/2, TNF-α, IL-1 and LTB4 diminished disease severity in the experimental EBA [126, 133-

137]. By contrast, inhibition of IL-6 exacerbated the EBA disease phenotype, while treatment with recombinant IL-6 ameliorated disease severity in experimental EBA through induction of IL1ra [138].

After migration into the skin, PMNs undergo further activation, which is mainly an FcγR-dependent process through binding to deposited immune complexes (ICs) at the DEJ. In Ab-transfer-induced EBA, compelling evidence suggests a resistance to skin inflammation in mice lacking either the common γ-chain of all activating FcγR, or the FcγRIV (activating variant of FcγRs in mice), while mice deficient in inhibitory FcγRIIB demonstrated stronger skin inflammation compared with wild-type controls [131]. Furthermore, the glycosylation of COL7 aAbs is essential for their interaction with PMNs' FcγRs. Thus the manipulation of glycosylation status of the aAbs might have a therapeutic importance in aAb-mediated diseases, where the aAb induce pathology through FcγR-mediated mechanisms. This hypothesis has been tested using EndoS, an endoglycosidase that exclusively hydrolyzes the glycan at Asn297 in the native IgG [139]. Treatment of the mice with EndoS led to the reduction of the clinical disease in experimental EBA [140, 141]. Pretreatment of anti-mCOL7 IgG with EndoS dramatically decreased split formation at the DEJ in the *ex vivo* model of EBA. Pathogenic anti-mCOL7 IgG pretreated with EndoS was not either capable of inducing the disease in Ab-transfer-induced EBA [140].

Engagement of PMNs' surface receptors (e.g., FcγRIV and integrins) elicits a signaling pathway initiating with early upstream molecules such as Src and Syk kinases. Deficient mice in these kinases are resistant to skin inflammation in the Ab-transfer-induced EBA [142-144]. Several downstream signaling kinases and regulators including phosphatidylinositol 3-kinase (PI3K)-β and -δ, p38 mitogen-activated protein kinase (MAPK), extracellular signal-regulated kinase (ERK)1/2, Akt, RORα, and phosphodiesterase-4 (PDE4) [103, 145-148] are involved in PMNs' activation in the experimental EBA. Inhibition of these molecules led to reduced disease manifestation in Ab-transfer-induced EBA. One of the ultimate pathologic events in the effector phase of experimental EBA which leads to tissue damage and clinically detectable disease is mediated by the release of ROS and proteases such as MMP-9 from IC-activated PMNs. ROS and MMP-9 are believed

to degrade proteins of DEJ causing DEJ separation and blister formation [130, 149]. To explain in more detail, in the Ab-transfer-induced EBA, a resistance to skin blistering was indicated in neutrophil cytosolic factor 1-deficient mice lacking functional NADPH oxidase [130]. Furthermore, using a combination of inhibitors against proteases, serine and matrix metalloproteases entirely blocked the DEJ separation induced by IC-activated PMNs in *ex vivo* model of EBA. Further investigation using MMP-9 selective inhibitor resulted in abolished DEJ separation, meaning that MMP-9 is an indispensable protease for DEJ separation in EBA [149]. All these findings make EBA as a prototype of an aAb-induced and neutrophil-driven disease.

The current knowledge on the pathogenesis of EBA presents monocyte/macrophage as a second cell type in addition to PMN that is involved in blister formation [135]. Besides PMNs as key players causing tissue injury in the effector phase of EBA, γδ and NK-T cells have been suggested to contribute to the efferent phase of EBA by augmentation of PMNs' recruitment to the site of inflammation [150]. Moreover, Tregs have been revealed as a PMN function modulators in the effector phase of EBA by regulation of cytokine production (e.g., IFN-γ) and the expression of PMN adhesion molecules (e.g., CD18). As a consequence, they are capable of modulating PMNs' recruitment to the skin [151]. Furthermore, an anti-inflammatory role of CD11b was observed in Ab-transfer-induced EBA. In this study, mice with CD11b-deficiency developed more severe diseased phenotype than wild type mice. They also expressed increased levels of T cell cytokines including IFN-γ and IL-4. Hence, possible mechanism of the anti-inflammatory role is that CD11b is contributed to a suppressive regulation of T cell responses [152].

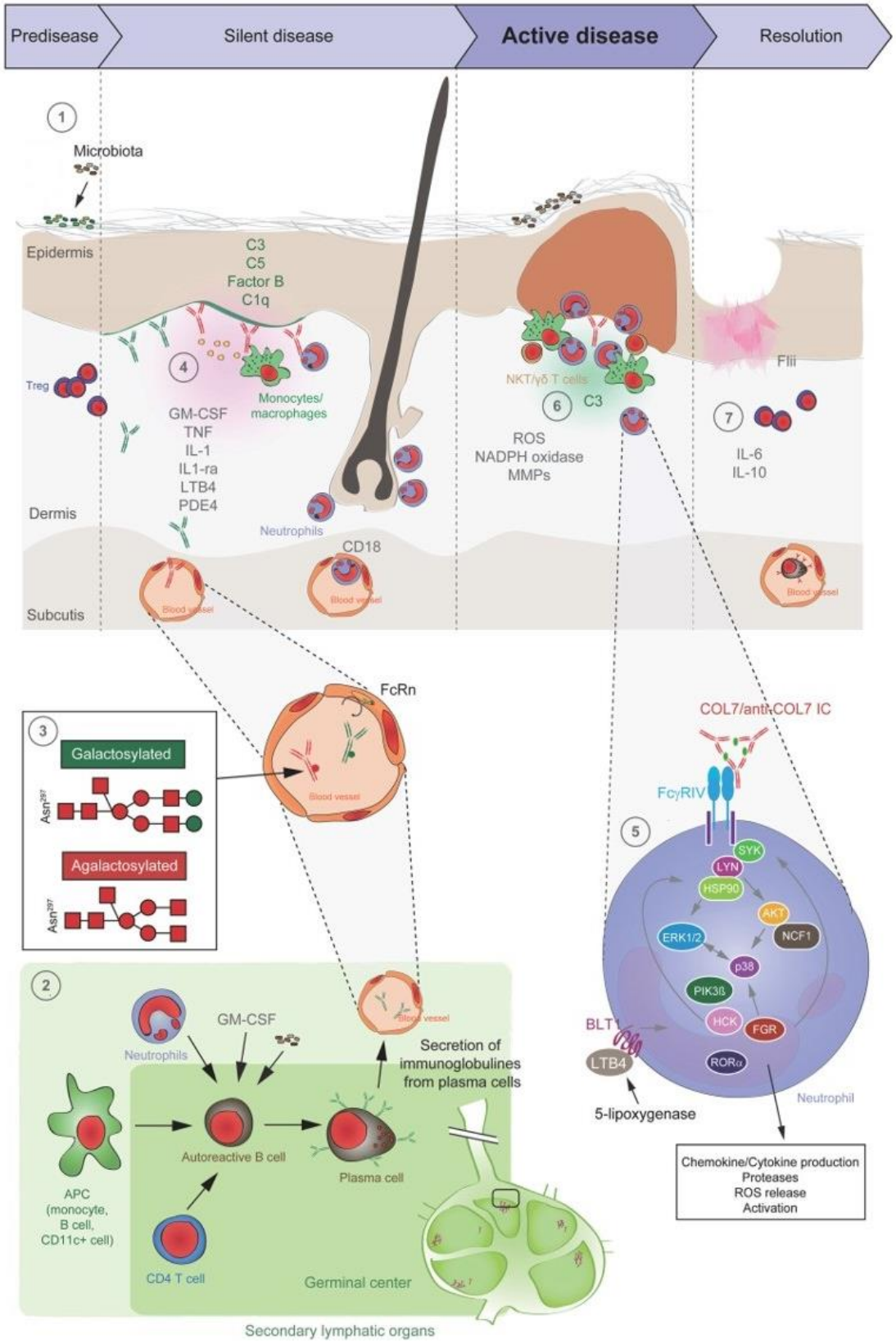

Figure 1. 7: Schematic demonstration of EBA pathogenesis. Explanation in following page.

(1) Loss of tolerance happens due to the genetic factors and the skin microbiome imbalance. (2) Breach of tolerance is associated with the interaction of APCs with autoreactive B and T cells which results in clonal expansion and differentiation into plasma cells. AAbs directing COL7 are released into the blood circulation and effector organs. (3) During inflammation, galactosylation of Abs may differ. High galactosylation of IgG is crucial for the anti-inflammatory properties, whereas low galactosylation is pro-inflammatory. (4) Binding of anti-COL7 Abs to COL7 at the DEJ, elicits the production and/or the release of a number of mediators such as cytokines and complement fragments. This milieu leads to an increased expression of endothelial adhesion molecules in cutaneous vessels and leukocyte recruitment particularly PMNs. (5) Immune complexes bind in an Fc-dependent manner to neutrophils and induce a signaling cascade leading to activation, including the (6) release of ROS and proteolytic enzymes. Besides neutrophils, other cell types are contributed to split formation, as shown for monocytes/macrophages, NKT and γδ T cells. However, Treg cells have an inhibitory effect on EBA progression. (7) Resolution of autoantibody-induced tissue injury will ultimately happen [153]. (Figure modified from [153])

1.5 Drug repurposing

Despite the increasing advancement in drug research and development (R&D) such as chemical genomic technologies and chemical libraries, the number of new drugs brought to the market has dramatically declined in recent decades [154]. De novo drug discovery is a time-consuming, laborious, costly and high-risk process. It usually takes 10-15 years to develop a new drug. However, the success rate of a newly discovered drugs is considerably small (<10%) in phase-II and -III of clinical trials or post-marketing phase [155, 156]. Finding new therapeutic indications for existing drugs, known as drug repurposing, propose one possible solution to such a problem [154]. Using this approach, a drug is repurposed for a new molecular target or for the same target in a different disease [157]. Typically, existing drugs have been already studied in terms of the safety, efficacy, and toxicity in order to gain approval by the United States Food and Drug Administration (FDA) and/or the European Medicines Agency (EMA) for a specific indication [158]. Thus, drug repurposing should notably help to decrease time, money, and risk of drug development compared with conventional drug discovery (Figure 1.8) [154]. Likewise, while only 10% of newly discovered drugs' applications obtain market approval, roughly 30% of repurposed drugs are approved [158]. As a consequence, drug repurposing is rapidly growing in popularity to develop a new medicine. In spite of the profound success shown by repurposed drugs, most of them are the consequence of "serendipity", i.e. based on the unexpected

observations made during or after late phase of clinical study [159] (Table1). For instance, in 1964, Dr. Sheskin used thalidomide to help a patient with leprosy to sleep but interestingly, thalidomide also healed the patient's sores and eliminated his pain [160, 161]. This discovery demonstrates that clinical outcome could be the most direct and reliable source of drug repurposing [162]. Systematic approaches of drug repurposing include (i) experimental approach such as (high-throughput) screening of marketed drugs, and targeted testing of a class of drugs for a new disease area, and (ii) computational approach utilizing *in silico* methods based on the drug-target interactions [162, 163]. For experimental repurposing, gaining a physical collection of approved drugs for screening has been considered as a major difficulty. Several companies have dealt with this problem by marketing some libraries containing from a few hundreds to thousands of approved or off-patent drugs. These encompass Enzo Life Sciences (Plymouth Meeting, PA, USA), Prestwick (Washington DC, USA), and Spectrum (Microsource, Gaylordsville, CT, USA). Apart from approved drugs, a number of compounds that have failed clinical trials because of lack of efficacy (not toxicity) also represent a substantial source for repurposing (Figure 1.8). For instance, the ineffective cancer drug zidovudine later became a widely used anti-human immunodeficiency virus (HIV) drug [163].

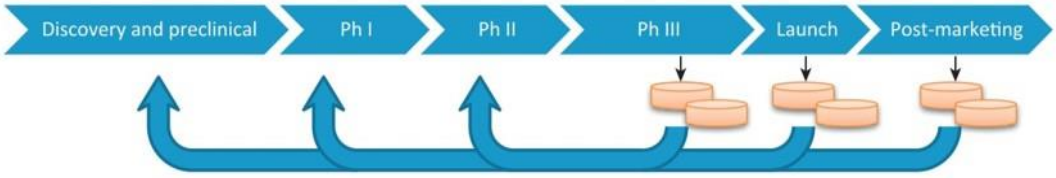

Figure 1. 8: Drug repurposing scheme.
When a compound is unsuccessful in the last steps of development or even marketed compounds are brought back into the pipeline for research and development for their new indication. Abbreviations: Ph, Phase. (From [164])

In the context of autoimmune diseases, some studies have been conducted concerning inflammatory bowel disease (IBD) [165, 166], MS [167], and psoriasis [168] using the literature mining and *in silico* methods. Another study utilized experimental approach for screening of the Prestwick chemical library (PCL) using a zebrafish system as an *in vivo* drug discovery platform to repurpose existing drugs for anti-inflammatory applications in atopic dermatitis (AD) [169]. To the best

of my knowledge, no experimental studies have been performed to repurpose any drug for AIBDs, including EBA.

Table 1. 1: List of repurposed compounds updated and supplemented with information on compound approval.

Drug	Original indication	New indication	Year*
Amphetamine	Stimulant	Hyperkinesis in children	1943
Allopurinol	Tumor lysis syndrome	Gout	1967
Zidovudine	Cancer	HIV/AIDS	1985
Minoxidil	Hypertension	Alopecia	1988
Bupropion	Depression	Smoking cessation	1997
Sibutramine	Depression	Obesity	1997
Finasteride	Benign prostatic hyperplasia	Alopecia	1997
Methotrexate	Cancer	Rheumatoid arthritis	1999
Fluoxetine	Depression	Premenstrual dysphoric disorder	2000
Atomoxetine	Parkinson's disease	ADHD	2002
Thalidomide	Morning sickness	Multiple myeloma	2003
Cymbalta	Depression	Diabetic peripheral neuropathy	2004
Topiramate	Epilepsy	Migraine	2004
Paclitaxel	Cancer	Restenosis	2004
Sildenafil	Angina	Erectile dysfunction	2005
Requip	Parkinson's disease	Restless legs	2005
Lumigan	Glaucoma	Hypotrichosis simplex	2009
Dapoxetine	Analgesia and depression	Premature ejaculation	2009
Milnacipran	Depression	Fibromyalgia syndrome	2009
Phentolamine	Hypertension	Dental anesthesia reversal agent	2009
Lidocaine	Local anesthetic	Arrhythmia	2010
Mifepristone (RU486)	Pregnancy termination	Cushing's syndrome	2012

* Year of first approval in new indications. Abbreviations: ADHD; Attention deficit hyperactivity disorder, HIV; human immunodeficiency virus, AIDS; acquired immunodeficiency syndrome. (From [164])

1.6 Aim of the study

Although autoimmune disorders are considered as relatively rare diseases, their mortality and morbidity rates are quite high [170]. Of these, incidence rate of AIBDs in Germany is 2,000 new cases and an overall prevalence of about 40,400 cases in the total population of 80,925 million inhabitants [13, 41]. EBA belongs to PDs, a subset of AIBDs, with an unfavorable prognosis. It is classified as an aAb-induced inflammatory disease. EBA is difficult to cure and its mainstay of therapy is the systemic corticosteroids at high doses and immunosuppressive agents. Despite the growth in drug development, there are no approved drugs used to cure EBA. The main objectives of the recently-discovered therapies for EBA is to develop specific, pathogenesis-based therapeutics with minimized side-effects [116]. As has been stated above, there is an unmet need to find a treatment for EBA with higher effectiveness and fewer drawbacks.

Drug repurposing, reuse of already existing drugs for their new indications, is an emerging strategy compared with traditional drug development with a swifter development time and an increased safety certainty. There have been no reported studies on drug repurposing for AIBDs. A previously well-established Ab-transfer-induced model of EBA in our laboratory provided a perfect tool for preclinical drug evaluation for PDs' treatment. Utilizing this model in the present study, I tested the effects of the candidate drugs which passed the primary screening. The ultimate aim of the current study is to identify potential therapeutics for treatment of PDs (EBA as a representative) through drug repurposing. To that end, the specific goals of my thesis were:

- Implementation of a primary screening applying an *in vitro* model of EBA (ROS release assay) to identify drugs with inhibitory effect on ROS generation by immobilized IC (iIC)-activated neutrophils (PMNs). Moreover, further *in vitro* validation to confirm effect of the promising identified drugs and to identify mechanism of action.

- Validation of candidate drugs using the Ab-transfer induced model of EBA. Verification aimed at identification of compounds that ameliorate EBA phenotype.

- Elucidation of *in vivo* mode of action of the effective drug(s) and identification of drug-induced gene expression signature by means of RNA sequencing (RNA-Seq).

2 Materials and Methods

All experimental procedures in this study were carried out by me unless otherwise stated.

2.1 Materials

All materials used in this work are listed in appendix.

2.2 *In vitro* screening

2.2.1 Ethical consideration

All procedures accomplished in this study comprising human participants were performed in accordance with the Helsinki declaration. The ethic committee at the University of Lübeck approved the study (V 242-7224.122.5 (23-3/14)) and all volunteers gave their written informed consent to the study participation.

2.2.2 Description of screening drug library

The Prestwick chemical library (PCL) was used for screening. The PCL is a recognized chemical screening library for high chemical and pharmacological diversity, as well as for known bioavailability and safety in humans. The PCL consists of 1,200 FDA-(formerly) approved, off-patent small molecules used as drugs for various diseases including infectious, neurodegenerative, psychiatric, and cardiovascular diseases and cancer [171, 172]. Compounds were provided in DMSO at the concentration of 10mM in 96-well plates.

2.2.3 Compound preparation

Compounds were diluted in DMSO to a concentration of 100µM in the non-binding 96-well microplates. Of this, a volume ratio of 1:100 (final concentration of 1µM) in 1% DMSO was used for screening.

2.2.4 Generation of recombinant human COL7 (h-COL7) fragments

Based on an already established protocol in the laboratory, h-COL7 fragments expressed and purified. In brief, h-COL7EF fragments comprising amino acid residues Thr^{394}-Ala^{600} of h-COL7 NC1 domain were produced by PCR from human skin cDNA. They were then cloned into pGEX-6P1 GST-fusion vector and the recombinant proteins were expressed in E. coli Novablue and purified by glutathione affinity chromatography [86]. Generation and isolation of recombinant h-COL7 was performed by Ms. C. Kauderer.

2.2.5 Expression of chimeric anti-h-COL7 IgG1

To generate anti-h-COL7 IgG1 Abs according to a previously established protocol, expression vectors of Ab heavy and light chains were co-transfected with pAdVAntage (expression enhancing vector) into human embryonic kidney cells 293 (HEK-293T cells) using the HEK freestyle system. Abs were purified from culture supernatants using HiTrap protein G sepharose [86]. These Abs were expressed by Dr. A. Recke and purified by Ms. C. Kauderer.

2.2.6 Isolation of primary human PMNs

Whole blood was drawn from healthy volunteers in EDTA-tubes and processed in less than 2 hours (h). Polymorphprep™ density gradient centrifugation was utilized for the isolation of human PMNs from whole blood. One volume of whole blood was overlaid on one volume of Polymorphprep™ and was centrifuged at 500×g for 35 minutes (min) at room temperature (RT), deceleration was without brake. Plasma and upper band of cells containing mononuclear cells were discarded and the lower ring of PMNs was harvested. One volume of half medium was added to one volume of PMNs and was centrifuged at 400×g for 10 min at RT. To lyse residual erythrocytes, the cell pellet was resuspended in 3 mL of cold lysis buffer for 30 seconds (s). Lysis was then stopped by adding RPMI1640 and mixture was centrifuged at 400×g for 10 min at RT and the cell pellet was subsequently washed with chemiluminescence (CL) medium (centrifugation at 400×g for 10 min at RT). PMNs were harvested and adjusted to the concentration of 2×10^6/mL in CL

medium. 100 µL of PMNs at concentration of 2×10^6/mL were seeded into each well.

2.2.7 *In vitro* model of EBA for screening; iIC-induced PMN activation

In our laboratory, to model the IC-induced PMN activation in EBA, an *in vitro* method called ROS release assay has been developed [145]. It was initially established for ICs comprising type XVII collagen (COL17) and anti-COL-17 Abs closely duplicating IC-mediated PMN activation in BP [173]. It is in principle a luminol-amplified chemiluminescence technique. Upon activation of PMNs using iICs comprising recombinant hCOL7 antigen and corresponding recombinant anti-hCOL7 Abs, NADPH oxidase, situated in the plasma membrane and in the membranes of specific granules of PMNs, generates superoxide anions (O2.-) from which further ROS derive. ROS are released into the ambient medium and lead to oxidation of luminol (5-amino-2,3-dihydro-1,4-phthalazinedione), a redox-sensitive compound, which emits blue luminescence upon oxidation. This method is very sensitive and is able to detect both intra- and extra-cellular ROS as it can diffuse into the cells [174]. In this *in vitro* model, iICs were formed by coating a 96-well white plate with 10µg/mL of recombinant h-COL7EF in 100µL of Carbonate-Bicarbonate buffer, pH 9.6 (coating buffer) per well at RT for 3 h. After 3-times washing with PBS-T (phosphate-buffered saline-0.05 % v/v Tween-20), wells were blocked overnight with 1% biotin-free bovine serum albumin (BSA) in PBS-T at 4°C. Following 3x washing, wells were incubated with 100µL of 2µg/mL of recombinant anti-h-COL7 IgG1 at RT for 2 h and subsequently washed. Isolated PMNs containing 1 mM luminol were then added to the already IC-immobilized plate in the presence of either compounds at a concentration of 1 µM or 1% DMSO as vehicle. To check the dose response of the 33 promising drugs (hits) from primary screening, 3 more concentrations were also used (0.1, 0.01, and 0.001 µM). 10 ng/mL of Phorbol-myristate-acetate (PMA) was served as positive control for stimulation of PMNs. Release of ROS into the supernatant was ultimately monitored using a luminometer for almost 2 hours. The aim of this experiment was to evaluate the inhibitory effect of 1,200 compounds of PCL on ROS generation by iIC-stimulated human PMNs. Screening of the 1,200 compounds was implemented with the assistance of Dr. W. Veldkamp, who

screened 700 compounds as part of her medical studies in Groningen (The Netherlands).

2.2.8 Cell-free/acellular enzymatic luminol-amplified chemiluminescence ROS release assay

To investigate the mechanisms of action of the drugs in ROS release reduction, an acellular enzymatic ROS release assay was carried out. This system comprises glucose/glucose oxidase (G/GOX), catalase (CAT), and myeloperoxidase (MPO) that enables regulated generation of hypochlorous acid (HOCl) and H_2O_2 that in fact simulates the oxidative burst of neutrophils [175]. This assay is briefly described as follows. Human MPO, CAT, and GOX were mixed at final concentrations of 10 mU/mL, 2 U/mL, and 0.5 U/mL, respectively. Assay buffer, color free Hank's Balanced Salt Solution (HBSS), was supplemented with 0.1% v/v Triton X100 and 5 mM glucose and 2 mM luminol in the presence of the 33 promising drugs at the concentrations of 1, 0.1, 0.01, and 0.001 µM or 1% DMSO as vehicle. *N*-acetyl-L-cysteine (NAC), an artificial antioxidant, at the concentration of 10 mM was used as a positive control [176]. ROS generation was monitored by luminometer in 60 repeats.

2.2.9 Flow cytometric assay for analysis of cytotoxic effects of promising drugs

The principle behind this flow cytometry-based cytotoxicity assay is detection of early and late apoptotic cells. During apoptosis, cells undergo a translocation of membrane phosphatidylserine (PS) from the inner side of the plasma membrane to the cell surface followed by the loss of membrane integrity. Annexin V (AV), a Ca^{2+}-dependent phospholipid-binding protein, has high affinity for PS. Staining for AV is typically accompanied by a vital dye such as propidium iodide (PI). Viable cells with intact membranes exclude PI, whereas the membranes of dead cells are permeable to PI. Therefore, cells that are considered viable are both AV and PI negative, while cells that are in early apoptotic stage are AV positive and PI negative, and cells that are in late apoptotic stage or already dead are both AV and PI positive [177]. In order to evaluate the drug-induced toxicity, PMNs were seeded into the plate (described in section 2.2.7) and were incubated with

compounds for 2 hours at 37°C. They were subsequently centrifuged at 300×g for 7 min and pellet was re-suspended in 50µL of AV-binding buffer. FITC-conjugated AV (AV-FITC) was then added to the cell suspension at a concentration of 1 µg/mL and incubated for 20 min at 4°C in the dark. After dark incubation, the plate was centrifuged at 300×g for 7 min and the pellet was re-suspended in 100µL of FACS buffer. After washing (centrifugation at 300×g for 7 min), the pellet was re-suspended in 300µL of FACS buffer. PI was added (at 1:300 dilution) to the samples before starting the measurement by BD FACSCalibur flow Cytometer. Dead cells (UV-killed cells) were served as a positive control to set up a proper measurement setting. Cytotoxicity assay for the 33 promising compounds (hits) was performed by Dr. W. Veldkamp using BD FACSCalibur flow Cytometer. I repeated drug-induced cytotoxicity analysis for the 6 candidate drugs using MACSQuant® Analyzer 10.

2.2.10 Flow cytometric assessment of compounds' impact on PMN function

To study the effect of the compounds on other PMN functions, the expressions of a neutrophil activation biomarker namely CD62L was analyzed on PMN surface. CD62L is constitutively expressed on leukocytes and is involved in the "rolling" of PMNs and in the inflammatory process. Upon activation, CD62L is shed from PMNs' surface [178]. CD66b is consistently expressed on human PMNs and it was here used as a PMN marker [179, 180]. Another PMN marker, CD15 was also used to improve the specificity of the staining [179]. To evaluate the effect of 6 candidate drugs on function of the PMNs, 2×10^5 PMNs in 100µL of CL medium were seeded into the wells (described at 2.2.7) and were incubated with compounds for 2 hours at 37°C. They were then centrifuged at 300×g for 7 min and pellet was re-suspended in 50µL of FACS buffer and 5µL of Fc receptor (FcR) blocking reagent from Miltenyi Biotech was added and incubated for 5 min at RT. Thereafter, cells were labeled with APC-conjugated anti-CD15 (1µg/1×10^6 cells), FITC-conjugated anti-CD66b (1µg/1×10^6 cells) and PE-conjugated anti-CD62L (1µg/1×10^6 cells). They were dark incubated at 4°C for 20 min followed by adding 100µL of more FACS buffer. Subsequently, they were centrifuged at 300×g for 7 min and the pellet was re-suspended in 300µL of FACS buffer and shortly before measurement PI was added (1:300). Samples were measured by MACSQuant

Analyzer 10 (Miltenyi Biotec, Bergisch Gladbach, Germany) and the data were analyzed using MACSQuantify software. Analysis of PMNs' activation state was performed by the use of three markers (CD15, CD66b and CD62L). PMNs were first gated by forward scatter and side scatter. After exclusion of dead cells using PI, $CD15^{pos}$ cells were gated. From $CD15^{pos}$ parent cell population, activated PMNs and resting PMNs were gated as $CD66b^{pos}CD62L^{neg}$ and $CD66b^{pos}CD62L^{pos}$, respectively.

2.3 *In vivo* validation

2.3.1 Ethical consideration

Local authorities of the Animal Care and Use Committee (Kiel, Germany) approved all mice experiments implemented in this project under authorization number of AZ 122-5(23-3/14) and all protocols were carried out by certified personnel.

2.3.2 Mice

Wild type C57BL/6J mice were used for Ab-induced transfer of EBA at the age of 8-12 weeks. Esr1/Esrα KO (B6.129P2-*Esr1*^{tm1Ksk}/J) and Esr2/Esrβ KO (B6.129P2-*Esr2*^{tm1Unc}/J) mice were purchased from The Jackson Laboratory and were bred heterozygously (het) × (het). Mice were genotyped for Esrα and Esrβ genes using polymerase chain reaction (PCR). Esrα and Esrβ deficient mice and the respective age- and gender-matched wildtype littermates were used for experiment. All mice were held at specific pathogen free conditions and fed acidified drinking water and standard chow *ad libidum*. Animals were maintained on a 12-hour light–dark cycle. All scoring processes of mice were performed under anesthesia using intraperitoneal (i.p.) administration of a mixture of ketamine (100µg/g) and xylazine (15µg/g).

2.3.2.1 Expression and purification of mCOL-7-vWFA2

The immunedominant m-COL7-vWFA2 subdomain (Figure 2.1) of NC1 domain (aa 1048-1238 with 5 additional amino acid residues [GRAMG] at the N terminus) was

expressed in E. coli ER2566 and purified according to an established protocol in the laboratory [70, 181] and performed by Ms. C. Kauderer.

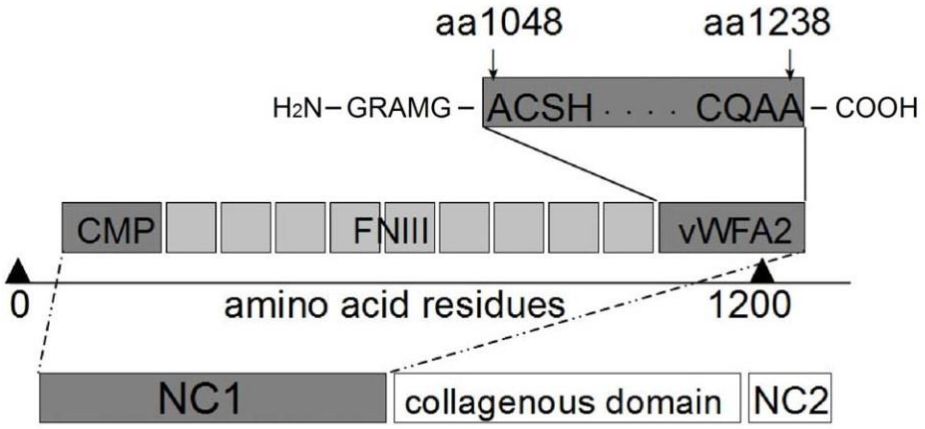

Figure 2. 1: Schematic representation of m-COL7-vWFA2 of NC1 domain used in this study.
Within the murine NC1 domain, the vWFA2 subdomain is located at amino acids of 1048–1238. For recombinant expression, 5 additional amino acids residues (GRAMG) at the N-terminus were added. (From [70])

2.3.2.2 Generation and purification of anti-m-COL7- vWFA2 antibodies

The obtained proteins from 2.3.2.1 were sent to Eurogentec GmBH, Belgium for immunization of New Zealand white rabbits. Rabbits were subcutaneously immunized with 250µg of 2mg/mL m-COL7-vWFA2 protein which was suspended in complete Freund's adjuvant (CFA). The animals were boosted three times (at 14-day intervals) with the same protein preparation in incomplete Freund's adjuvant (IFA). 2 months after the first immunization, immune sera were obtained and followed by a weekly blood collection and sent back to the Lübeck Institute of Experimental Dermatology (LIED). IgG purification was performed based on an established protocol in the laboratory. The protein G Sepharose fast flow affinity column chromatography was utilized for purification of IgG fractions against vWFA2 subdomain (anti-mCOL7 IgG). In brief, after adding the serum mixed with 1 volume of binding buffer to the already prepared column through a filter paper, the column was closed and incubated on a rocking platform for 1-4 hours at 4°C. Subsequently, I let the flow through to drain and washed column with the binding

buffer until the OD280 <0.1. Anti-mCOL7 IgG was eluted with 0.1M glycine buffer (pH 2.8) and neutralized with 1M Tris-HCl (pH 9). Anti-mCOL7 IgG was transferred into dialysis tubes and put on PEG for 2h at RT. Then the tubes containing IgG fractions were dialyzed against 1X PBS (pH 7.2) at 4°C for 2x 3 hours followed by an overnight procedure. Anti-mCOL7 IgG was concentrated by Amicon Ultra (30 KDa) at 4°C using maximum speed centrifugation [26]. Purified IgG fractions were then sterilized using 0.22 µm filters and the concentration was assessed by Nano-Drop 2000c spectrophotometer. Reactivity of the IgG fractions was analyzed by DIF microscopy on murine skin sections. The titer should be higher than 1:4000 for using in mice experiment.

2.3.2.3 Disease induction in Ab-transfer induced EBA

Purified rabbit anti-mCOL7 IgG was subcutaneously injected into the adult mice, aged 8-12 weeks, at a concentration of 3.5 mg/ 20 gBW every other day for 6 times (on days 0, 2, 4, 6, 8, and 10). The experimental set-up was designed for a period of 16 days. Mice were weighed and examined for their general conditions and for the presence of cutaneous lesions (i.e., erythema, blisters, erosions, and crusts) every 4 days. On day 16 mice were euthanized and blood and tissue specimens were harvested for further investigation (Figure 2.2).

Figure 2. 2: Schematic representation of disease induction and treatment strategy in Ab-transfer induced EBA.
Purified rabbit anti-mCOL7-IgG was subcutaneously injected into the mice every other day for 6 times. Mice were treated with the drugs one day before starting total IgG injection over a period of 16 days. Mice were scored for the presence of cutaneous lesions (i.e., erythema, blisters, erosions, and crusts) every 4 days. On day 16 mice were euthanized and blood and tissue specimens were harvested.

2.3.2.4 Evaluation of disease severity in experimental EBA

Scoring system of the experimental EBA basically incorporates the determination of involved body surface area that is expressed as percentage at different time points (days 4, 8, 12, 16). Affected body surface area (ABSA) was quantified by allocating individual fraction to each part of the body to reach overall score of ABSA in percentage [98] (Figure 2.3). The area under the curve (AUC) was then calculated using scores at different time points, taking both disease onset and maximal disease severity into account. To protect against bias, the evaluation of the disease symptoms was performed by a blinded observer, Dr. K. Matsumoto.

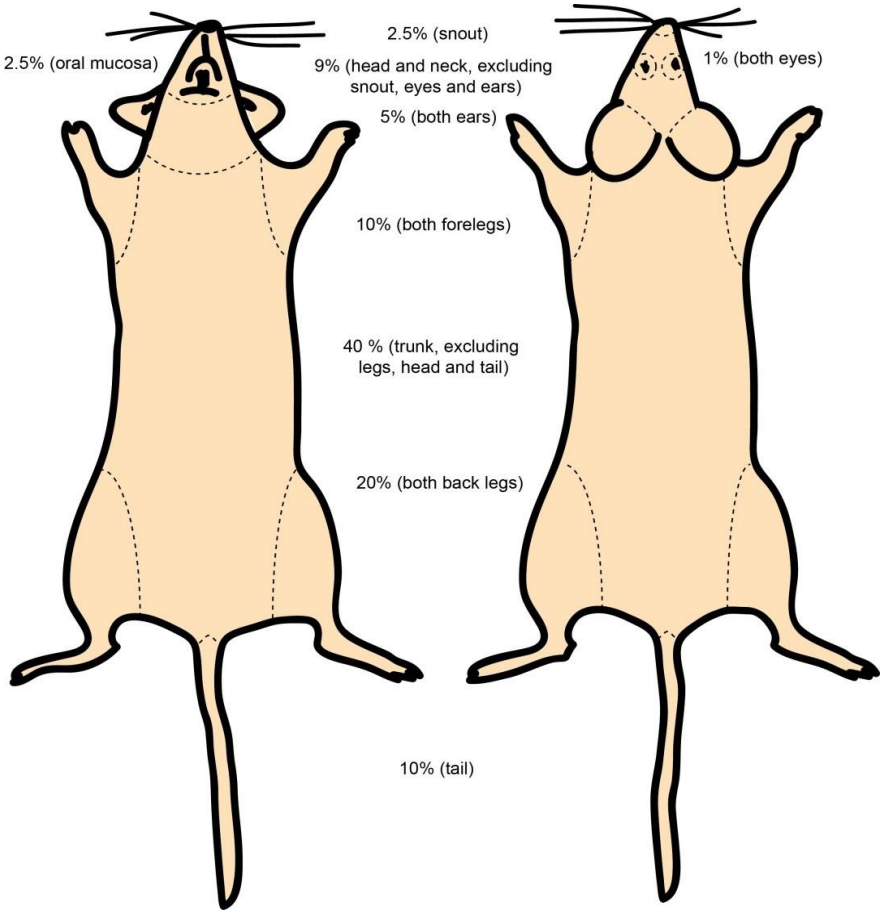

Figure 2. 3: Calculation of disease severity in experimental EBA based on the percentage of the ABSA.
Involved body surface area is calculated by allotting individual section to each part of the body (both ears-5%, both eyes-1%, snout-2.5%, oral mucosa-2.5%, head&neck-9%, both front legs-10%, both rear legs-20%, tail-10% and trunk-40%). (From [98])

2.3.3 Treatment regimens in the experimental EBA

The best method to investigate the potential of candidate compounds to interfere with complex physiological processes is to assess their effects *in vivo* [169] . To determine conservation of activity of candidate drugs from primary screening, the impact of the identified candidate drugs (amodiaquine, apomorphine, auranofin, dobutamine, niclosamide, and tamoxifen) was investigated on disease onset and progression in the Ab-transfer induced EBA. Mice were treated with these compounds at the doses recommended by literature or methylprednisolone as a reference treatment in a prophylactic approach, in other words, mice were treated with the compounds one day before initiating of total IgG injection (Figure 2.2). Furthermore, the effects of two candidate compounds (apomorphine and tamoxifen) were tested in combination treatment approach and their possible *in vivo* dose responses were studied as well.

2.3.3.1 Amodiaquin dihydrochloride dihydrate

Amodiaquin dihydrochloride dihydrate ($C_{20}H_{28}Cl_3N_3O_3$, Amo) is an antimalarial agent and has extensively been used in the treatment or prevention of malaria [182]. In addition to its anti-malarial effects, its beneficial roles have been reported in controlling cancer, through the inhibition of autophagy [183] and chronic inflammatory diseases such as RA and SLE via its immunosuppressive activity [184-186]. In this study, Amo was intraperitoneally administered to the mice (n = 5 / group) at the concentration of 50 mg/kg BW on the daily basis for 16 consecutive days in the Ab-transfer induced EBA model. Mice in control group received daily intraperitoneal (i.p.) injection of vehicle (distilled water).

2.3.3.2 Apomorphine

R(-) Apomorphine hydrochloride hemihydrate ($C_{34}H_{38}Cl_2N_2O_5$, Apo), is a dopamine-receptor agonist possessing high affinity for all known dopamine receptors (D1, D2, D3, D4, and D5) [187]. This compound has been used for treatment of different diseases including Parkinson's disease [188], erectile dysfunction [189] and alcohol dependency [190]. Mice (n = minimum 8 / group in

two independent experiments) were subcutaneously given Apo at a concentration of 10 mg/kg BW twice weekly for a period of 16 days in the Ab-transfer induced EBA model. In control group, 5% (v/v) DMSO in PBS 1X was given to the mice at the same route of administration and same timeframe as drug-treated group.

2.3.3.3 Auranofin

Auranofin ($C_{20}H_{34}AuO_9PS$, Au) is a gold compound which was developed in the 1980s as a potential anti-rheumatic agent [191]. More recently, its anti-proliferative and pro-apoptotic activities have been observed in a variety of human tumor-derived cell lines [192, 193]. Potential mechanisms of anti-neoplastic activity include modulation of secretion of tumor-promoting cytokines such as IL-6 and IL-8 by monocytes and macrophages [194], modulation of intracellular signaling and survival pathways such as Nuclear factor kappa-light-chain-enhancer of activated B cells (NF-κB), Signal transducer and activator of transcription 3 (STAT3) [192, 195] and intracellular generation of ROS [193]. Mice (n= minimum 8 / group in two independent experiments) intraperitoneally received either vehicle (5% (v/v) DMSO in 1X PBS) or Au at a concentration of 3 mg/kg BW twice daily for 16 successive days in the Ab-transfer induced EBA model.

2.3.3.4 Dobutamine

Dobutamine hydrochloride ($C_{18}H_{24}ClNO_3$, Dob) is a β1-receptor agonist that increases cardiac output. As such, it is used clinically in the treatment of acute heart failure [196]. In order to administer Dob to the mice (n = 5), they were subjected to a subcutaneous implantation of osmotic pumps (ALZET model 1002). Briefly, mice were undergone an incision on the back, slightly posterior to the scapula and a subcutaneous pocket was created and the pump containing Dob or vehicle (n= 5) was located towards the flank. Pumps were already filled with either vehicle (PBS 1X) or Dob at a concentration calculated to deliver 4 ng/min/g BW for up to 16 days. During the surgical intervention mice were anesthetized with a mixture of ketamine (100µg/g) and xylazine (15µg/g). The wound was closed with an interrupted suture using a skin closure thread (SERALON USP 3/0).

2.3.3.5 Methyprednisolone

Methylprednisolone (MP) is a synthetic corticosteroid- a chemical modification of a natural glucocorticosteroid, hydroxycortisone [197]. It has been demonstrated that MP hinders neutrophil activation, it hence barricades aAb-induced tissue damage in the experimental EBA [148]. Therefore, it was used here as a reference treatment. MP (dissolved in distilled water) was intraperitoneally applied to the mice on the daily basis at the concentration of 20 mg/kg BW for the entire duration of each experiment (16 days). Number of the mice in this group was different in each experiment from 5-10 mice. Since MP was served for comparison of the relative magnitude of the candidate drugs' effect on EBA, allocation of its specific vehicle group was not needed.

2.3.3.6 Niclosamide

Niclosamide ($C_{13}H_8Cl_2N_2O_4$, Nic) is an anti-helminthic drug with a series of recently reported activities such as antitumor [198, 199] and antiviral [200] activities. In addition, Nic can modulate dendritic cells' activation and function [201] and ameliorate joint inflammation in RA [202]. Mice (n = 5 / group) were intraperitoneally treated on the daily basis with vehicle (5% (v/v) DMSO, 15% (v/v) cremophore in water) or niclosamide at a concentration of 20 mg/kg BW for 16 consecutive days. In order to prepare the drug for injection, Nic was dissolved in 5% (v/v) DMSO followed by adding 15% (v/v) cremophore. Subsequently, the mixture was incubated at 37°C for 15 min for better dissolving. Ultimately, 80% (v/v) water was added to the mixture.

2.3.3.7 Tamoxifen

Tamoxifen ($C_{32}H_{37}NO_8$, Tam) is a well-established and approved drug widely used for the treatment of estrogen receptor-positive breast cancer. It is a selective estrogen receptor modulator (SERM) which exerts variable, context-dependent agonist and antagonist effects on estrogen receptor (ER)-expressing cells [203, 204]. Tam is also broadly utilized for the induction of genomic recombination in mice [205]. Tam, as one of the 6 candidate drugs, was used here for treatment of

the mice (n= minimum 8 mice / group in two independent experiments) at the concentration of 20 mg/kg BW twice a week for the entire duration of the experiment (16 days). Tam and corresponding vehicle (5% (v/v) DMSO in 1X PBS) were applied subcutaneously.

For *in vivo* validation of three compounds (Apo, Au and Tam), a single vehicle (5% (v/v) DMSO in 1X PBS) was used. In *in vivo* efficacy studies of the two most potent drugs (Apo and Tam) in ameliorating EBA symptoms, drug-specific vehicles were used i.e. 1X PBS was administered to control groups in Apo *in vivo* efficacy assay and control mice in Tam *in vivo* efficacy study received 5% (v/v) DMSO in 95% corn oil.

2.3.4 Specimen collection and processing

Blood was collected through a retro-orbital puncture while mice were under terminal anesthesia. After coagulation of the blood samples, sera were separated by centrifugation at 13,000×g for 20 min at 4°C. Following euthanizing the mice by cervical dislocation whilst they were anesthetized, tissue biopsies were harvested from ear and back skin. Left ears were snap frozen in liquid nitrogen whereas right ears were divided into two pieces; one was embedded in Tissue-Tek® optimum cutting temperature (O.C.T) medium and then frozen on dry ice, while the other piece was fixed in 4% histofix solution. Sera and frozen samples were thereafter stored at -80°C until further use.

2.3.5 Skin histopathology

In EBA, biopsies from lesional skin show variable findings depending on the stage of the disease development. The immune cell infiltration can be found around vessels, around hair follicles and in the interstitium [35, 40]. The infiltrate may be rich in neutrophils or mixed with variable numbers of eosinophils, monocytes and lymphocytes in the upper dermis. The current diagnostic gold standard is the DIF microscopy of a perilesional skin biopsy. Linear deposits of IgG, IgA and/or C3 are also seen along the BMZ in the skin specimens [33].

2.3.5.1 Hematoxylin & eosin (H&E) examination

Histopathology technique was used to verify the clinical phenotype of EBA in the mice. For histological analysis, fixed ears and lesional back skin specimens in 4% histofix solution were de-hydrated with a series of alcohol, cleared with xylene and ultimately embedded in paraffin. They were cut at 6 µm thickness, deparaffinized, rehydrated, stained with H&E and finally cover-slipped with xylene based mount medium [206]. This process was performed by Ms. R. Cames. All sections were visualized and images were captured using the BZ-9000E series Keyence microscope. Images have been taken at multiple magnifications that each contains important information for further investigations.

2.3.5.1.1 Inflammation quantification

To evaluate immune cell infiltration in the biopsied murine tissues, ImageJ, a license-free image analysis software (https://imagej.nih.gov/ij/), was used. In order to quantify infiltrated cells into the tissue, H&E stained sections were visualized under bright field illumination using Keyence microscope. Five fields per section were randomly chosen and 400× magnified images were captured. These images were then opened in ImageJ software and from toolbar, “Multi-point”  was selected. This button allows you to enumerate the cells you wish to count simply by clicking. Once counting was done “Analyze” menu was selected and then by clicking on “Measure”, a total number of the cells was appeared in the “Results” window. The results can be copied and pasted and/or saved as Excel sheet.

2.3.5.1.2 Epidermal thickness assessment

In the present study, epidermal thickening was another histologic feature that has been measured in murine H&E stained skin sections. Using bright field illumination, sections were visualized by Keyence microscope. Images were captured at 100× magnifications from whole section and the calibration scale was inserted to the images using Keyence analyzer software. Pictures consisting of calibration scale were opened in ImageJ software and “Straight line”  was

chosen from toolbar. A straight line was drawn on the scale bar (known distance), and in the “Analyze” menu, “Set Scale” was selected. In the opened dialog box, the distance in pixels would be automatically filled in based on the length of the line you already drew. In “Known Distance” the value of the corresponding scale bar was entered and in the “Unit of Length” the unit of the scale bar was inserted. “Global” was selected so that the calibration would be applied to all images for further measurements. Afterwards, in 5 fields of the image, epidermis was measured at the sites of splits and/or crusts using “Straight line”  in toolbar. After each assessment, “Analyze” and then “Measurement” were clicked. Ultimately, the values of all 5 lengths were shown in “Results” window and they exported to Excel sheet. This procedure was repeated for all images of an individual section and an average value was reported per section. For healthy sections 5 fields of the epidermis were randomly selected for measurement.

2.3.5.1.3 Split formation evaluation

Split formation, a histologic hallmark of EBA, was also examined in H&E stained skin sections in mice samples. In order to assess the sub-epidermal split present in the sections, they were analyzed by bright field illumination in Keyence microscope. Several 100× magnified images were taken to cover whole section and calibration scale bar was inserted to the pictures using Keyence analyzer software. Images were then opened in ImageJ software and setting the scale was performed as explained above (in 2.3.5.1.2 section). After setting the scale, by right clicking on “Straight line” from toolbar “Segmented or free-hand” button was chosen. This button enables you to create a straight, and segmented line along the dermis. By means of this option, entire dermis was measured and from “Analyze” menu and subsequently “Measurement”, the value of the complete dermis would be displayed in the “Results” window. The length of the splits was also assessed in the similar way, exported to the Excel sheet and finally percentage of the split formation was calculated by:

$$\% \text{ Split} = (\text{Split length} / \text{Entire dermis length}) * 100$$

2.3.5.2 IF microscopy; overlapped depositions of anti-COL7-IgG and C3

To detect tissue-bound anti-COL7-IgG and/or C3 at the DEJ, I established an IF microscopy technique which was performed on pre-lesional skin specimens. In principle, a fluorochrome-conjugated anti-IgG or anti-C3 antibodies were used to detect rabbit IgG or murine C3 depositions at the DEJ and the excitation of the linked fluorochrome enabled the visualization of the target protein by fluorescent microscopy. In detail, frozen 6 µm sections were cut using microtome from biopsied tissues by either Ms. A. Fischer or Ms. D. Scheppan. Sections were air-dried for 10 min at RT to prevent sections from falling off the slides during staining process. Sections were then fixed in ice-cold acetone (already stored at -20°C) for 10 min at 4°C, were air-dried and were washed 3 times for 5 min in TBS-T 1X (tris-buffered saline-Tween 20) wash buffer. The tissue was surrounded with a hydrophobic barrier using a barrier pen (Dako-pen). Non-specific binding of the primary antibody was blocked by incubating of the sections in the first blocking buffer, 5% goat serum in 1X PBS, for 1h at RT. After removing the excessive buffer, sections were immediately incubated with the second blocking buffer, 1% BSA in 1X PBS, for 1h at RT. Subsequently, primary antibody against murine C3 (C3b/iC3b/C3c) (diluted 1:50 in the second blocking buffer), and isotype control antibody (Rat anti-mouse IgG1) (diluted 1:250 in the second blocking buffer, tthis dilution gives the same concentration to the primary Ab) were applied to the sections for 1h at RT. After washing the slides 3 times each for 7 min in wash buffer, they were incubated for 1h at RT with secondary antibodies including Alexa Fluor 594-conjugated Goat anti-rat IgG and FITC-conjugated Donkey anti-rabbit IgG diluted in second blocking buffer at dilutions of 1:600 and 1:100, respectively. Slides were then washed with wash buffer 3 times each for 7 min and nuclei were counterstained with 4′,6-Diamidino-2-phenylindole dihydrochloride (DAPI) for 1min at RT diluted 1:1000 in dH_2O. After washing in wash buffer (3 times each for 1 min), slides were mounted with Fluoromount-G® and were incubated at 4°C overnight. This staining protocol led to exhibition of green and red signals that overlap to a yellow yield, and DAPI-stained nuclei which exhibit a bright blue fluorescence. Sections were visualized using Keyence microscope.

2.3.6 Enzyme-linked immunosorbent assay (ELISA)

2.3.6.1 Detection of circulating rabbit anti-mCOL7-vWFA2 IgG

In order to determine level of the rabbit anti-mCOL7-vWFA2 IgG in murine sera an ELISA was conducted. In detail, 96-well microtiter plates (Maxisorb) were coated with 250 ng of murine vWFA2 protein per well in 100µL of coating buffer. After 1-hour incubation at RT, wells were then washed with PBS-T for 3 times. Nonspecific binding was reduced by blocking plates with 1% BSA in PBS-T at RT for 1h. After 3X washing, plates were subsequently incubated with 100µL of mouse sera (dilutions of 1:400 and 1:800 in blocking buffer) and standards at RT for 1h. After 3X washing the wells with PBS-T, plates were incubated with 100 µL of detection antibody, HRP-conjugated goat anti-rabbit IgG (dilution of 1:2000 in blocking buffer) for 1h at RT. After washing step 3X, development was performed by adding 100 µL of Chromogen (TMB) Substrate solution. The reaction was terminated by adding 100µL of H_2SO_4 1M. The colorimetric measurements were performed at 450nm using a GloMax® Discover System microplate reader. All samples were tested in duplicates and from the mean OD value for each serum sample, the mean OD value of the blank was subtracted. A purified rabbit anti-mCOL7-vWFA2 IgG with a known concentration served as a standard sample to plot a standard curve. This protein was diluted in two-fold steps starting from 23 µg/mL. A four-parameter logistic (4-PL) standard curve was created to calculate the concentrations of rabbit anti-mCOL7-vWFA2 IgG in the sera samples using a Graph-Pad Prism software v7.

2.3.6.2 Detection of circulating murine anti-rabbit IgG

Serum levels of mouse anti-rabbit IgG were also determined by an ELISA established by me. In detail, 250 ng of purified total rabbit IgG in 100µL of coating buffer was added to 96-well microtiter plates (Maxisorb) and plates were incubated for 1h at RT, followed by a 3X-washing step. Afterward blocking (described above in 3.3.6.1) for 1h at RT and 3x washing step, the plates were incubated with mouse sera (dilutions of 1:400 and 1:800) and standard samples for 1h at RT. Following washing step 3X, 100 µL of detection antibody, HRP-conjugated goat

anti-mouse IgG (1:50,000 dilution), was applied to the wells. Wells were subsequently washed 3X and color was developed using 100µL of Chromogen (TMB) Substrate solution. The reaction was stopped by adding 100 µL of H_2SO_4 1M. The colorimetric measurements were implemented at 450nm using a GloMax® Discover System microplate reader. All samples were tested in duplicates and from the mean OD value for each serum sample, the mean OD value of the blank was subtracted. In order to prepare standard samples, serial two-fold dilutions of a mouse anti-rabbit IgG was used in sequential wells beginning from 15 µg/mL. To calculate the concentrations of murine anti-rabbit IgG in the sera samples a four parameter logistic (4PL) standard curve was plotted using a Graph-Pad Prism software v7.

2.4 Identification of a drug-associated gene expression signature

The identification of genes whose expressions are altered by a drug provides precise information about its molecular mechanisms. Here, transcriptome RNA-Seq analysis was served as a tool to comprehensively elucidate gene expression profile in murine skin after drug treatment compared with vehicle treated group. The workflow of operating procedures for gene expression profiling is illustrated in Figure 2.4.

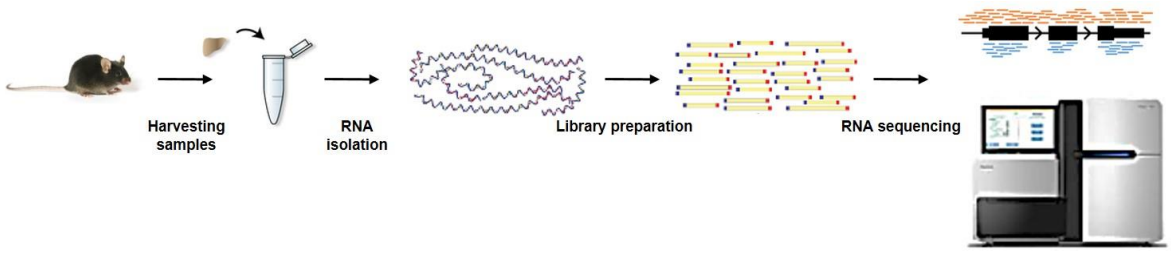

Figure 2. 4: Overview of the procedures to identify the drug-induced transcriptional alteration in drug-treated mice compared with the vehicle.
Total RNA was isolated from snap-frozen murine ear specimens. After evaluation of the RNA quality using Bioanalyzer (not shown), library was prepared and RNA-Seq was then performed on NextSeq® 500. Data processing and statistical analysis was conducted afterwards. (Figure adopted from [207-209])

2.4.1 RNA isolation

Total RNA was purified from snap-frozen murine skin samples using a QIAamp RNA Blood Mini Kit according to the manufacturer's instructions with minor modifications. The principle behind it, is mainly a silica-membrane-based purification of cellular RNA. Frozen tissues in liquid nitrogen were grinded to a fine powder by mortar and pestle. The powder under the liquid nitrogen was transferred into an RNase-free, liquid-nitrogen-cooled 1.5 mL micro-tube. Once, the liquid nitrogen was evaporated (but the tissue was not thawed), 500µL buffer RLT (lysis buffer) was added and lysate was pipetted directly into a QIAshredder spin column placed on a 2mL collection tube, and centrifuged at maximum speed (16,000×g) for 2min to homogenize the sample. Flow-through was used to proceed to next step and the QIAshredder spin column was discarded. 1 volume (500µL) of 70% ethanol was added to the cleared lysate and mixed well by pipetting. 500µL of the lysate was pipetted into a QIAamp spin column in a new 2 mL collection tube. Any precipitation in the lysate was taken as well. Tube was then centrifuged for 15s at 13,500×g. This step was successively repeated for the rest of the lysate. To wash the QIAamp spin column, it was transferred into a new 2 mL collection tube and 350µL buffer RW1 was pipetted into the QIAamp spin column. It was centrifuged for 15s at 13,500×g and the flow-though was discarded. Genomic DNA was completely removed using RNase-Free Dnase Set (Qiagen) and it was performed according to the manufacturer's instruction. In detail, 10µL DNase I stock solution was added to 70µL buffer RDD and the DNase I incubation mixture (80 µl) was added directly to the QIAamp spin column membrane, and placed on the benchtop at RT for 15min. 350 µl Buffer RW1 was then loaded on the QIAamp spin column and centrifuged for 15s at 13,500×g and flow-through was discarded. In order to wash QIAamp spin column, it was placed onto a new 2 ml collection tube and 500µL buffer RPE was pipetted into the column and centrifuged for 15s at 13,500×g and both the flow-through and collection tube were discarded. The QIAamp spin column was transferred into a new collection tube and 500 µl of buffer RPE was added. Tube was centrifuged for 3 min at 16,000×g and the collection tube with the flow-through was discarded. The QIAamp spin column was placed onto a new 2mL collection tube and was solely centrifuged for 1 min at 16,000×g. The QIAamp spin column was transferred into a 1.5 ml micro-

tube, and 35 µL of RNase-free water was directly pipetted onto the QIAamp membrane. It was incubated at RT for 5min and centrifuged for 1 min at 13,500×g to elute. Eluate was re-loaded on the spin column membrane and centrifuged for 1 min at 13,500×g. Three RNA aliquots have been made for RNA-Seq, RNA integrity evaluations, and RT-qPCR analyses and stored at -80°C for further use.

2.4.2 Assessment of RNA integrity

The evaluation of the RNA integrity in order to use intact RNA is a critical first step in obtaining meaningful gene expression data [210]. The process is based on an automated capillary-electrophoresis system which generates information on RNA concentration and allows a visual inspection of RNA integrity and creates ribosomal ratio which is considered as RNA integrity number (RIN) value. RIN is developed to remove individual interpretation in RNA quality control and it takes the entire electrophoretic trace into account. It enables to classify total RNA, based on a numbering system from 1 to 10, with 1 being the most degraded RNA and 10 being the most intact one (representative electropherogram in Figure 2.5) [210]. To determine RNA quality and quantity, here, Agilent RNA 6000 Nano Kit and Agilent 2100 Bioanalyzer system were used. The procedure was performed according to the manufacturer's manual. In brief, RNA chip consisting of gel-dye mix was firstly primed using chip priming station (supplied with Agilent 2100 Bioanalyzer system). Following adding 5µL of RNA marker and 1µL of ladder into the distinct wells on the chip, 1µL of RNA samples was added to the sample wells. Chip was vortexed for 1 min at 2,400rpm in the IKA vortexer (supplied with Agilent 2100 Bioanalyzer system). Chip was ultimately run in the Agilent 2100 Bioanalyzer system. When the chip run was finished, results can be exported as a PDF file. Results created by Bioanalyzer software are displayed as an electrophoregram and gel-like images with a RIN value for each sample (Figure 2.5).

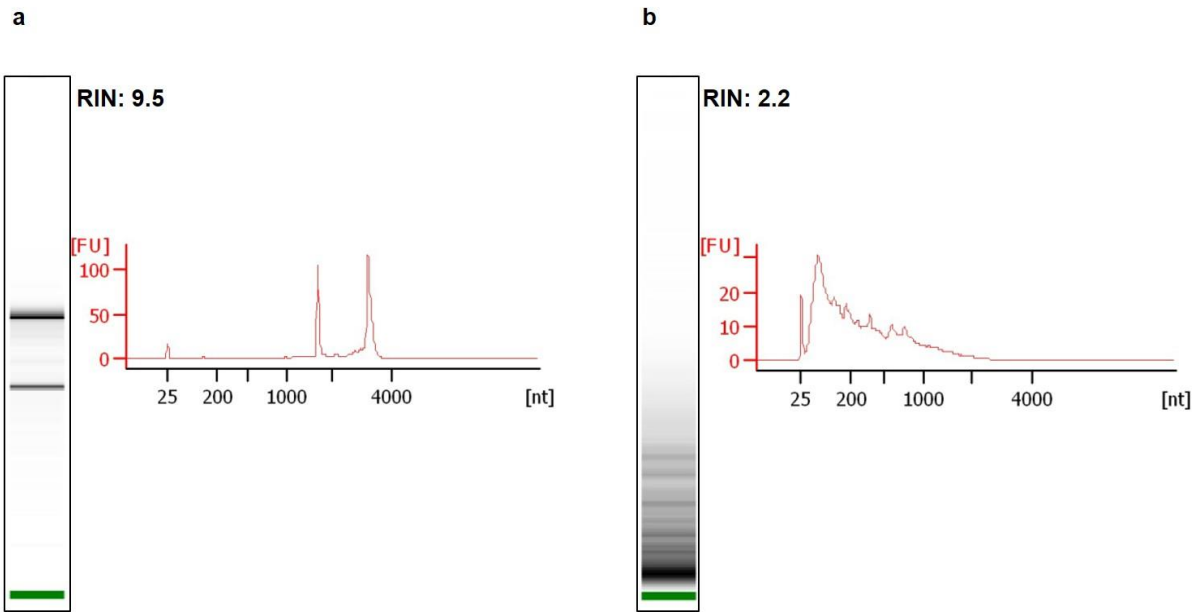

Figure 2. 5: Representative electropherograms and corresponding electrophoretic traces of 2 total RNA samples with RIN values of 9.5 and 2.2, respectively.
a) The most intact total RNA sample with the RIN value of 9.5 with the distinct 18S and 28S peaks. b) The RNA sample with RIN value of 2.2 is a degraded total RNA sample which is characterized by a decrease in the 18S to 28S ribosomal band ratio and an increase in the baseline signal.

2.4.3 RNA sequencing

Library preparation and RNS-Seq were implemented by Dr. S. Künzel at Max Planck Institute for Evolutionary Biology, Plön, Germany. The library preparation was performed using TruSeq® stranded mRNA library preparation kit. 1 µg of total RNA per sample was used for mRNA library preparation. During the first step, polyA containing mRNA molecules using oligo-dT attached magnetic beads were purified through 2 rounds. During the second elution of the polyA RNA, the RNA was fragmented and primed for cDNA synthesis. Subsequently, the cleaved RNA fragments which were already primed with random hexamers underwent reverse transcription and generated first strand cDNA. The addition of Actinomycin D to the first strand cDNA prevents spurious DNA-dependent synthesis. RNA template is then removed and is replaced with a strand that incorporates dUTP in place of dTTP to generate ds cDNA. The incorporation of dUTP quenches the second strand during amplification. Using AMPure XP magnetic beads the ds cDNA was separated from the second strand reaction mix. The result is blunt-ended cDNA. The cDNA was end-repaired, 3’-adenylated and unique indexing adaptors ligated

onto the fragments ends. The library was enriched using PCR. The quality of the prepared library and the size distribution were analyzed using DNA 7500 Kit on Agilent 2100 bioanalyzer. The sample content was quantified with Nano-Drop 2000c spectrophotometer and adjusted to 40 ng in 10 µL per sample to generate the clusters on the surface of a flow cell before sequencing. RNA-Seq was performed using NextSeq 500 High Output Kit, 150 cycles on NextSeq® 500 generating a 75 bp paired-end reads. Both basic and advanced analyses of the RNA-Seq data was performed by Dr. Y. Gupta and is briefly described: To analyze the original data generated by sequencer, data were converted from per-cycle BCL base call files to FASTQ files using bcl2fastq2 Conversion Software (Illumina, San Diego, USA). Following a quality control of raw data using FastQC, files were trimmed using Trimmomatic tool (q > 30) and high-quality reads (min read length 36 bp and Phred Score > 20) were retained for further downstream processing. The sequence was then aligned and mapped to the reference mouse genome (mm10), build GRCm38 v79 using Spliced Transcripts Alignment to a Reference (STAR) software [211]. Genomic coordinates for known mouse genes were downloaded as GTF file from Ensembl genome browser (https://www.ensembl.org/index.html). HTseq-count was used to quantify expression of each gene and it enabled us to count for each gene how many aligned reads overlap its own exon and to discard reads aligned to multiple positions or overlapping more than one gene. These counts were finally utilized for gene-level differential expression analysis using DESeq2 R package with a cut-off of adjusted *P* value <0.01 and -1 > $\log_2$fold change (FC) > 1. To identify if the DEGs are associated with a certain biological process or molecular function, the Gene ontology (GO) database (ftp://ftp.geneontology.org/go/www/GO.tools_by_type.database.shtml) was utilized. Kyoto Encyclopedia of Genes and Genomes (KEGG) database (https://www.genome.jp/kegg/kegg1.html) was also implemented for pathway detection [212, 213]. Fisher's exact statistical tests were used for calculation of *P*-values.

2.4.4 Complementary DNA (cDNA) synthesis

Total RNA was converted to cDNA using RevertAid™ First Strand cDNA Synthesis Kit, following the manufacturer's instruction. Forthcoming reagents were added to 500 ng of purified total RNA in a sterile, nuclease-free 200µL tube on ice on the indicated order:

- 1µL of oligo $(dT)_{18}$ primer
- nuclease-free water up to 12µL
- 4µL of 5X reaction buffer
- 1µL of Ribolock RNase inhibitor (20U/µL)
- 2µL of 10mM dNTP Mix
- 1µL of RevertAid M-MuLV RT (200U/µL)

The total volume of each reaction mixture would be 20µL. It was gently mixed and spun down. Reaction mixture was subsequently incubated for 60 min at 42°C and the reaction was terminated by heating at 70°C for 5 min in S1000TM Thermal Cycler. Minus reverse transcriptase (MRT) reaction was also performed as a control for Real-Time quantitative Polymerase Chain Reaction (RT-qPCR). MRT contains all components except for RevertAid M-MuLV RT. All reaction products were then stored at -20°C until future use.

2.4.5 Real-Time quantitative PCR (RT-qPCR)

Confirmation of the RNA-Seq data was examined using RT-qPCR. Primers for RT-qPCR reactions were designed using NCBI Primer BLAST (www.ncbi.nlm.nih.gov/tools/primer-blast/) and Gene Runner (http://www.generunner.net/). Primers were designed to span intron boundaries to avoid amplification of genomic DNA. In order to avoid designing primers with secondary structures such as hairpin loop and primer dimer, characteristics of the designed primers were checked using Gene Runner and OligoAnalyzer 3.1 (https://eu.idtdna.com/calc/analyzer). Primers (Table 2.1) were produced at and purchased from Biomers (Biomers.net GmbH, Ulm, Germany) at a concentration of 100µM. RT-qPCR reactions were conducted using SYBR™ Green PCR Master

Mix. The following 10 µL reaction mix was prepared in an individual well in an optical 96-well PCR plate on ice:

- 5µL of SYBR™ Green PCR Master Mix
- 0.5 µL of forward or reverse primers
- 1µL of cDNA
- 3µL of nuclease-free water

To optimize RT-qPCR assays a standard curve was generated using a 2-fold dilution of a cDNA template for each gene. The standard curves were constructed by plotting the log of the dilution factor against the C_T value obtained during amplification from each dilution. The r^2 value and the slope were calculated for calculation of slope amplification efficiency using (https://www.chem.agilent.com/store/biocalculators/calcSlopeEfficiency.jsp). Amplification efficiencies ranged between 80% and 111% for the genes of interest and reference genes (Table 2.2). All RT-qPCR reactions were performed in duplicate on an Eppendorf Mastercycler® ep realplex Real-Time PCR system (Eppendorf AG, Hamburg, Germany). A two-stage cycling protocol was performed comprising single cycle of 95°C for 10 min to activate AmpliTaq Gold® Polymerase, followed by 30 cycles of denaturation step at 95°C for 15s, annealing and extension steps of 60°C for 1min. To check for nonspecific product formation, melt curve was plotted. Melting rate was performed from 60°C to 95°C at 0.3°C/s. Four different housekeeping genes (HKGs) namely *Hprt* (hypoxanthine phosphoribosyl transferase) [214], *MLN51/Casc3* (cancer susceptibility candidate 3) [214], *Actb* (β-*actin*) [215], and *β2m* (β2-*microglobulin*) [216] were utilized as reference genes and $2^{-\Delta\Delta CT}$ method was used for data normalization [217].

Table 2. 1: List of 4 HKGs and top 8 differentially expressed genes (DEGs) selected for confirmation using RT-qPCR and their designed primers.

Gene name	Gene bank accession number	Forward primer (5'->3')	Reverse primer (5'->3')	Amplicon size (bp)
Prr7	NM_001030296.4	ACCCACACCATCACGCAC	AGCACCGCCTCCTCGTAG	127
Plaur	NM_011113.4	AGGCTTAGATGTGCTGGGAAAC	AGCAGGAGACAGAGACGTTGAG	122
Cyp4f18	NM_024444.2	ACACAGTCTTCTACCGTTTCC	TGGAAGGCAGGTGTCAGC	106
Ccdc88b	NM_001081291.1	TCTGGTGTGGAATGGGATG	TGAGGGAAGGGGTAAGGAAC	115
Mmp9	NM_013599.4	TCCCCAGAGCGTCATTCG	GAAACTCACACGCCAGAAG	124
S100a7a	NM_199422.1	TCTGCTCTTGGATAGTGTGC	TAGTCCTTCACCAGCTTGC	156
Lce3c	NM_033175.3	TCTTCAGCACAGCCTTCTTC	ACTTTGGAGAGGGACACTTG	118
Cebpd	NM_007679.4	AGGCAGGGTGGACAAGC	TGGTTGCTGTTGAAGAGGTC	189
Hprt (HKG)	NM_013556.2	TGATTAGCGATGATGAACCAGG	ACATCTCGAGCAAGTCTTTCAG	133
Casc3 (HKG)	NM_138660.2	AGCACTTGGATGACGATGAGG	AGCGACCCTCATCTTTCCATAG	150
Actb (HKG)	NM_007393.5	CTCCTAGCACCATGAAGATC	ACGCAGCTCAGTAACAGTC	189
β2m (HKG)	NM_009735.3	TGGTCTTTCTGGTGCTTGTC	AGTTCAGTATGTTCGGCTTCC	114

Table 2. 2: R^2, slope and efficiency values for optimization of RT-qPCR reactions for genes of interest.

Gene	R^2 Value	Slope value	Efficiency
Prr7	0.998	-3.469	96%
Plaur	0.986	-3.365	97%
Cyp4f18	0.964	-3.931	80%
Ccdc88b	0.993	-3.678	86%
Mmp9	0.995	-3.457	95%
S100a7a	0.977	-3.709	86%
Lce3c	0.999	-3.730	86%
Cebpd	0.973	-3.705	86%
Hprt (HKG)	0.995	-3.596	89%
Casc3 (HKG)	0.983	-3.074	111%
Actb (HKG)	0.998	-3.641	90%
β2m (HKG)	0.997	-3.786	83%

2.5 Statistical data analysis

GraphPad Prism v7 (GrapgPad Software, San Diego, CA, USA) was used for statistical analysis of the data. Values demonstrate mean ± standard error of the mean (SEM) and Shapiro-Wilk test was performed to examine normal distribution of data. For comparison of means and *P*-value determination of two groups, unpaired t test or Mann-Whitney-U test was used. For comparison of means and *P*-value determination of more groups, one-way analysis of variance (ANOVA) method or Kruskal Wallis test was conducted. A two-way ANOVA test was performed for comparison of means of two groups in a time frame with taking the treatment into account as independent variable. All tests were followed by Sidak's or Dunn's multiple comparison test and adjusted *P*-value<0.05 was considered statistically significant.

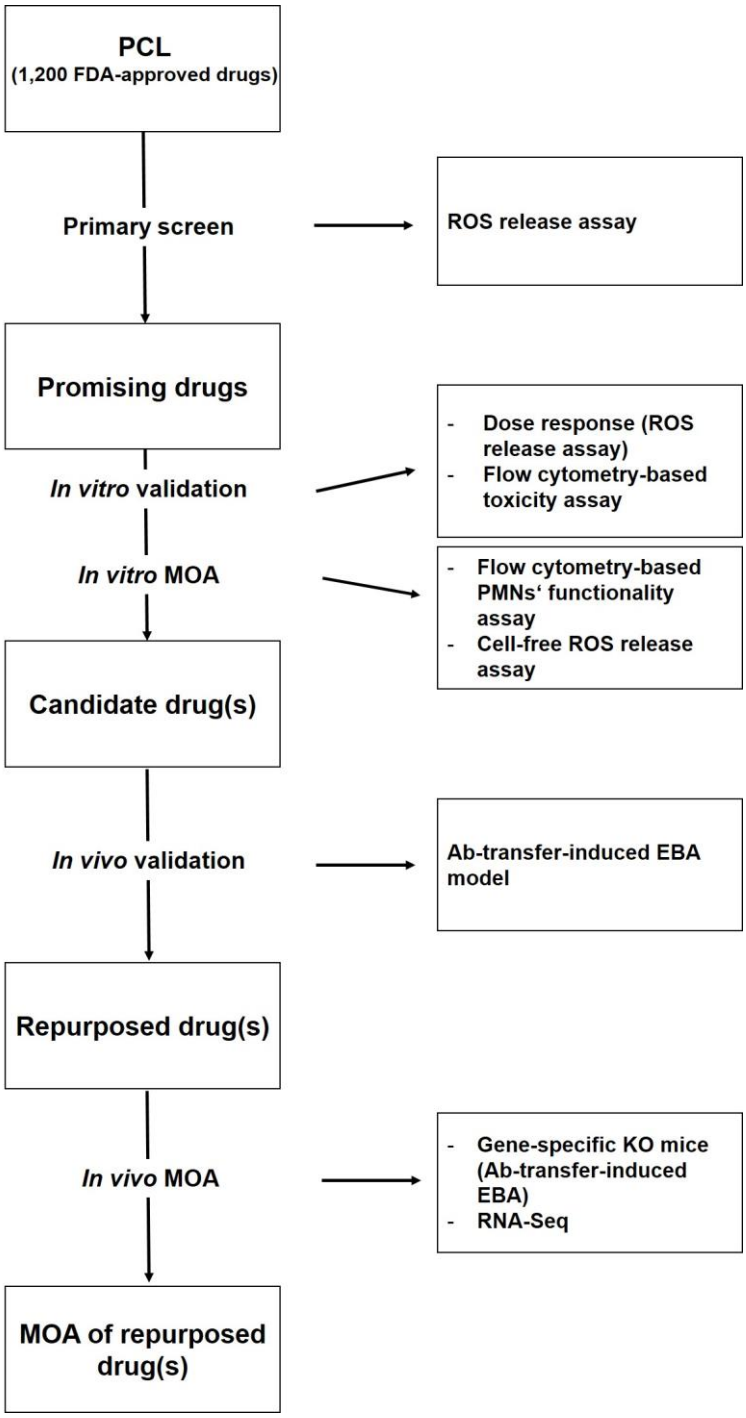

Figure 2. 6: A flowchart illustrating methodological approaches taken in my thesis.
Abbreviations: PCL; Prestwick chemical library, MOA; mechanism of action, KO; knockout, RNA-Seq; RNA-Sequencing.

3 Results

3.1 Primary screen

3.1.1 PMN-based screen identified 33 potential drugs (hits) for treatment of EBA

A cell-based approach for drug screening allows to determine impact of the compounds in complex biological systems rather than investigating the impact of the drugs on a single pathway. This allows to identify potential drug candidates without knowing the actual molecular target(s) and may provide a more disease relevant readout for screening [218]. Therefore, I here hypothesized that a disease-relevant cell (PMN)-based approach is a proper screening platform for identification of the potential drugs for treatment of EBA in the absence of any insights on molecular targets. ROS generation by iIC-activated primary human PMNs in the presence of either the drugs (n= 1,200 from PCL) or vehicle (1% DMSO) was evaluated using luminol-enhanced chemiluminescence assay. Screening platform was designed to assess PMNs' ROS production under the influence of these compounds at a concentration of 1 µM. The compounds that repressed ROS detection by more than 50% (mean from 4 independent experiments) of the vehicle were considered as potential inhibitors of iIC-induced PMN activation (Figure 3.1a, c). Amongst the 1,200 screened compounds 33 promising drugs (hits), 2.75% of screened drugs, (shown in green dots in figure 3.1b) were identified. Analysis of the therapeutic groups represented by the 33 promising drugs (hits) suggested a high degree of diversity in terms of therapeutic and biological activities. Anti-microbial agents (n=11, 33.3%) were the most represented drug class (Figure 3.1d).

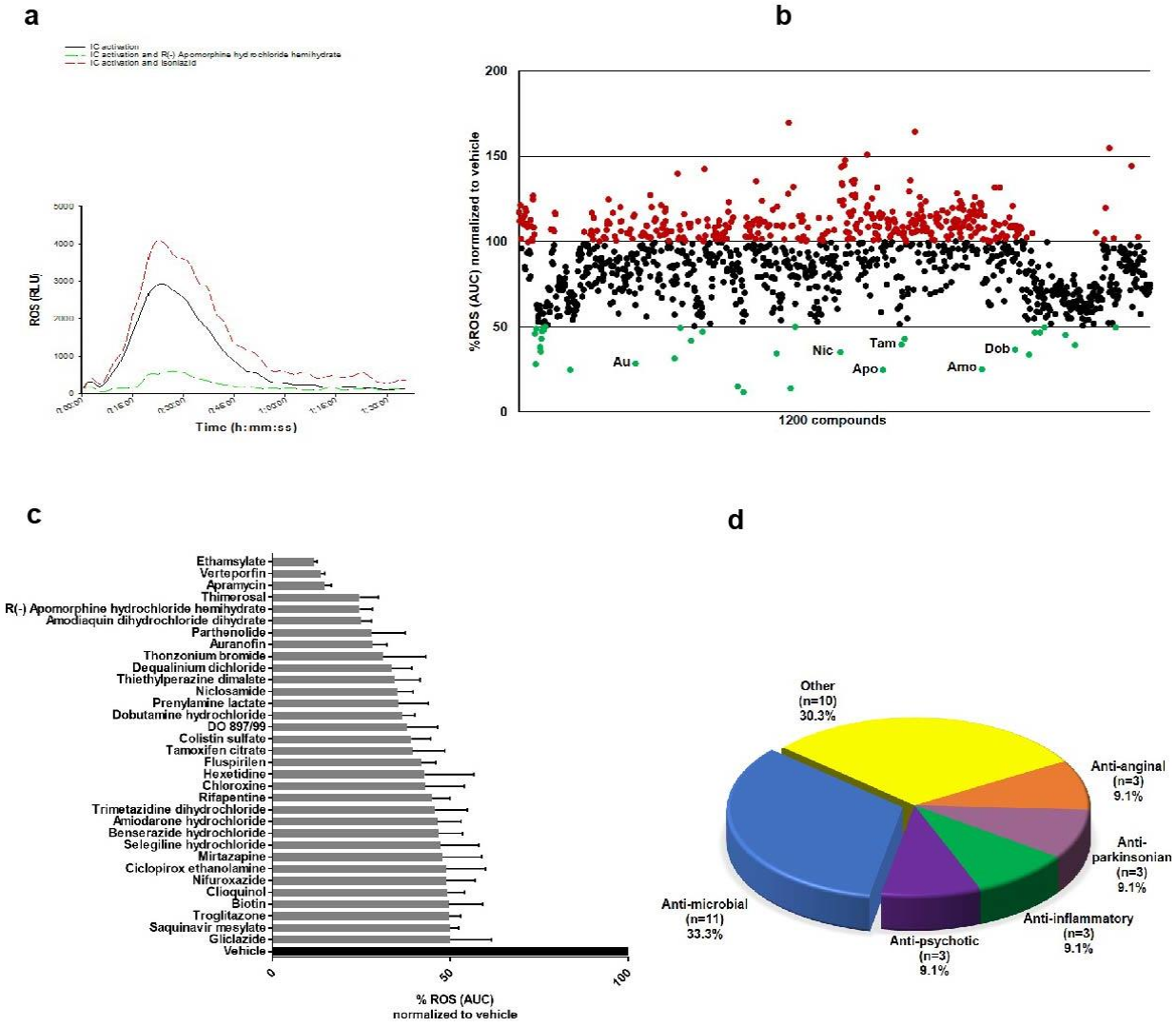

Figure 3. 1: Schematic summary of PMN-based screening.
a) Representative real-time kinetics of ROS production measured by luminol-enhanced chemiluminescence. Impact of the drugs was assessed through the addition of 1 µM of drugs to the iIC-activated primary human PMNs and ROS production was measured by luminol-enhanced chemiluminescence. Red dotted curve illustrates a PMNs' ROS enhancer (isoniazid) and green dotted curve displays a PMNs' ROS inhibitor (Apo) in comparison with vehicle treated PMNs, plotted as the solid black line. b) Scattergram for 1,200 screened compounds. Each dot represents one compound's value which is calculated as the AUC of total chemilluminescence normalized to vehicle-treated PMNs. Red dots demonstrate compounds that enhanced PMNs' ROS generation. Green dots depict the 33 effective drugs suppressing PMNs' ROS release by more than 50% of the vehicle-treated PMNs. 6 candidate drugs which were then identified as survivors of *in vitro* validation are designated. c) AUC values of the 33 promising drugs (hits) were incorporated over time (2 hours) and expressed as a percentage of the normalizer (vehicle-treated PMNs). The data are shown as mean ± SEM of 4 different PMN donors. d) Pie chart displays distribution of hits by drug class. It shows the number and proportion of the various therapeutic class amongst the 33 promising drugs. Anti-microbial agents with number of 11 (33.3%) were identified as the most abundant drugs. Anti-psychotic, anti-parkinsonism and anti-anginal agents each composed of 3 (9.1%) drugs. The category "Other" represents therapeutic groups containing ≤ 2 drugs.

3.2 *In vitro* validation

3.2.1 Six among the 33 promising drugs (hits) suppressed iIC-induced ROS by PMNs in a dose-dependent fashion

To take a closer look at *in vitro* efficacy of the 33 promising drugs (hits), each compound was tested in a dose response series in 10-fold dilutions at 4 different concentrations (ranging from 0.001 to 1 µM). The response readout was normalized using the vehicle-treated PMNs to provide the response measurement (% ROS release). Among the 33 promising drugs (hits), 6 compounds exhibited a dose-dependent response as well as a sustained effectiveness at the 1 µM concentration at which compounds were primarily screened. Figure 3.2 depicts representative dose-responses of the 6 candidate drugs which were then identified as candidate drugs through the *in vitro* validation.

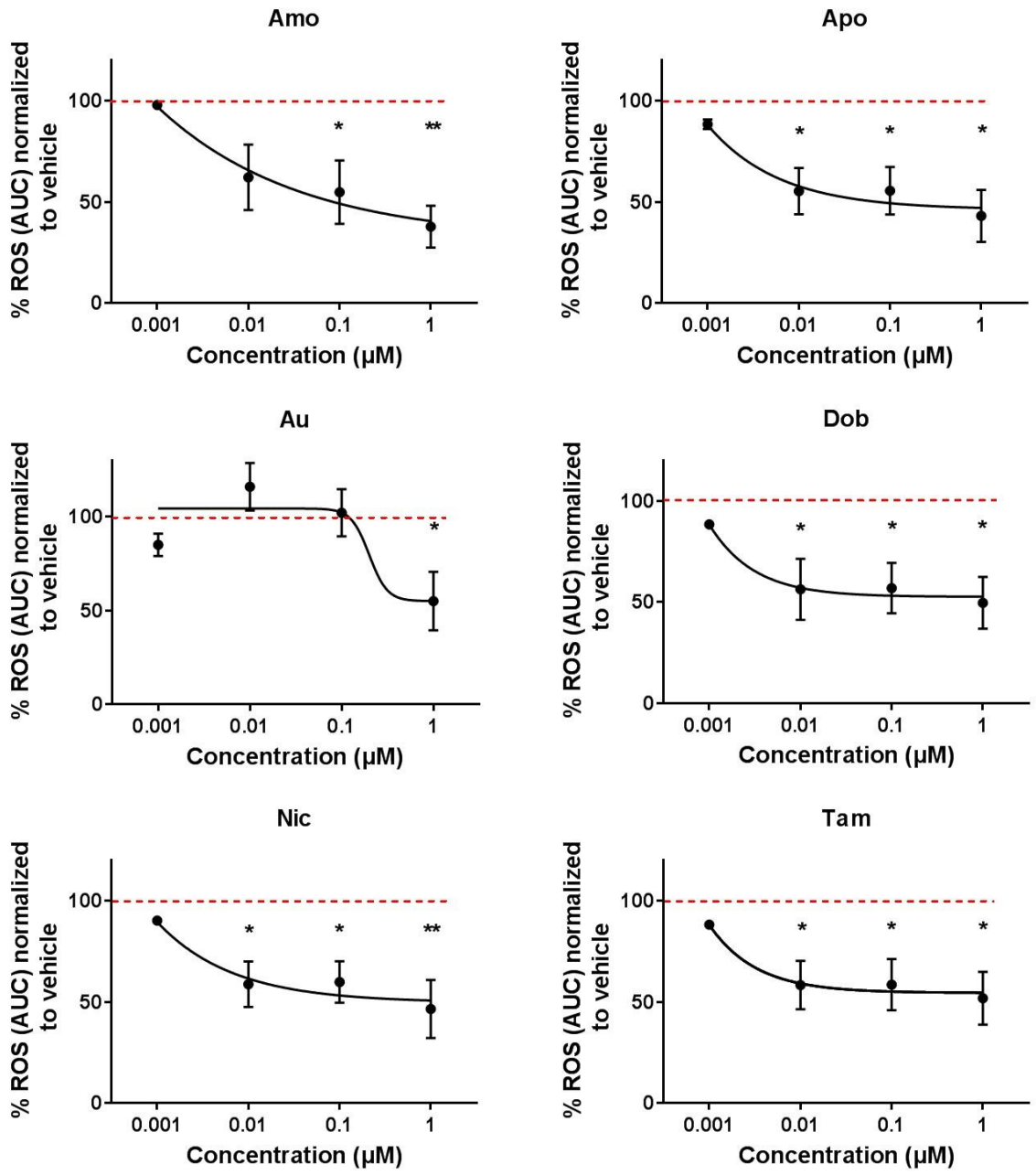

Figure 3. 2: Representative dose-response curves of the 6 candidate drugs show their efficacies as the dosage is increased.

Dose response curves were generated for the 33 hits exhibiting more than 50% reduction at ROS production from iIC-activated primary human PMNs. To perform it, PMNs were incubated with a series of 10-fold dilutions of the 33 drugs ranging from 0.001 µM to 1 µM and their ROS release was monitored. Of those 6 compounds showed dose response reduction at ROS production as well as maintained efficacy at 1 µM concentration. The data are mean ± SEM of 5 different PMN donors. AUC value of % ROS release by vehicle-treated PMNs is indicated by a red dashed line. One-way ANOVA test, Sidak's multiple comparisons test.

3.2.2 *In vitro* validation identified verteporfin as a toxic compound to primary human PMNs

In an effort to exclude drugs with cytotoxicity impacts on PMNs, the compounds were studied under the same conditions as of that for the primary screening. In other words, iIC-activated human PMNs were incubated with the compounds at the concentration of 1 µM for 2 hours. Verteporfin was found as the only toxic compound to human PMNs. This observation was in line with the previous findings that proposed verteporfin as a cytotoxic agent to inhibit proliferation of hepatocellular carcinoma cells and retinoblastoma cells. Verteporfin is an FDA-approved drug that is typically used for the treatment of age-related macular degeneration [219]. Figure 3.3 illustrates the flow cytometric analysis for the cytotoxicity effects of the 6 candidate drugs.

Taken together, through the *in vitro* validation study, 6 candidate drugs (Amo, Apo, Au, Dob, Nic and Tam) were revealed. These drugs repressed ROS release by iIC-stimulated PMNs in a dose-dependent manner. More importantly, they sustained their ROS modulatory activity at the concentration (1 µM) that was primarily used for screening. Moreover, they did not affect PMNs viability.

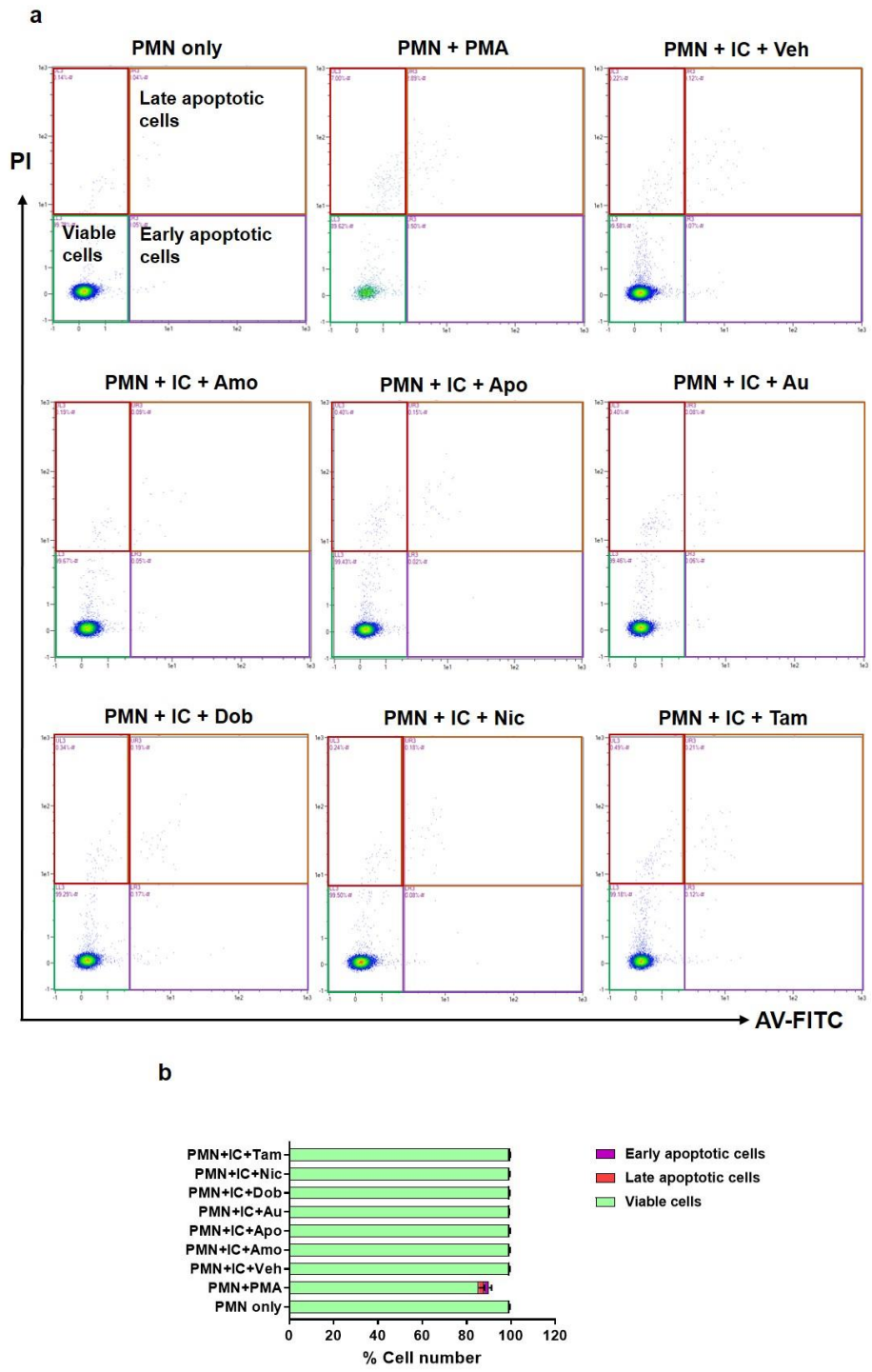

Figure 3. 3: Representative flow cytometry-based cytotoxicity results of the 6 candidate drugs.

Following incubation of human PMNs with the 33 hits (1 µM) for 2 hours, they were stained with FITC-conjugated AV and PI. a) Representative demonstration of flow cytometric plots of AV and PI in iIC-stimulated human PMNs in the presence of 6 candidate drugs. b) The number of double negative cells (viable cells) were calculated and normalized against vehicle-treated PMNs. Data are represented as mean ± SEM of 3 different donors. One-way ANOVA test, Sidak's multiple comparisons test. UV-killed cells were used as a positive control to conduct a proper flow-cytometric setting (data not shown).

3.3 *In vitro* mechanism of action (MOA)

3.3.1 No impact of the 6 candidate drugs on CD62L expression on iIC-activated human PMN

In order to assess whether the 6 candidate drugs affect other PMNs' activation phenotype such as expression of CD62L (an L-selectin involved in PMNs' rolling), the expression level of this cell surface marker was evaluated using a flow-cytometric analysis. Since upon activation, PMNs shed CD62L [178], its expression level was evaluated as PMN activation marker in human PMNs in the presence of either 6 candidate drugs or vehicle. Following 2-hour incubation of the iIC-activated primary human PMNs with the drugs at a concentration of 1 µM, they were stained with APC- conjugated anti-CD15 (a PMN marker), FITC-conjugated anti-CD66b antibodies (a PMN marker) and PE-conjugated anti-CD62L (PMN activation marker). The $CD66b^{pos}CD62L^{neg}$ cells and $CD66b^{pos}CD62L^{pos}$ cells were considered as activated and resting PMNs, respectively. Figure 3.4 illustrates that none of the 6 drugs exert significant effects on PMNs' activation state. The relative expression levels of the target proteins (CD66b and CD62L) were normalized against the vehicle-treated control sample.

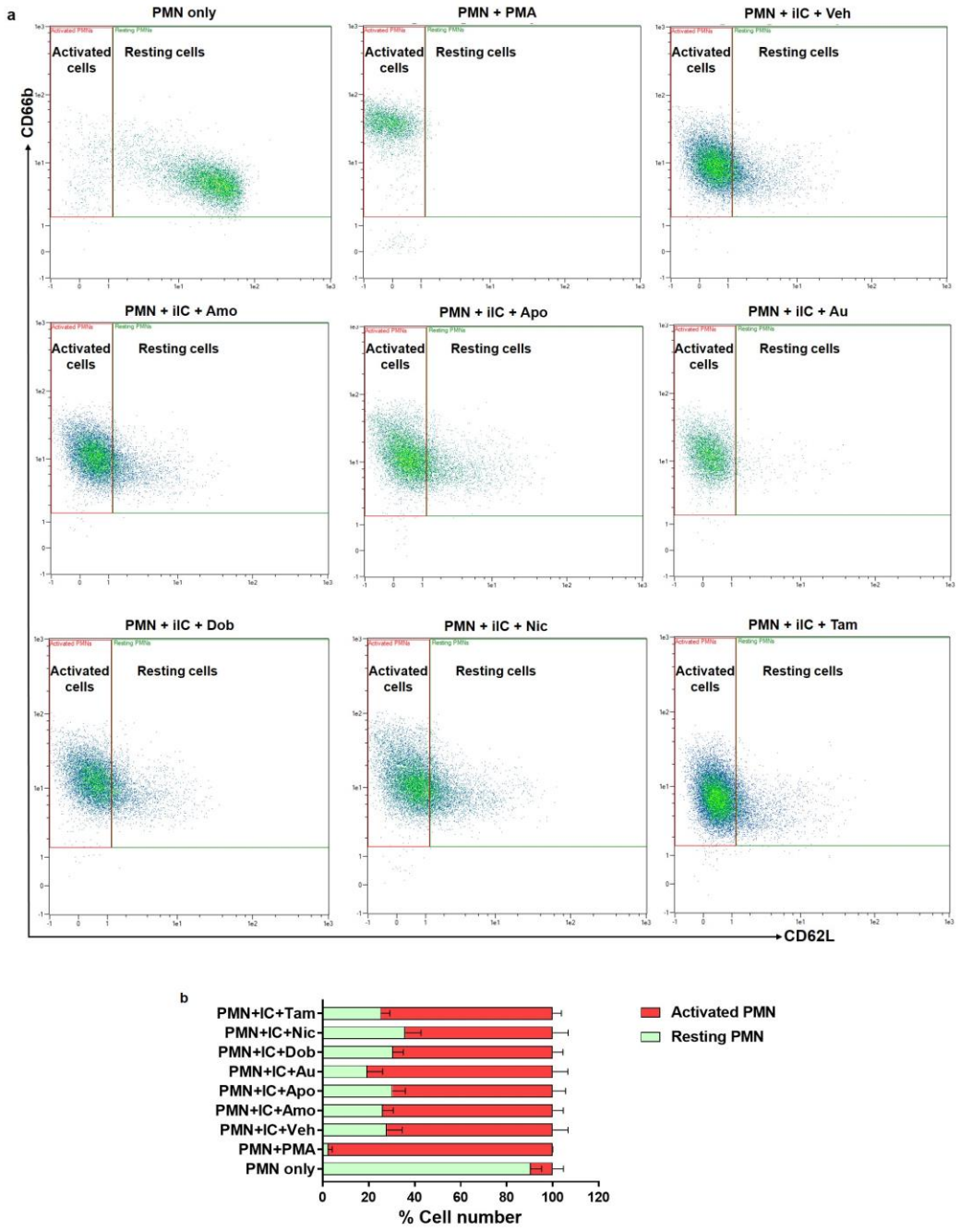

Figure 3. 4: Six candidate drugs demonstrated no influence on primary human PMNs' activation status.

a) Representative demonstration of flow cytometric plots of CD66b and CD62L expressions on iIC-stimulated human PMNs. Expression level of CD62L did not significantly change on PMNs incubated with the 6 candidate drugs compared with vehicle (1% DMSO). PMA was utilized as a positive control for PMN stimulation and PMN only means PMNs without any stimulations. b) To evaluate the relative expression level, the individual protein (CD62L and CD66b) values were normalized against value of the vehicle-treated control. CD62L and CD66b double positive cells and $CD66b^{pos}CD62L^{neg}$ cells were considered as resting and activated PMNs, respectively. One-way ANOVA test, Dunn's multiple comparisons test. Data are represented as mean ±SEM from 3 different donors.

3.3.2 Four compounds exhibited ROS scavenging capabilities

For understanding the casual mechanisms leading to the reduction of ROS generation by the 6 candidate drugs, an acellular ROS release assay was performed. This is an enzymatic model mimicking the oxidative burst of activated neutrophils [175]. Of the 6 candidate drugs, four had a ROS scavenging activity namely Amo, Apo, Dob, and Nic. Figure 3.5 depicts results of the cell-free ROS release assay for the 6 candidate drugs. *N*-acetyl-L-cysteine (NAC), an agent with a known anti-oxidant activity, was used here as a positive control at a concentration of 10 mM [176]. Amo was the only compound amongst the candidate drugs with the potent ROS scavenging ability since it reduced ROS generation at all tested doses. Apo and Dob demonstrated anti-oxidant activity at their highest dose (1 µM), while Nic decreased ROS release at the concentrations of 1µM and 0.1µM.

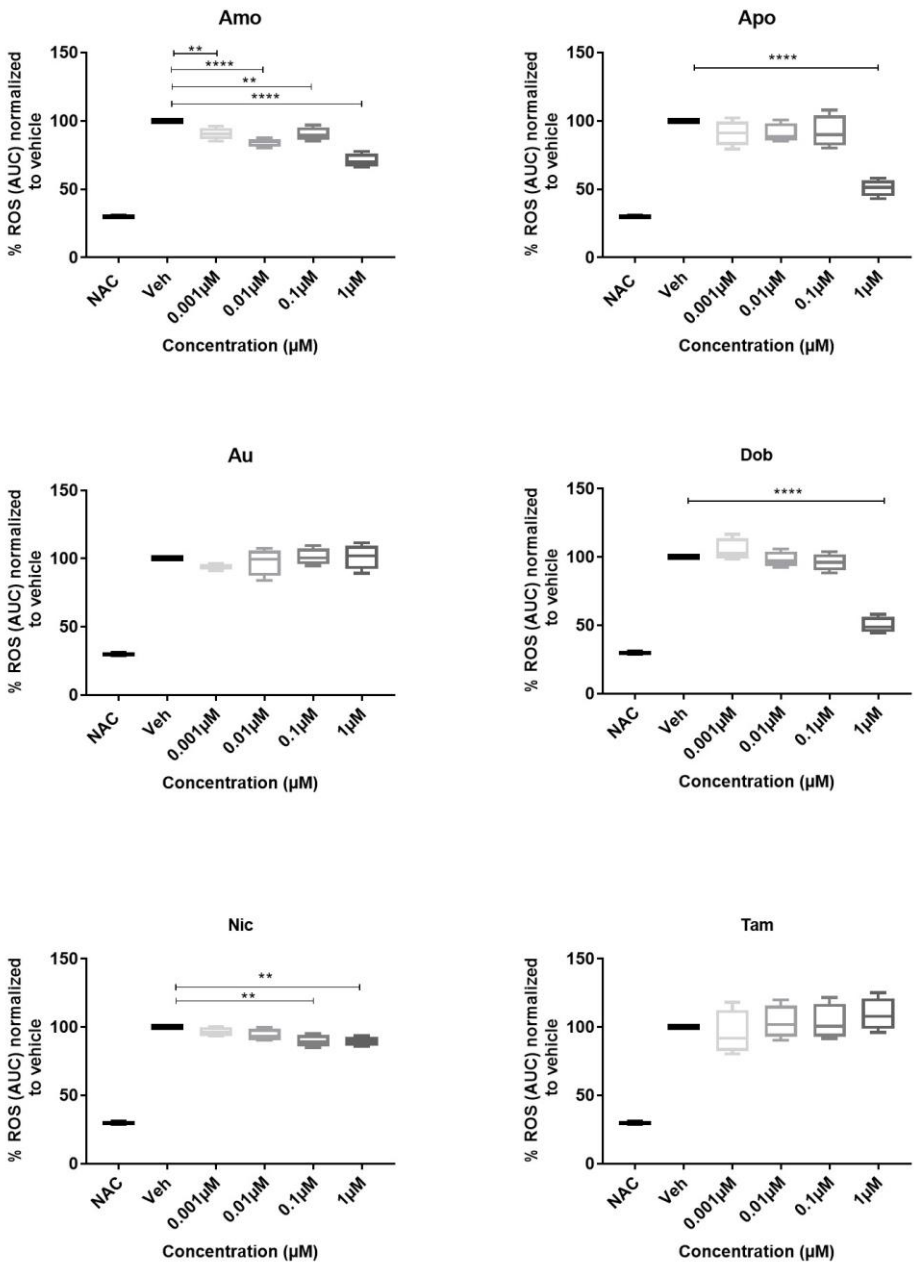

Figure 3. 5: Results of the cell-free ROS release assay for the 6 candidate drugs.
Using an enzymatic model simulating the oxidative burst of neutrophils, antioxidant activities of the 6 candidate drugs were tested. Among them, 4 compounds significantly scavenged ROS compared with vehicle (1% DMSO). Evidently, Amo at all concentrations (1, 0.1, 0.01, 0.001 µM) depicted a significant ROS scavenging capability compared with vehicle. Whereas Apo and Dob scavenged ROS only at the highest concentration and Nic demonstrated ROS scavenging capability at the concentrations of 1 µM and 0.1µM. 10mM of NAC was utilized as a positive control which is an artificial ROS scavenger. Data are illustrated as mean ± SEM from 4 replicates. One way ANOVA, Dunn's multiple comparisons test.

Collectively, *in vitro* studies (primary screen, *in vitro* validation and *in vitro* MOA studies) revealed six candidate drugs namely Amo, Apo, Au, Dob, Nic, and Tam. These drugs repressed ROS generation from iIC-activated PMNs by more than 50% in a dose-dependent manner and they did not have any impact on PMNs' viability and function. As release of ROS is a key driver of inflammation in EBA [130], it was hypothesized that ROS modulatory activity of candidate drugs may contribute to a potential ameliorative effect *in vivo*. Therefore, they were selected for further *in vivo* validation studies.

Table 3. 1: An overview of *in vitro* validation of the 33 promising drugs.
Data are shown as mean ± SEM relative to the vehicle control treatment. Asterisks mark the 6 candidate drugs chosen for further *in vivo* validation.

Compound	Therapeutic field	% ROS release	Dose response	% acellular ROS release	% Viability
Amiodarone hydrochloride	Anti-anginal	46.32 ± 6.77	No	92.57 ± 0.27	100.1 ± 2.4
Amo*	Anti-inflammatory	24.92 ± 2.89	Yes	71 ± 2.4	99.1 ± 0.2
Apramycin	Anti-microbial	14.71 ± 1.75	No	93.62 ± 1.38	101.6 ± 1.3
Au*	Anti-inflammatory	28.21 ± 3.96	Yes	101 ± 4.6	98.85 ± 0.2
Benserazide hydrochloride	Anti-parkinsonian	46.76 ± 6.78	No	8.06 ± 0.45	100.4 ± 1.3
Biotin	Vitamin	49.54 ± 9.58	No	96.46 ± 5.60	103.9 ± 1.7
Chloroxine	Anti-microbial	42.87 ± 11.1	No	77.52 ± 0.94	106.8 ± 8.5
Ciclopirox ethanolamine	Anti-microbial	48.84 ± 11.1	No	93.5 ± 2.03	100.8 ± 2.6
Clioquinol	Anti-microbial	49.16 ± 4.87	No	67.13 ± 2.78	100.0 ± 1.6
Colistin sulfate	Anti-microbial	39.09 ± 5.41	Yes	94.6 ± 2.40	102.7 ± 1.8
Dequalinium dichloride	Anti-microbial	33.62 ± 5.57	No	90.55 ± 4.21	98.6 ± 2.3
DO 897/99	Anti-psychotic	37.77 ± 8.67	No	74.8 ± 1.74	100.6 ± 2.6
Dob*	Analeptic	36.47 ± 3.56	Yes	50 ± 3.0	98.8 ± 0.5
Ethamsylate	Anti-platelet	11.57 ± 0.96	No	28.7 ± 0.86	98.9 ± 1.8
Fluspirilen	Anti-psychotic	41.77 ± 4.09	No	99.42 ± 1.08	94.6 ± 2.2
Gliclazide	Anti-coagulant	49.99 ± 11.6	No	92.2 ± 2.34	102.1 ± 1.5
Hexetidine	Anti-microbial	42.77 ± 13.8	No	94.7 ± 0.32	101.2 ± 3.6
Mirtazapine	Anti-psychotic	47.84 ± 11.0	No	102.8 ± 5.72	99.7 ± 1.9
Nic*	Anti-microbial	35.00 ± 4.50	Yes	90.0 ± 1.6	98.84 ± 0.4
Nifuroxazide	Anti-microbial	48.99 ± 7.95	No	75.8 ± 6.26	99.9 ± 4.1
Parthenolide	Anti-inflammatory	27.89 ± 9.39	No	107 ± 2.31	101.3 ± 2.2
Prenylamine lactate	Anti-anginal	35.30 ± 8.50	No	97.02 ± 2.98	102.5 ± 1.5
Apo*	Anti-parkinsonism	24.49 ± 3.64	Yes	51.0 ± 3.1	98.9 ± 0.2
Rifapentine	Anti-microbial	44.86 ± 5.07	No	20.66 ± 1.60	102.7 ± 2.0
Saquinavir mesylate	Anti-microbial	49.91 ± 2.54	No	96.53 ± 1.29	97.9 ± 5.0
Selegiline hydrochloride	Anti-parkinsonian	47.19 ± 10.8	No	92.07 ± 1.57	103.9 ± 1.6
Tam*	Anti-neoplastic	39.25 ± 9.20	Yes	109.2 ± 6	99.1 ± 0.2
Thiethylperazine dimalate	Anti-emetic	34.25 ± 7.24	No	103.3 ± 4.07	104.2 ± 1.9
Thimerosal	Anti-septic	24.48 ± 5.24	No	74.54 ± 1.35	105.1 ± 1.9
Thonzonium bromide	Anti-septic	31.09 ± 12.0	No	99.24 ± 1.48	96.4 ± 2.2
Trimetazidine dihydrochloride	Anti-anginal	45.79 ± 8.97	No	98.44 ± 6.77	101.8 ± 1.8
Troglitazone	Anti-diabetic	49.65 ± 3.29	No	46.15 ± 3.51	104.3 ± 2.0
Verteporfin	Photosensitizer	13.58 ± 1.08	Yes	71.51 ± 2.86	21.9 ± 1.7

3.4 *In vivo* validation and mode of action

To validate the *in vivo* efficacy of the 6 candidate drugs, the Ab-transfer induced model of EBA was chosen for the following reasons. (i) This model finely represents the effector phase of EBA pathogenesis in which Fc-dependent PMN activation is the main contributor to induction of inflammation and blister formation [130, 131]. (ii) It is a phenotypically well-characterized model providing the opportunity to nicely study the influence of the therapeutics on the effector phase of EBA as the clinical symptoms are visible within days after the IgG transfer [98]. (iii) Likewise, this model is a proper replication of the clinical conditions [87]. Aside from providing a model to investigate the underlying molecular and cellular mechanisms of the blister formation, it offers a platform to examine the prophylactic effects of several therapeutic options. In addition, using this model, interrogation of the novel drugs' efficacy on treatment of EBA is straightforwardly feasible as the readout can be obtained in several days compared with 10-14 weeks in immunization-induced model [153]. Furthermore, several studies demonstrated that the compounds which were effective in inhibition of ROS release assay were successfully validated in Ab-transfer-induced EBA [134, 146, 148].

Mice here were treated in a prophylactic approach with the 6 candidate drugs (Amo, Au, Apo, Dob, Nic, and Tam) as previously described (2.3.3). Mice were clinically investigated on each scoring day (days 4, 8, 12, 16) and the disease severity, expressed as percentage of the affected body surface area (ABSA), was documented. It is already shown that EBA mice lose body weight or fail to gain weight as a functional relevance of anti-COL7 Abs causing tissue damage in gastrointestinal tract [220]. Due to this fact, body weight was also measured on the scoring days. Recent data demonstrated a xenogeneic immune reaction to rabbit anti-mouse COL7 IgG that may contribute to IC-driven inflammation and tissue damage in this model [221]. As a consequence, serum levels of the circulating rabbit anti-mCOL7 and mouse anti-rabbit IgGs were evaluated. Dermal infiltration of the immune cells, epidermal thickness, and percentage of split (%split) formation were also determined in the H&E-stained skin sections of the mice. Treatment of mice with Dob or Nic did not exert any effect on manifestations of the

experimental EBA at any time points of the observation. While mice on Au treatment showed disease reduction only on day 12 of the experiment. Three out of the 6 candidate drugs (Amo, Apo and Tam) significantly alleviated clinical signs of the disease in the experimental EBA compared with vehicle on day 16 of the observation. The results of 4 treatment groups (Amo, Apo, Au and Tam) are in detail reported below. Of note, the primary efficacy endpoint of the *in vivo* validation study is the magnitude of disease (%ABSA) on the latest time point (day 16) of the experiment.

3.4.1 Amo diminished the clinical and histological symptoms in Ab-transfer induced EBA

Mice received 50 mg/kg BW [222] i.p. injection of either Amo or vehicle (distilled water) on a daily basis. Mice treated with Amo, developed significantly less blistering disease (Figure 3.6a and c). On day 16, mean value of the disease severity of the mice treated with Amo was 7.4 ± 1.9 while mice treated with vehicle had a disease severity with a mean value of 13.45 ± 2.8 ($p=0.0068$, Two-way ANOVA, Sidak multiple comparison test). Mice on Amo treatment almost maintained their weight during the 16 days. They did not generally demonstrate significant difference in relative body weight loss compared with vehicle-treated mice except for day 4 (Figure 3.6b). Assessment of the skin histological alterations revealed a significant reduction in the epidermal thickness in mice treated with Amo (57.73 µm ± 9.03) compared with vehicle-treatment group (91.57µm ± 3.66; Figure 3.7a and b). Moreover, Amo-treated mice demonstrated significantly decreased leukocyte infiltration at the dermis (163.2 ± 13.03) in comparison with vehicle-treated mice (255.4 ± 23.82; Figure 3.7a and c). In contrast, no significant changes were observed in Amo-treated mice compared with vehicle-treated mice in terms of split formation (Figure 3.7a and d). Consistent with the observation in experimental EBA, murine complement C3 and rabbit IgG depositions were detected at the DEJ in the skin sections of both mice treated with the drug and the vehicle demonstrating proper induction of the disease in both groups (Figure 3.6c). Evaluation of the serum levels of murine anti-rabbit IgG showed no significant difference between Amo-treated group and vehicle-treated mice (Figure 3.7f).

Similarly, no significant difference was observed in the amount of rabbit anti-mouse IgG levels in sera of the mice in both groups (Figure 3.7e).

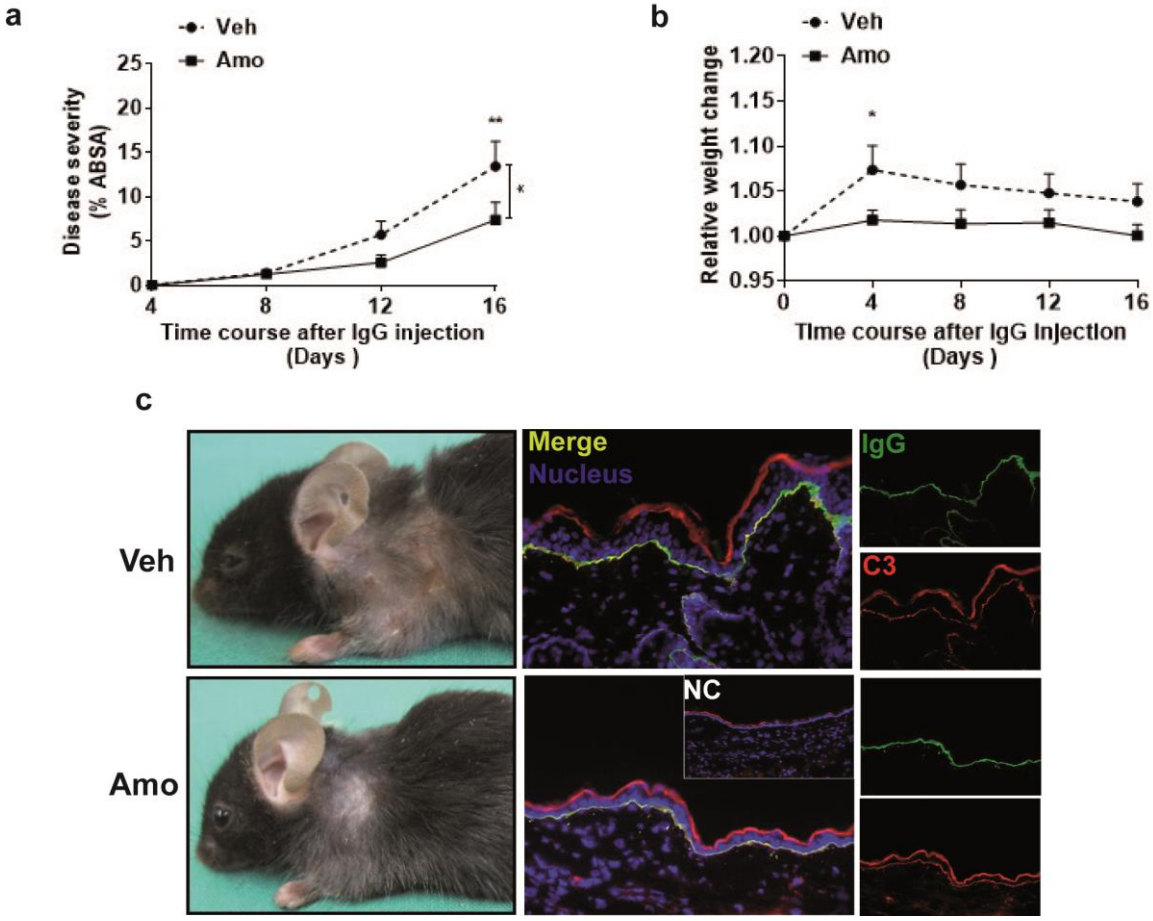

Figure 3. 6: Amo hindered clinical disease progression in Ab-transfer induced EBA. Injection of mice with 3.5 mg/20 g BW of rabbit anti-mCOL7 total IgG was performed at days 0, 2, 4, 6, 8, and 10. One day prior to the total immune IgG injection, mice were treated either with Amo or the corresponding vehicle (distilled water). %ABSA was recorded 4, 8, 12, and 16 days after the first injection of anti-mCOL7 IgG. a) %ABSA was decreased in Amo-treated mice. b) Body weight loss was not significant compared with control group throughout the observation except for day 4. c) Clinical pictures of mice at day 16 after injection of rabbit anti-mCOL7 IgG showed a reduced clinical disease severity in mice treated with Amo compared with vehicle. Immunofluorescence staining of deposited rabbit anti-mCOL7 IgG (green) and murine C3 (red) yields to a yellow signal (merge). No difference was observed in IgG and C3-deposition at the DEJ between mice receiving Amo and control. Two-way ANOVA, Sidak multiple comparison test, (*$p < 0.05$, **$p < 0.01$), mean (± SEM), n=minimum of 5 mice per group. NC: negative control section is stained in the absence of anti-rabbit IgG and in the presence of the corresponding isotype control of rat anti-mouse IgG1. Veh; vehicle.

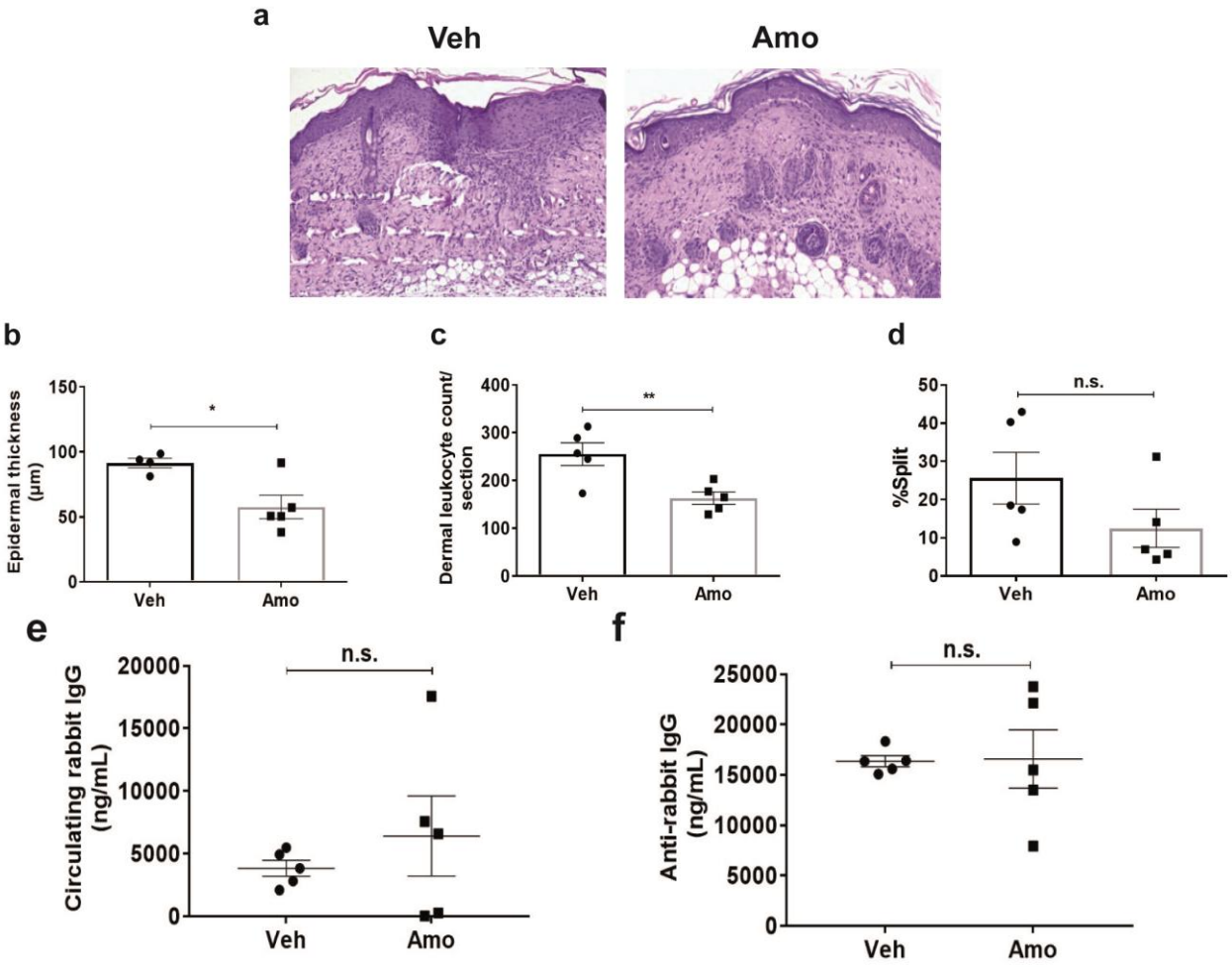

Figure 3. 7: Amo reduced histological disease in Ab-transfer-induced EBA.
a) H&E stained sections of back skin show b) decreased epidermal thickness and c) reduced inflammation in drug-treated mice in comparison with vehicle. Whereas, d) no significant change was seen in split formation between the 2 groups. e and f) Similar levels of rabbit anti-mouse and murine anti-rabbit IgGs in sera of Amo-treated and Vehicle-treated mice were detected. Unpaired t test or Mann-Whitney-U test, (*$p < 0.05$, **$p < 0.01$), mean (± SEM), n= minimum of 5 mice per group. n.s.; not significant, Veh; vehicle.

3.4.2 Au treatment ameliorated disease activity in experimental EBA at day 12

Remark: Please note that in sections 3.4.2, 3.4.3 and 3.4.4 the same vehicle (5% (v/v) DMSO in 1X PBS) was used as a solvent for Au, Apo and Tam. These 3 drugs were tested in 2 independent experiments. In sections, 3.4.3.1, 3.4.4.1 and 3.4.4.2 in which Apo and Tam were tested for further validation, the drug specific vehicles were used, i.e, 1X PBS and 5% (v/v) DMSO in 95% corn oil were served as Apo's vehicle and Tam's vehicle, respectively.

Treatment of the mice with Au began one day before injection of the rabbit anti-mCOL7 total IgG and continued for 16 days. Au was administered at a concentration of 3 mg/kg BW twice daily [223] by an i.p. injection. Score of the disease severity was recorded at days 4, 8, 12, and 16 of the experiment and the experiment was terminated on day 16. There was a disease reduction tendency in Au-treated group in comparison with vehicle group with a significant impairment at day 12. Mean value of the disease severity of the mice in Au-treatment group at day 12 was 4.96 ± 1.26 compared with vehicle group with a mean of 7.6 ±1.26 ($p= 0.018$, Two-way ANOVA, Sidak multiple comparison test; Figure 3.8a). Interestingly, histological examination of the skin obtained on day 16 from Au-treated mice demonstrated a significant reduction in both the dermal leukocyte infiltration and the sub-epidermal blistering in comparison with vehicle-treated mice, although no significant difference in clinical disease was observed on that day between the 2 groups (Figure 3.9a, c and d). In contrast, no significant difference was observed in epidermal thickness in the skin of the mice treated with Au compared with vehicle (Figure 3.9a and b). Body weight of the mice on Au treatment did not dramatically change compared with their initial weight. However, in vehicle treatment group, animals started a significant weight loss from day 8 compared with drug treatment group (Figure 3.8b). Serum concentrations of the mouse anti-rabbit and rabbit anti-mCOL7 IgGs did not significantly change between drug-treated mice and vehicle (Figure 3.9e and f). IgG and C3 deposition along the DEJ were identical in both groups (Figure 3.8c).

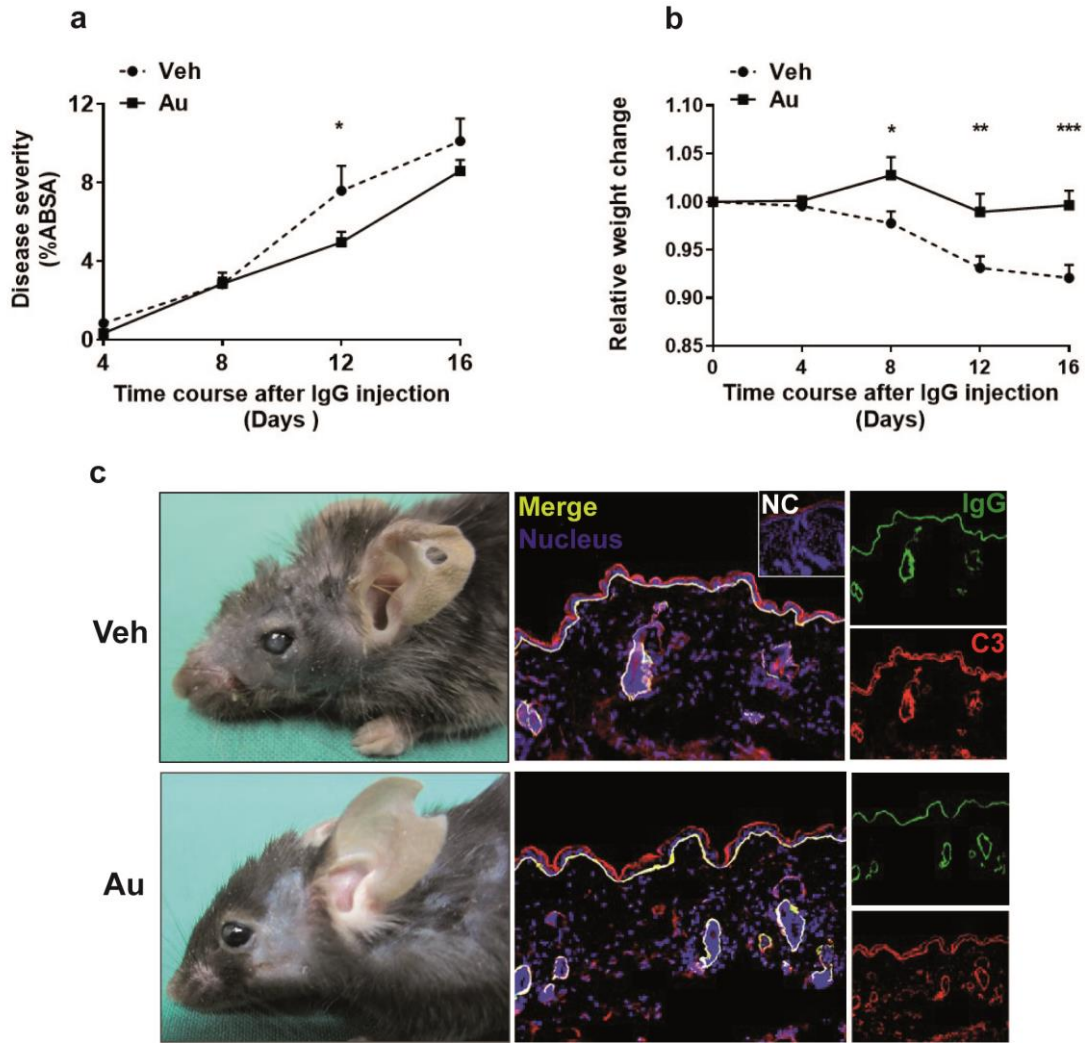

Figure 3. 8: Decreased disease activity in Au-treated mice 12 days after injection of anti-mCOL7 IgG.

Mice were intraperitoneally treated with either 3 mg/kg BW of Au or vehicle (5% (v/v) DMSO in 1X PBS) twice daily starting on a day before anti-mCOL7 IgG injection. Injection of anti-mCOL7 total IgG (3.5 mg/20g BW) initiated at day 0 and clinical disease score was monitored on days 4, 8, 12, and 16. a) There was a downward trend with a significant reduction on day 12 of observation in disease severity in the mice treated with Au compared with vehicle group. b) In comparison with vehicle-treated mice, Au-treated mice did not dramatically lose weight. c) Clinical manifestation of the disease 16 days after the initial anti-mCOL7 IgG injection in the indicated treatment group. Immunofluorescence staining of rabbit anti-mCOL7 IgG (green) and murine C3 (red) produce a yellow signal in merged image. No difference was observed regarding rabbit anti-mCOL7 IgG- and C3-depositions along the DEJ betwwen 2 groups. Two-way ANOVA, Sidak multiple comparison test, (*$p < 0.05$, **$p < 0.01$, ***$p < 0.001$), mean (± SEM), n = minimum of 8 mice /group, these are cumulative data from 2 independent experiments. NC: negative control section is stained in the absence of anti-rabbit IgG and in the presence of the corresponding isotype control rat anti-mouse IgG1.

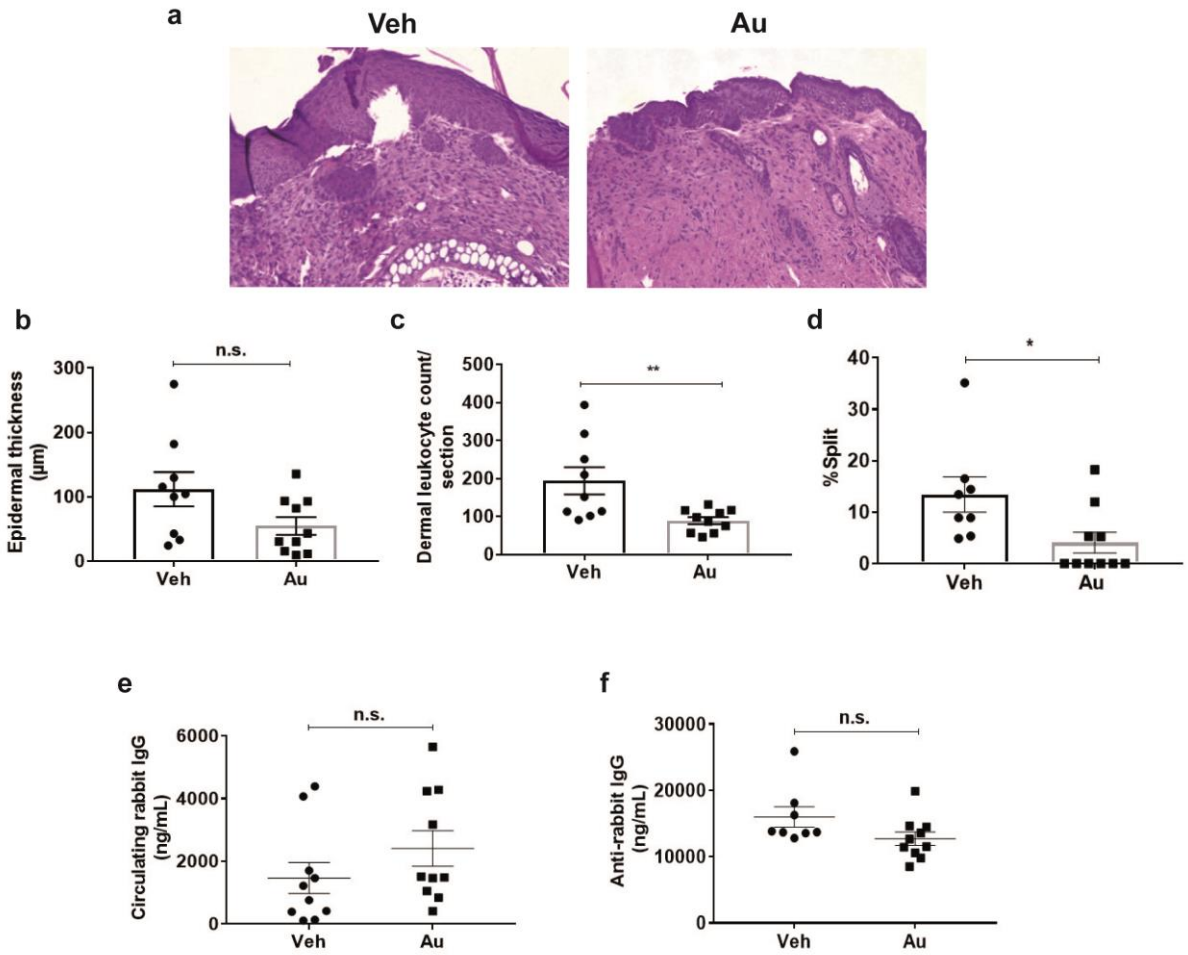

Figure 3. 9: Histological symptoms of the disease in experimental EBA was alleviated by Au-treatment.

a) Representative H&E-staining from skin specimens obtained from mice treated with Au and respective vehicle. b, c and d) Histological findings showed statistically significant reduction at both the leukocyte infiltration to the dermis and split formation in mice treated with Au in relation to vehicle treated group. While, no difference was observed in the epidermal thickness between two groups. e and f) No alterations in serum levels of the murine anti-rabbit and the rabbit anti-mouse IgGs were detected between 2 groups. Unpaired t test or Mann-Whitney-U test, (*$p < 0.05$, **$p < 0.01$), mean (± SEM), n = minimum of 8 mice /group, these are cumulative data from 2 independent experiments. n.s.; not significant, Veh; vehicle.

3.4.3 Apo treatment was effective in ameliorating disease symptoms in experimental EBA

10 mg/kg BW Apo or vehicle (5% (v/v) DMSO in 1X PBS) was subcutaneously administered to the mice one day earlier to the total anti-mCOL7 IgG injection and it was proceeded twice weekly for 16 days. Apo alleviated the disease clinical activity throughout the experiment by 50%, with mean AUC of the % ABSA of 44.2 ± 6.7 compared with mean AUC of 88.2 ± 12.2 in vehicle-treated group ($p= 0.0045$, unpaired t test; Figure 3.10a, c). Mice in Apo treatment group nearly sustained their body weight. While, mice on vehicle treatment showed a dramatic body weight loss compared with Apo treatment (Figure 3.10b). Histological analysis of the skin sections demonstrated a significant reduction in sub-epidermal blistering (mean of 7.82 ± 2.51 in Apo treatment compared with 19.42 ± 6.69 in vehicle treatment), accompanied by a decreased leukocyte infiltration to the dermis (mean of 116 ±12.18 in Apo-treated mice in comparison with 193.9 ± 35.88 in vehicle-treated group) (Figure 3.11a, c and d). On the contrary, epidermal thickness was not significantly changed in Apo treatment mice compared with vehicle treatment group (Figure 3.11a and b). No difference was detected in linear DEJ deposition of the rabbit anti-mCOL7 IgG and murine C3 between both groups (Apo and vehicle) (Figure 3.10c). Serum concentrations of the mouse anti-rabbit and rabbit anti-mCOL7 IgGs did not alter between mice treated with Apo and vehicle control group (Figure 3.11 e and f).

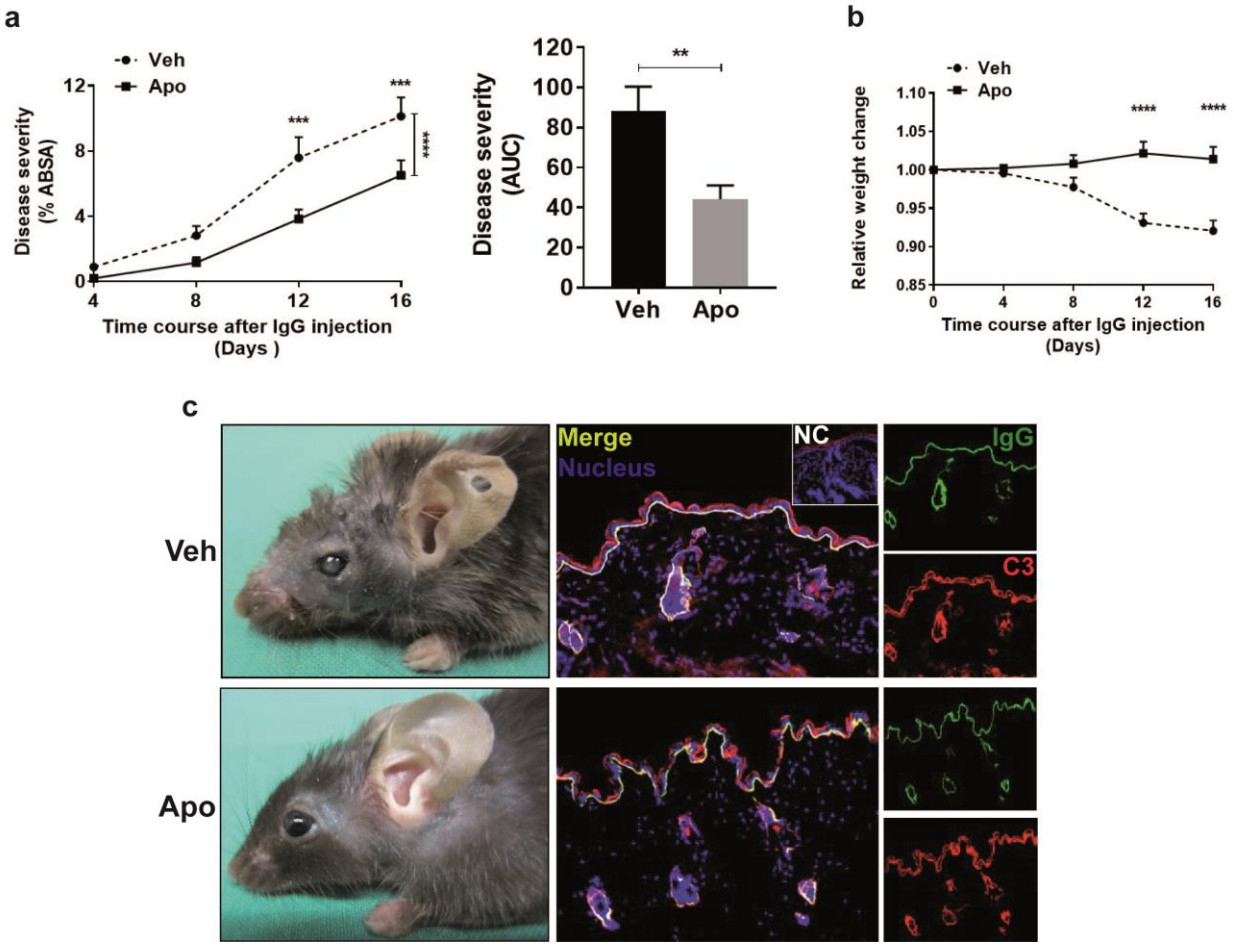

Figure 3. 10: Improvement of disease symptoms in experimental EBA following Apo treatment.

Experimental EBA was induced in mice by subcutaneous injection of 3.5 mg/20g BW of anti-mCOL7 IgG. Subcutaneous administration of 10mg/kg BW Apo or vehicle (5% (v/v) DMSO in 1X PBS) was initiated one day before total IgG injection and was continued twice weekly for entire duration of the experiment. a) Disease-alleviating activity of Apo was observed starting from day 12 and continued to the end of the observation time. Disease severity in the indicated groups is expressed as the AUC calculated from the ABSA on 4, 8, 12, and 16 days after the initial anti-mCOL7 IgG injection. Apo-treated mice showed 50% decrease in disease severity in relation to control. b) No weight loss was monitored in Apo treatment group. However, vehicle treatment group lost an average of 10% of their initial body weight until the end of the observation period and compared with Apo treatment group they had a significantly reduced weight. c) Representative clinical pictures, and immunofluorescence investigation of the mice in Apo- and vehicle-treated mice. Disease was induced in both groups due to the similar depositions of rabbit IgG (green) and murine C3 (red) in immunofluorescent staining. Overlapped rabbit IgG (green) and murine C3 (red) deposition merged to a yellow exhibition. Two-way ANOVA, Sidak multiple comparison test, (*$p < 0.05$, **$p < 0.01$, ***$p < 0.001$, ****$p < 0.0001$), mean (± SEM), n= minimum of 8 mice/group, these are the cumulative data from 2 independent experiments. NC: negative control section is stained in the absence of anti-rabbit IgG and in the presence of the corresponding isotype control, rat anti-mouse IgG1.

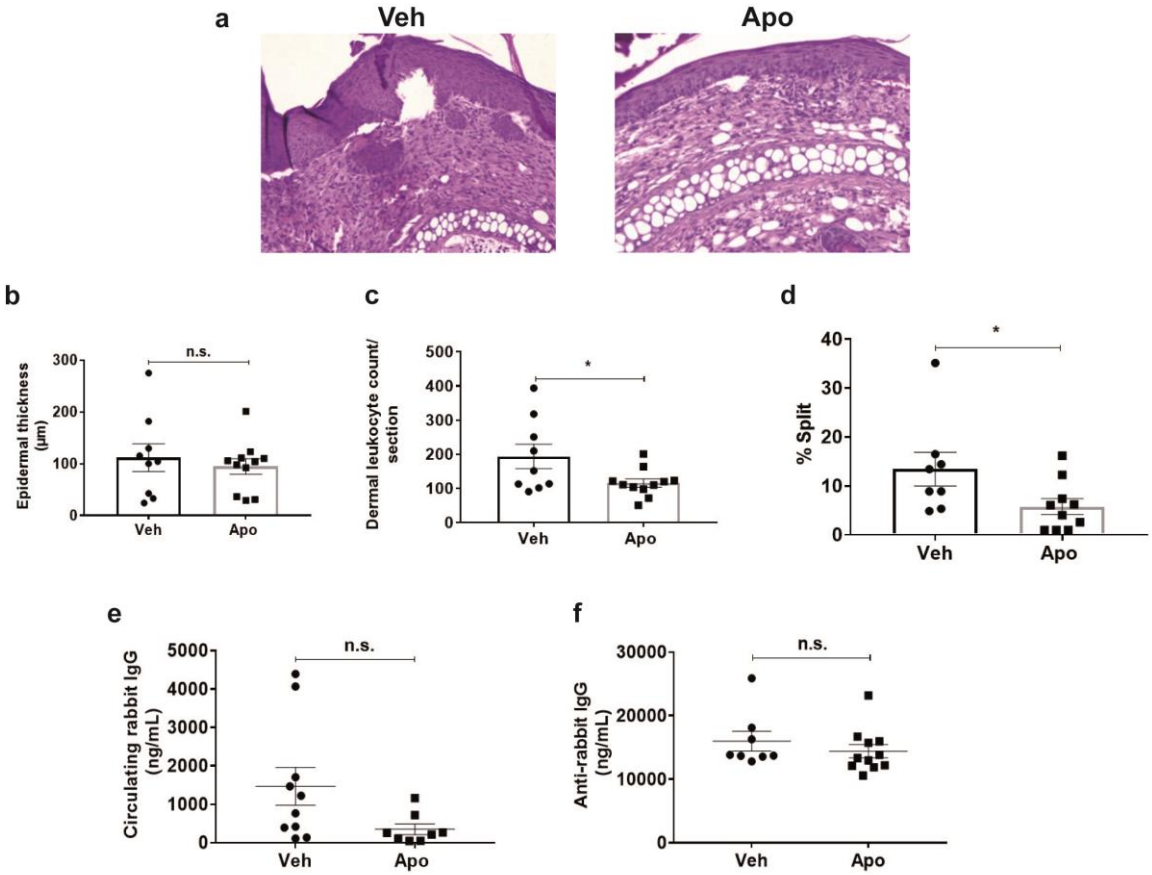

Figure 3. 11: Alleviated histological features was observed after Apo-treatment in experimental EBA.

a) Representative H&E stained skin sections. b, c and d) Histological examination in H&E stained sections of the skin demonstrated a statistically significant decrease both in the dermal leukocyte count and the %split formation in Apo-treated mice in comparison with vehicle-treated group. While similar epidermal thickness was shown in both groups. e and f) There was no difference between Apo- and vehicle- treated mice in terms of serum concentrations of the mouse anti-rabbit and rabbit anti-mCOL7 IgGs. Unpaired t test or Mann-Whitney-U test, (*$p < 0.05$), mean (± SEM), n= minimum of 8 mice/group, these are the cumulative data from 2 independent experiments. n.s.; not significant.

3.4.3.1 Identification of the effective dose of Apo at improvement of disease symptoms in experimental EBA

In order to establish a possible dose-response relationship of Apo in the alleviation of disease activity in experimental EBA, mice were given subcutaneous injections of 10 mg/kg BW of drug once (Apo 1x/w), twice (Apo 2x/w) and three times (Apo 3x/w) a week. Drug or vehicle (1X PBS) administration initiated one day earlier than total anti-mCOL7 IgG injection (day -1) and proceeded until the end of the experiment (day 16). As Figure 3.12a, and d demonstrate, interestingly the only effective dose of Apo was Apo 2x/w, with a 43% reduction of disease severity in relation to vehicle group. This was the dose that had been previously used for the *in vivo* validation study (section 3.4.3). Even though Apo 2x/w was the only effective dose at ameliorating disease severity, examination of H&E stained skin sections of mice treated with all doses showed a significant decrease in the dermal leukocyte infiltration. Mean values of the leukocyte counts were 79 ± 8.28, 89.3 ± 4.15, and 83.2 ± 5.51 for Apo 1x/w, Apo 2x/w, and Apo 3x/w, respectively in comparison with vehicle with the mean of 121.7 ± 6.13 (Figure 3.13a and c). However, compared with the vehicle control mice, drug-treated mice at all doses showed no alterations in epidermal thickness and split formation (Figure 3.13a, b and d). Linear DEJ deposition of rabbit anti-mCOL7 IgG and murine C3 were comparable in all treatment groups (Figure 3.12a). Mice receiving drug at all treatment regimen groups as well as vehicle did not lose any body weight throughout the entire course of the experiment (Figure 3.12b). Serum levels of the mouse anti-rabbit and rabbit anti-mCOL7 IgGs remained unchanged between different doses groups in relation to vehicle group (Figure 3.13e and f).

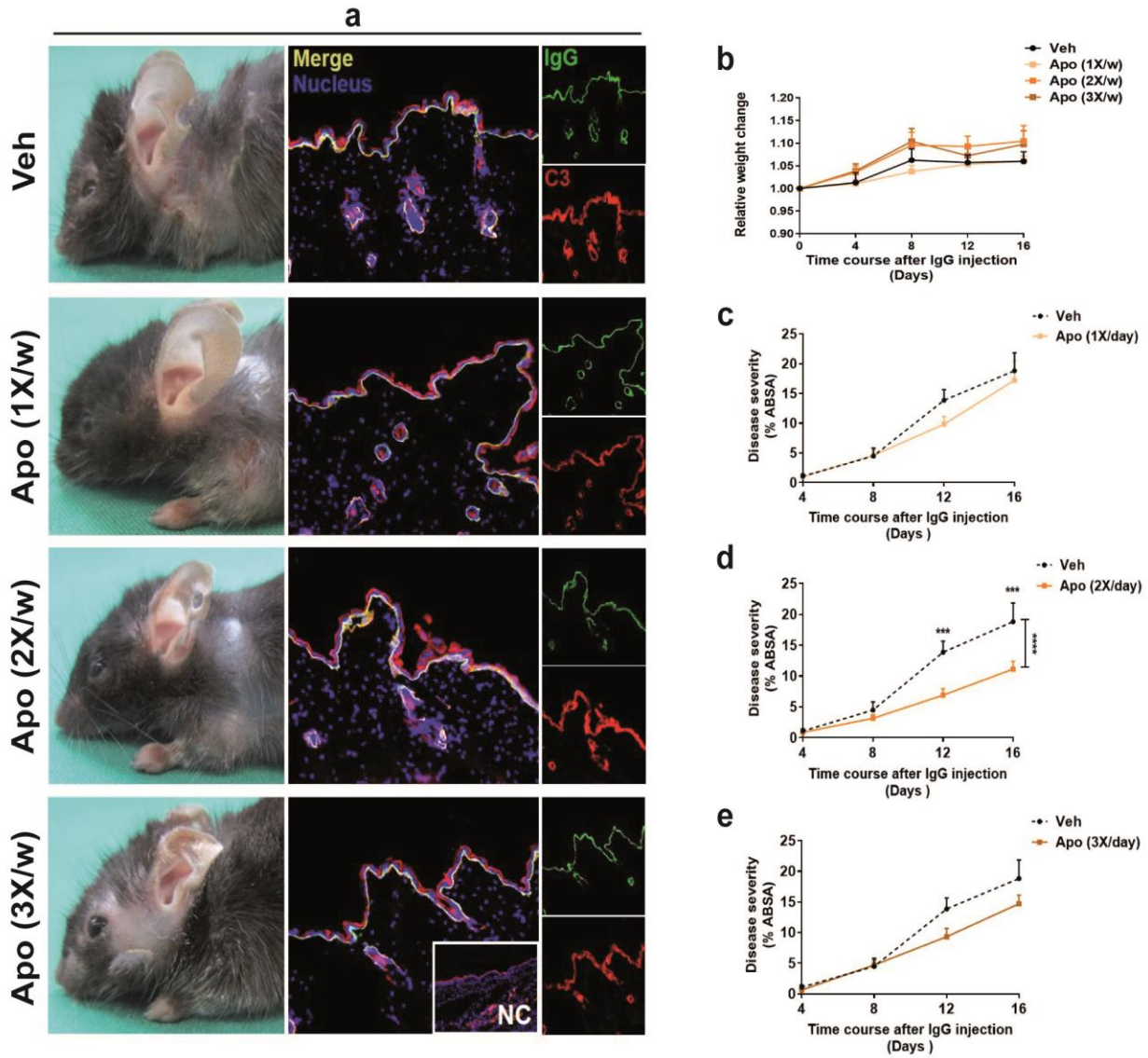

Figure 3. 12: Comparative effectiveness of Apo at different doses.
One day prior to total anti-mCOL7 IgG injection, mice received a subcutaneous injection of Apo. 10mg/kg BW of drug was administered at different frequencies to the mice as follows, once (Apo 1x/w) or twice (Apo 2x/w) or three times (Apo 3x/w) a week. Disease severity and body weight were monitored at days 4, 8, 12, and 16. a) Representative clinical pictures of the mice in the indicated groups, and fluorescence microscopy images in different treatment groups are shown. Comparable depositions of rabbit anti-mCOL IgG (green) and murine C3 (red) yielding to a yellow emission were depicted in all Apo treatment groups and vehicle. b) Mice in Apo treatment groups and vehicle showed no body weight decrement during the entire time of the experiment. c, d and e) Clinical scores of the experimental EBA in mice at different doses of Apo treatment demonstrated that Apo 2x/w was the only efficient dose at reduction of the disease severity in comparison with vehicle (1X PBS). Two-way ANOVA, Sidak multiple comparison test, (*$p < 0.05$, **$p < 0.01$, ***$p < 0.001$, ****$p < 0.0001$), mean (± SEM), n= minimum of 8 mice/group. NC: negative control section is stained in the absence of anti-rabbit IgG and in the presence of the corresponding isotype control, rat anti-mouse IgG1.

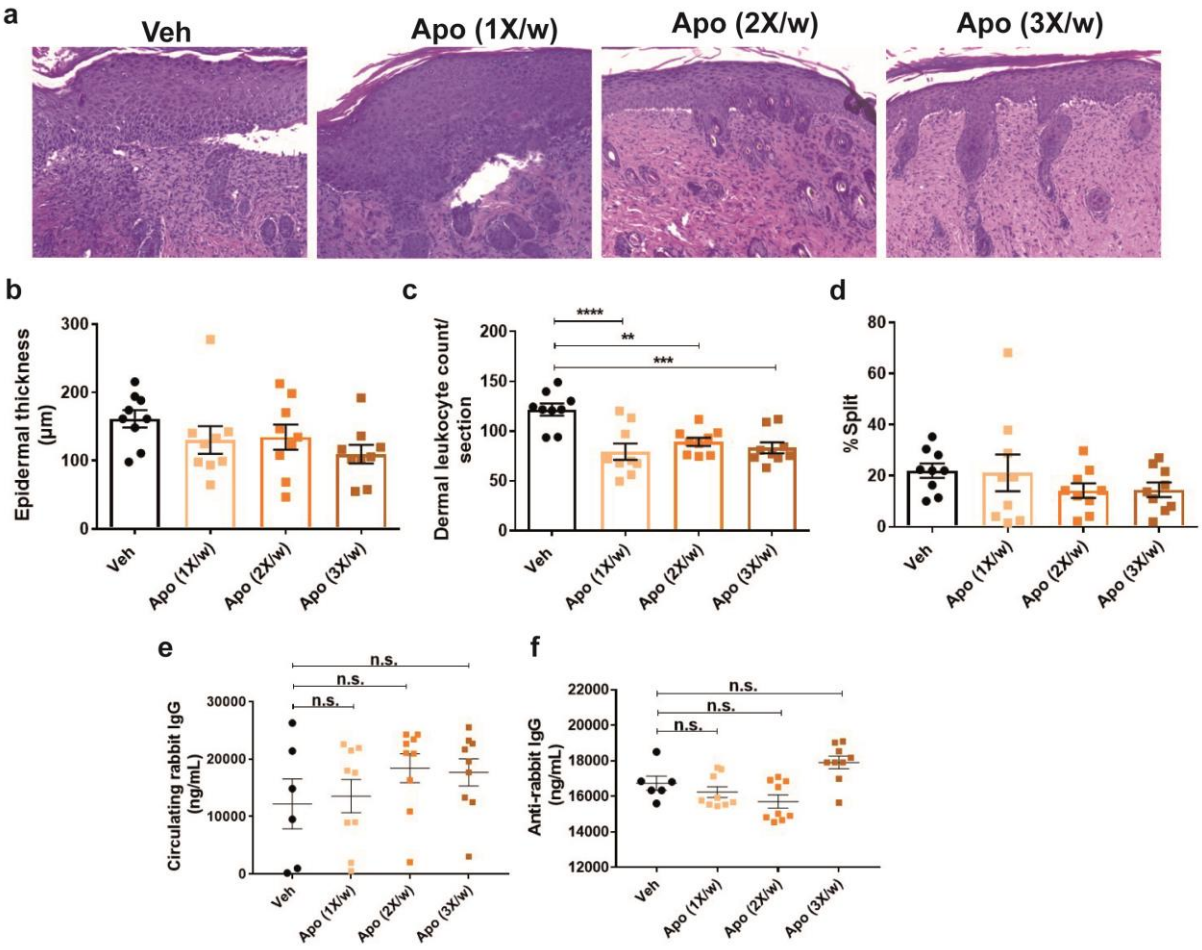

Figure 3. 13: Leukocyte infiltration to the dermis was hindered following Apo-treatment.

a) Representative H&E stained skin sections. b, c and d) Histological analysis of the H&E stained skin sections revealed that Apo at all doses diminishes dermal infiltration of the leukocyte compared with vehicle. Whereas it had no significant effect on the epidermal thickness and blister formation. e and f) There was no significant changes in the serum levels of mouse anti-rabbit and rabbit anti-mCOL7 IgGs between Apo treated groups and vehicle. One-way ANOVA, Sidak multiple comparison test, (*p < 0.05, **p < 0.01, ***p < 0.001, ****p <0.0001), mean (± SEM), n= minimum of 8 mice/group.

3.4.4 Tam markedly attenuated the disease symptoms in experimental EBA

The subcutaneous injection of 20mg/kg BW [224] of Tam began a day prior to initiation of the total anti-mCOL7 IgG injection (day -1). Drug or vehicle (5% DMSO (v/v) in 1X PBS), were applied twice a week for the entire duration of the experiment (until day 16). Mice were monitored for their body weight change and disease severity every four days (days 4, 8, 12, and 16). As Figure 3.14a, and c evidently illustrate, Tam treatment led to a significant attenuation of disease severity (assessed by a mean AUC of the ABSA of 46.62 ± 12.4) versus the vehicle (with a mean AUC of the ABSA of 88.2 ± 12.2). Tam treatment (the mean of the % ABSA of 4.5 ± 0.5) on day 16 of the experiment was equally effective as reference treatment (MP) (the mean of the % ABSA of 4.0 ± 0.6) (data not shown). Furthermore, histological findings revealed that Tam markedly diminished leukocyte infiltration into the dermis associated with significant reductions in both the blister formation and the epidermal thickness versus vehicle (Figure 3.15a, b, c and d). IF staining of skin sections exhibited a similar deposited rabbit anti-mouse IgG and C3 at the DEJ in both groups (Figure 3.14c). A maintained body weight was observed in Tam-treated mice during the entire course of the experiment. While mice on vehicle treatment started a significant body weight loss from day 8 compared with Tam treated group (Figure 3.14b). It was also shown that the concentrations of the mouse anti-rabbit and rabbit anti-mCOL7 IgGs did not differ in sera of the mice treated with Tam in relation to the vehicle treated mice (Figure 3.15 e and f).

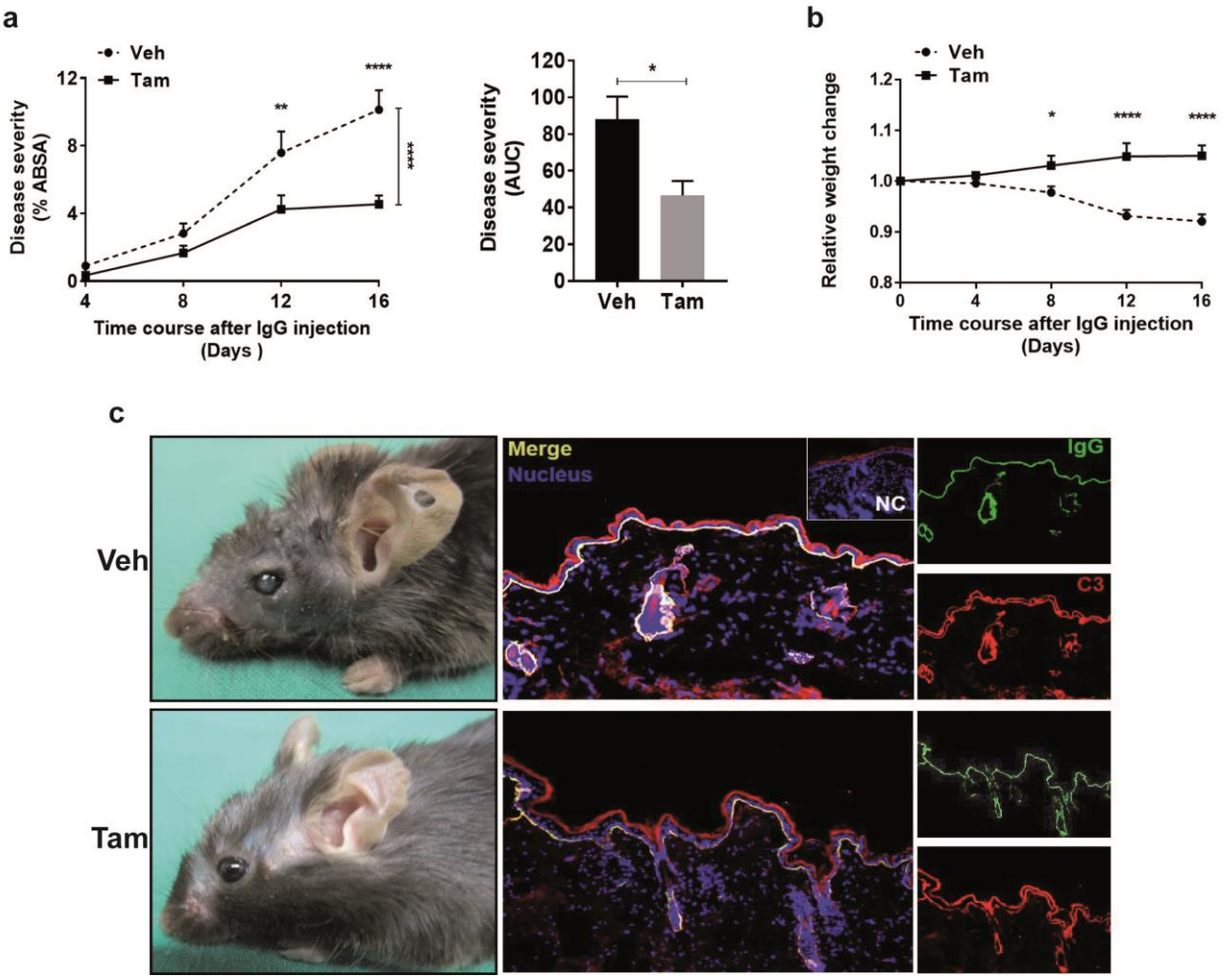

Figure 3. 14: Disease symptom was significantly reduced in Tam-treated mice in experimental EBA.

Mice were subcutaneously given 20mg/kg BW twice weekly of Tam or vehicle starting from a day before total IgG injection (day -1) until day 16. a) Mice treated with Tam demonstrated a statistically significant improvement in % ABSA versus the vehicle group. b) Tam-treated mice sustained their body weight during the entire time of the observation, whereas vehicle treated mice lost about 10% of their initial body weight on day 16. c) Representative clinical manifestation and IF images confirming disease induction in indicated groups. Identical depositions of rabbit anti-mCOL IgG (green) and murine C3 (red) yielding to a yellow emission were depicted in both groups. Two-way ANOVA, Sidak multiple comparison test, Mann-Whitney-U test, (*$p < 0.05$, **$p < 0.01$, ***$p < 0.001$, ****$p < 0.0001$), mean (± SEM), n= minimum of 8 mice/group. These are the cumulative data from 2 independent experiments. NC: negative control section is stained in the absence of anti-rabbit IgG and in the presence of the corresponding isotype control, rat anti-mouse IgG1.

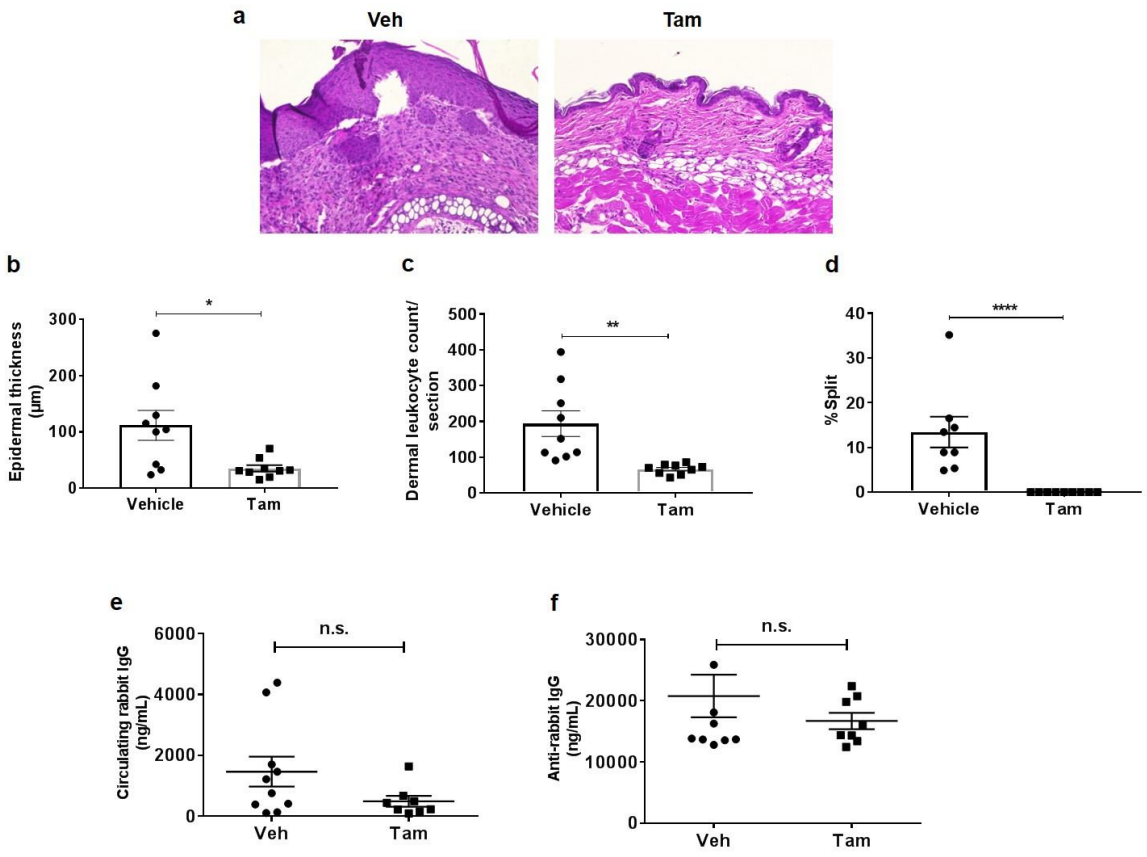

Figure 3. 15: Improved histological manifestations of the disease in experimental EBA in Tam-treated mice.

a) Representative H&E stained skin sections of the mice on Tam treatment and corresponding vehicle. b, c and d) Histological examination of the H&E stained section of the skin revealed a statistically significant decline in epidermal thickness, accompanied by a decrease in both the dermal infiltration of the leukocytes and split formation. e and f) ELISA analysis of the sera showed no difference between Tam- and vehicle- treated mice in concentrations of the mouse anti-rabbit and rabbit anti-mCOL7 IgGs. Unpaired t test, Mann-Whitney-U test, (*$p < 0.05$, **$p < 0.01$, ***$p < 0.001$, ****$p < 0.0001$), mean (± SEM), n= minimum 8 mice/group, these are the cumulative data from 2 independent experiments.

3.4.4.1 Different dosing regimens of Tam efficaciously mitigated disease severity in experimental EBA

In an effort to establish a possible dose response impact of Tam in melioration of experimental EBA, mice subcutaneously received varying doses of the drug. To do so, 10 mg/kg BW or 20 mg/kg BW or 40 mg/kg BW of Tam or corresponding vehicle (5% DMSO (v/v) in 95% corn oil) were administered twice per week, initiating from a day prior to total IgG injection. Mice were thereafter checked for clinical disease progression and body weight every 4 days (days 4, 8, 12, and 16). Tam treatment at all doses indicated an efficacious impact on clinical disease score compared with vehicle treatment (Figure 3.16a and d). Mean disease severity throughout the disease course calculated as AUC was 46.2 ±5.2, 47.0 ± 7.2, and 42.0 ± 4.3 for Tam (10 mg/kg BW), Tam (20 mg/kg BW), and Tam (40 mg/kg BW), respectively compared with vehicle treated controls with the mean value of 86.3 ± 11.3 (Figure 3.16b). Although, mice that received 10 mg/kg BW of Tam clinically showed a significant improvement in disease severity, the histological examination of their H&E stained sections demonstrated no statistically significant difference in relation to vehicle treatment group (Figure 3.17a, b, c and d). Consistent with clinical observation, mice treated with Tam (20 mg/kg BW), or Tam (40 mg/kg BW) had a thinner epidermis, along with a decreased dermal leukocyte infiltration versus the vehicle group (Figure 3.16a, b and c). Histological findings further revealed that Tam (40 mg/kg BW) markedly reduced split formation compared with vehicle, while this effect was not observed in Tam (20 mg/kg BW) treatment (Figure 3.16a and d). Confirmation of the disease induction was demonstrated in all groups of the mice by IF staining of the perilesional skin sections. Linear depositions of C3 and rabbit anti-mCOL7 IgG were depicted in Figure 3.16a. Mice under the drug treatment did not lose weight at the entire time of the observation (Figure 3.16c). The concentrations of the mouse anti-rabbit and rabbit anti-mCOL7 IgGs did not significantly change in sera of the mice treated with different doses of Tam versus the vehicle treated mice (Figure 3.17e and f).

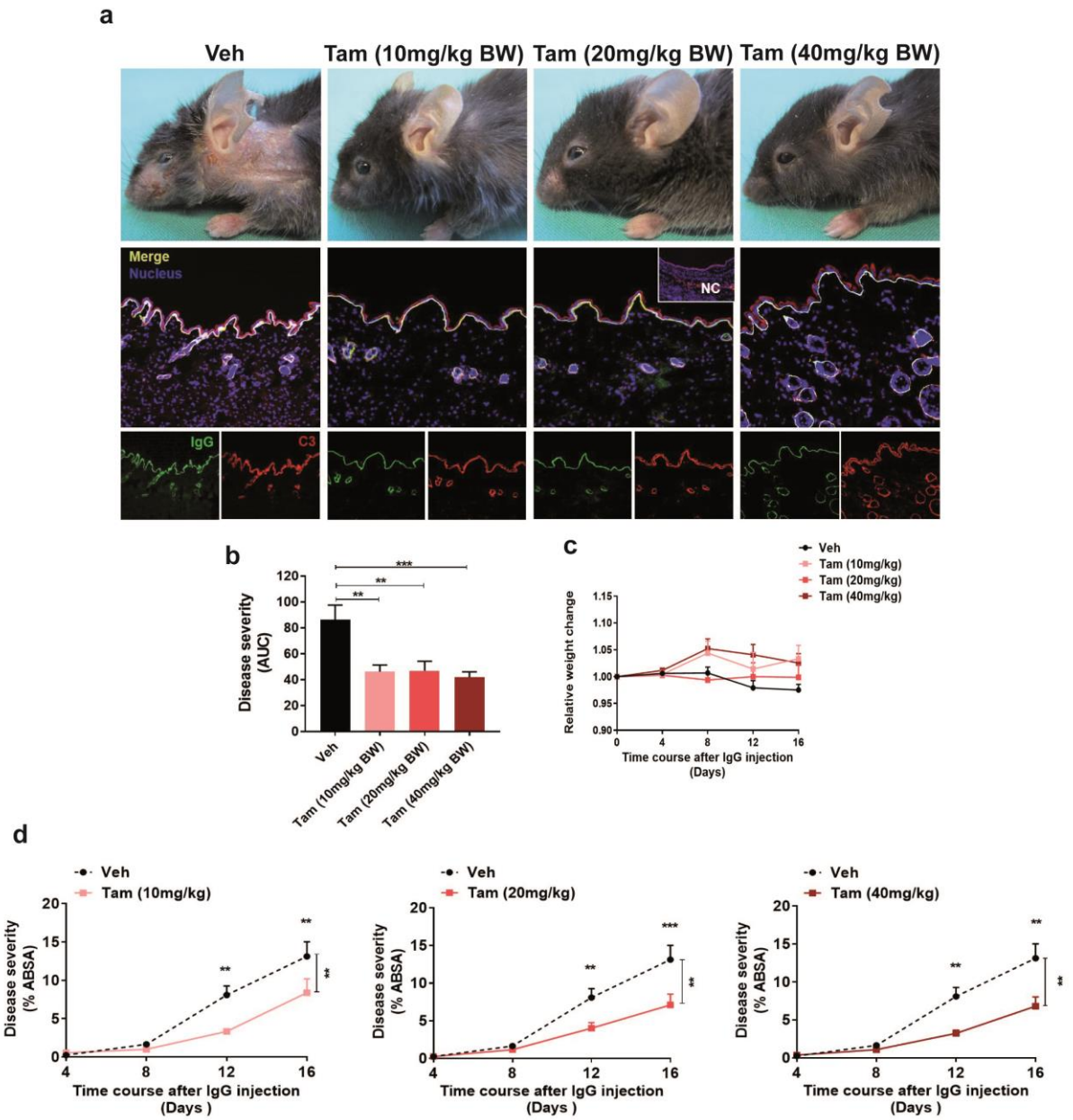

Figure 3. 16: Effectiveness of different doses of Tam at mitigating disease activity in experimental EBA.

Subcutaneous treatment of Tam at 10 mg/kg BW or 20 mg/kg BW or 40 mg/kg BW or respective vehicle was performed a day before total IgG injection until day 16. a) Clinical presentation of the disease in indicated groups and representative IF-stained skin sections. IF staining revealed a comparable rabbit anti-mouse IgG (green) and murine C3 (red) deposition (merged in yellow) at DEJ of the indicated groups. b and d) A relative 47% reduction was observed in clinical disease score of the mice under treatment of Tam at different doses in proportion to vehicle group. c) In contrast to vehicle treated animals, mice receiving Tam at all doses did not lose their body weight at the entire time of the observation. Two-way ANOVA, One-way ANOVA, Sidak multiple comparison test, (*p < 0.05, **p < 0.01, ***p < 0.001, ****p <0.0001), mean (± SEM), n ≥ 7/group. NC: negative control section is stained in the absence of anti-rabbit IgG and in the presence of the corresponding isotype control, rat anti-mouse IgG1.

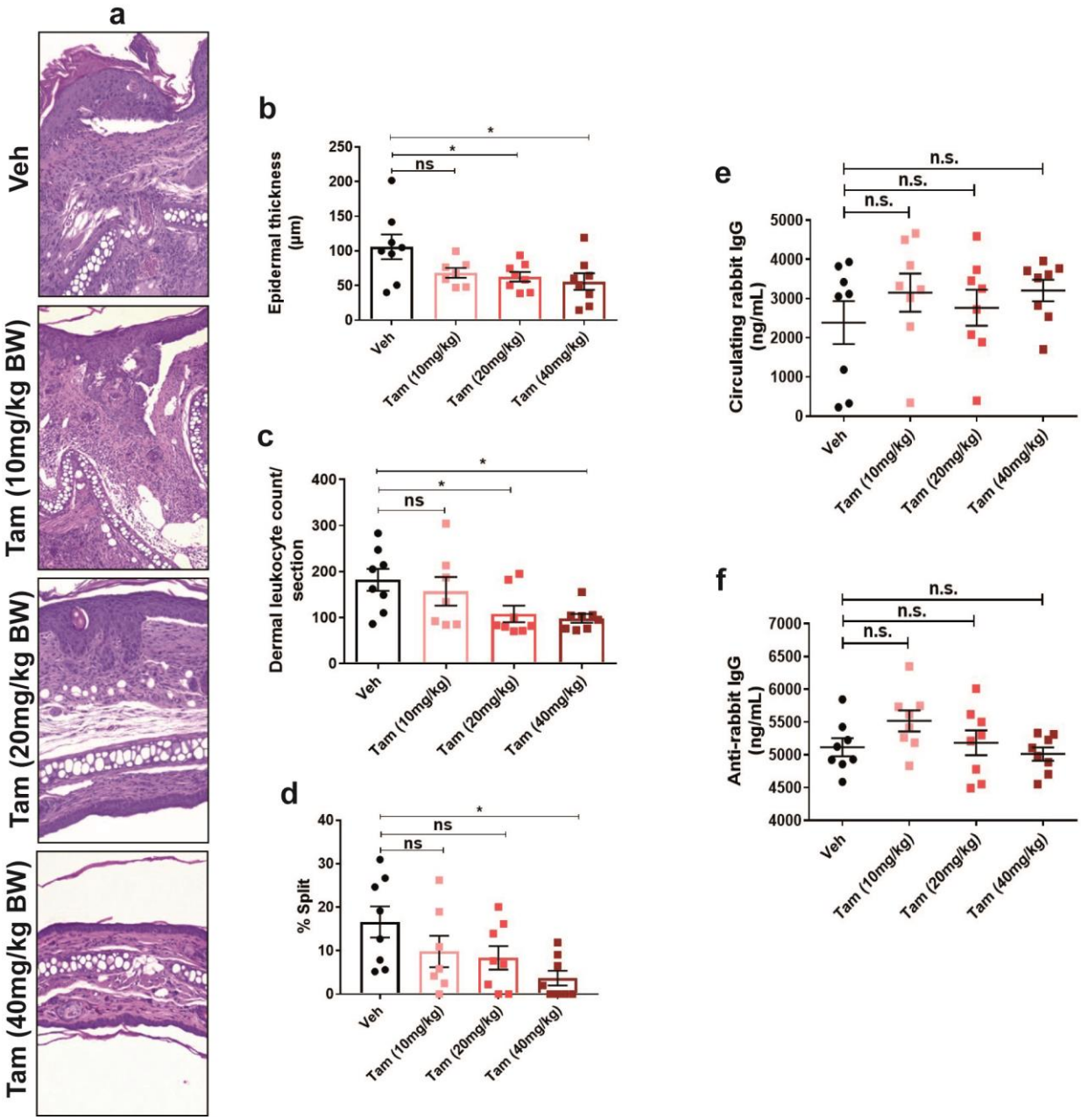

Figure 3. 17: Tam treatment at 2 doses led to the significantly milder infiltration of immune cells to the dermis and decreased epidermal thickness.

a) Representative H&E histological stained ear sections. b, c and d) Tam (10 mg/kg BW) exerted no marked impact on epidermal thickness, dermal leukocyte infiltration and %split in relation to vehicle. However, the highest dose significantly reduced epidermal thickness, dermal leukocyte infiltration, and %split versus vehicle. The middle dose (previously used in *in vivo* validation study) prominently decreased epidermal thickness and dermal leukocyte infiltration compared with vehicle, with no effect on %split. e and f) No significant alteration was revealed at serum concentrations of the mouse anti-rabbit and rabbit anti-mCOL7 IgGs in the mice treated with different doses of Tam versus the vehicle-treated mice. One-way ANOVA, Sidak multiple comparison test. (*p < 0.05, **p < 0.01, ***p < 0.001, ****p <0.0001), mean (± SEM), n ≥ 7/group.

3.4.4.2 Tam exerts its disease-alleviating activity through estrogen receptor (ER)-dependent mechanism

Due to a more robust impact of Tam among effective drugs at meliorating disease severity in experimental EBA along with the maintenance of its inhibitory effects at different doses, this drug was selected for further investigation. Tam, a selective estrogen receptor modulator (SERM), is an ER-binding compound acting as either an agonist or antagonist in a tissue-specific manner [225]. There are two known ERs in mammals: ERα (ER1) and ERβ (ER2) [226], operating as ligand-dependent transcription factors which ultimately modulate several gene expressions [227]. ERs are expressed on both lymphoid and myeloid cells and the effect of estrogen on immune cells has been already reported [228]. The immunomodulatory effects of Tam can be mediated through an ER-dependent [229-232] or ER-independent [233, 234] pathways. In order to gain deep insights into the possible mechanisms involved in alleviating activity of Tam in experimental EBA, ERα knockout (αERKO) and ERβ knockout (βERKO) mice were used. KO mice (n=8) and their wild type littermates (n=8) were treated with Tam (20 mg/kg BW) or vehicle (5% DMSO (v/v) in 95% corn oil). As Figure 3.18a and b show, Tam treatment compared with vehicle led to a significant relief of the disease symptoms in WT mice. In contrast, Tam treatment failed to show such an effect in αERKO mice in relation to the vehicle. Although in βERKO mice, compared with vehicle, Tam treatment slightly reduced disease severity, the difference was not statistically significant (Figure 3.18a and b). Thus, the therapeutic effect of Tam in EBA is directly mediated through interaction with ER. Examination of the IF-stained sections indicated an equal exhibition of rabbit anti-mouse IgG and murine C3 depositions at DEJ verifying similar disease induction in all mice (Figure 3.19a). Over the whole observation time, weights of the WT and βERKO mice under Tam treatment did not significantly alter compared with vehicle treatment group (Figure 3.18c). Whereas, αERKO mice in both Tam- and vehicle treatment groups lost up to 10% of their initial body weight (Figure 3.18c). There were no differences in serum concentrations of the mouse anti-rabbit and rabbit anti-mCOL7 IgGs between Tam-treated mice versus vehicle-treated mice in the αERKO and their

WT littermates (Figure 3. 19b). In sera of the βERKO mice no changes was observed at the level of rabbit anti-mCOL7 IgG while a significant reduction was demonstrated at serum level of the mouse anti-rabbit IgG in Tam-treatment group in proportion to vehicle (Figure 3. 19c). When the disease severity was compared between WT and ERKO mice regardless of the treatment, αERKO demonstrated similar magnitude of the disease to WT mice. While, βERKO mice developed significantly reduced disease compared with their WT littermates on day 16 of the experiment (Figure 3.20).

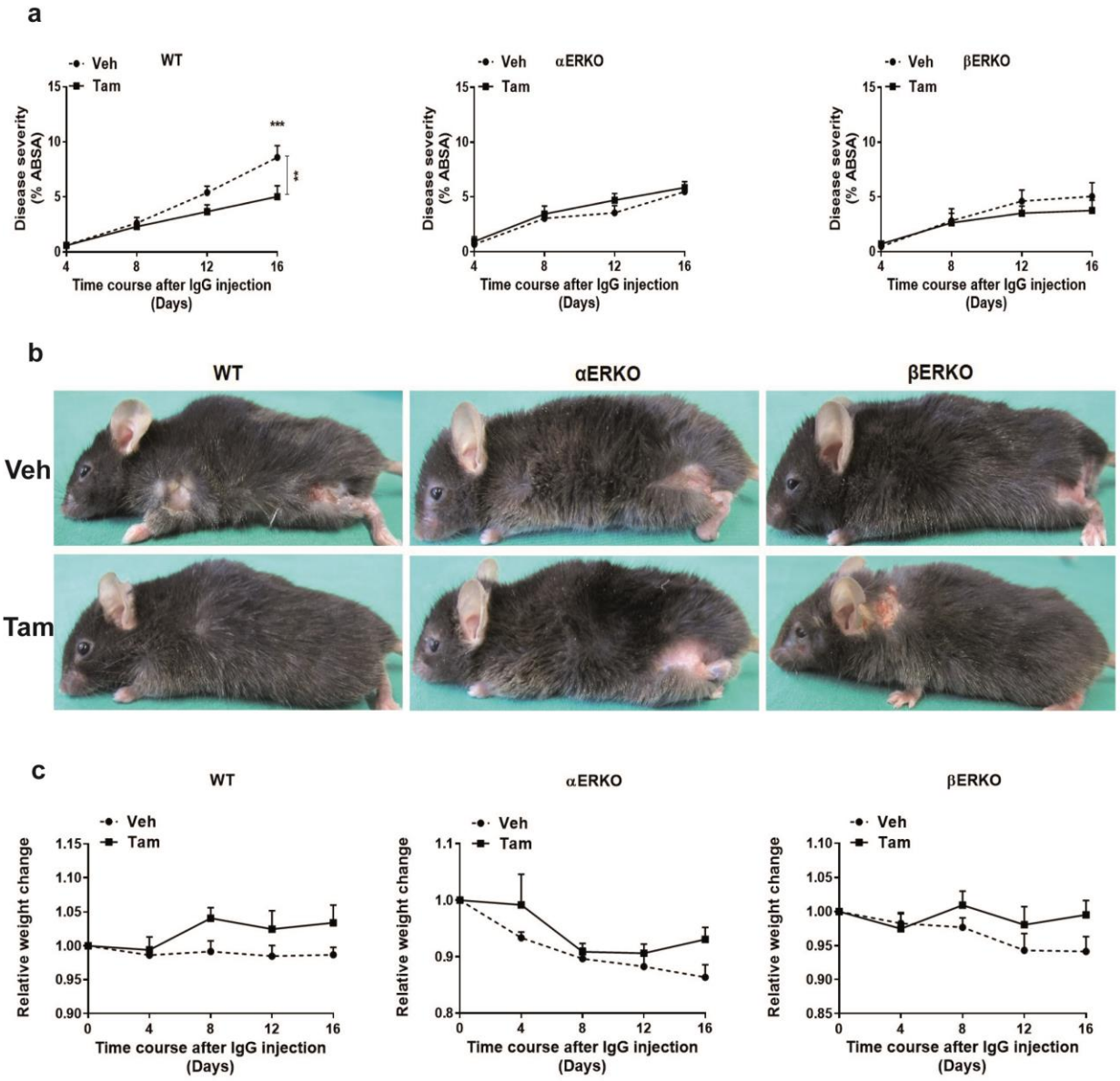

Figure 3. 18: In experimental EBA, disease-modifying effects of Tam are mediated through ER.

Disease induction started at day 0 by 6 repeated subcutaneous injection of anti-mCOL7 IgG every other day over a period of 16 days. On day -1, mice were given a subcutaneous treatment of 20 mg/kg BW Tam or vehicle twice per week. a) Analysis of disease score severity showed a significant reduction in EBA symptoms in WT mice receiving Tam compared with vehicle. While, this effect was not observed in αERKO and βERKO mice. b) Clinical manifestation of αERKO and βERKO mice and their wild type littermates treated with Tam or vehicle. c) Monitoring of the body weight change demonstrated no body weight loss in WT and βERKO mice, whereas 10% body weight loss was observed in αERKO mice. Two-way ANOVA, Sidak multiple comparison test, (***$p < 0.001$), mean (± SEM), n = 7-8/group.

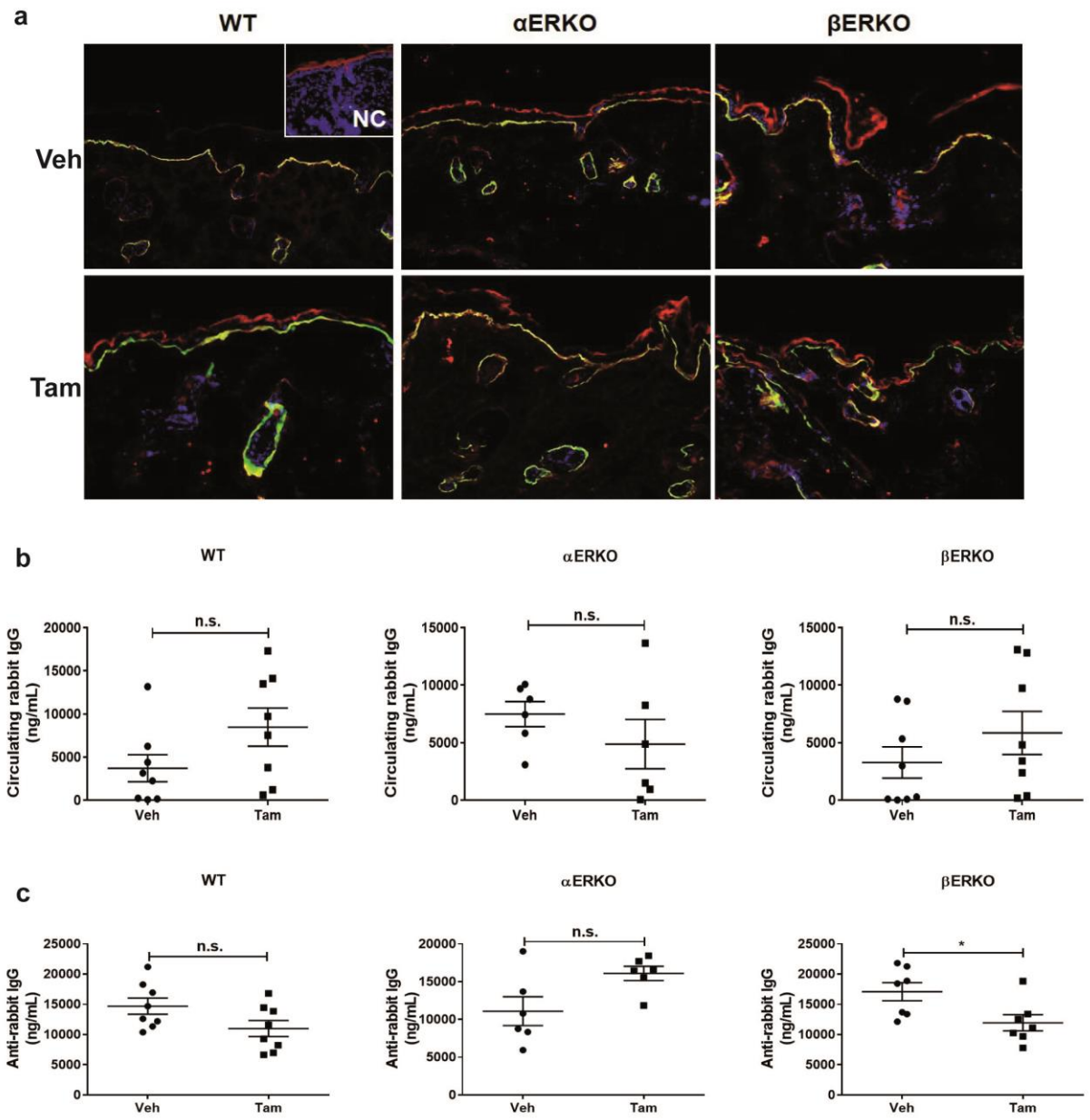

Figure 3. 19: Similar disease induction in αERKO and βERKO mice and their wild type littermates receiving Tam and vehicle.

a) Representative IF microscopy images. Deposition of rabbit anti-mouse IgG (green) and murine C3 (red) merged to yellow exhibition. b) There was no difference at serum level of circulating rabbit anti-mouse IgG in Tam-treated mice in KO mice and their WT littermate compared with vehicle. c) Serum level of anti-rabbit IgG did not change in Tam- and vehicle-treated groups in αERKO and WT littermates whereas, in βERKO mice it was significantly reduced in Tam-treated group compared with vehicle. Unpaired t test or Mann-Whitney-U test, (*$p < 0.05$, **$p < 0.01$, ***$p < 0.001$, ****$p < 0.0001$), mean (± SEM), n= minimum 7-8 mice/group. NC: negative control section is stained in the absence of anti-rabbit IgG and in the presence of the corresponding isotype control, rat anti-mouse IgG1.

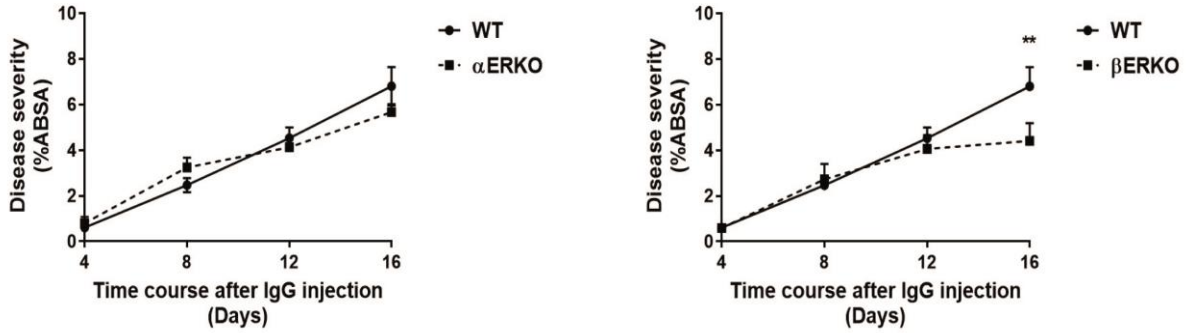

Figure 3. 20: βERKO mice developed significantly less sever disease compared with WT littermates in experimental EBA On day 16 of the observation.
αERKO and WT mice developed similar disease magnitude.

3.5 Identification of the Tam-induced gene expression signature

3.5.1 Expression of 488 genes were significantly altered by Tam treatment

RNA-Seq is a widely utilized technology for profiling gene expression. It aims at identification of genes or molecular pathways that are differentially expressed between two or more biological conditions [235]. In an attempt to discern the molecular mechanisms driving ameliorative effect of Tam in experimental EBA, the RNA-Seq approach was used. For RNA-Seq experiment, a subcutaneous administration of either Tam (20 mg/kg BW) or vehicle to the mice (n=8) was performed at day -1 and proceeded on a twice weekly basis for 16 days. Mice received their first total anti-mCOL7 IgG injection on day 0 and thereafter 6 repetitive injections were administered every second day. On day 16, animals were euthanized by cervical dislocation while they were fully anesthetized and ears were excised. After total RNA extraction from the snap frozen tissues, 1 µg of RNA was used to construct an RNA sequencing library. Libraries were then sequenced on an Illumina NextSeq500 by using 75-bp paired-end reads. Quality control was performed using FastQC software. Read were trimmed by trimmomatic software and high-quality reads (min read length 36 base pair and Phred Score > 20) were retained for further downstream processing. Afterwards, reads were aligned to the reference mouse genome (mm10), build GRCm38 v79 using STAR. Genomic coordinates for known mouse genes were downloaded as GTF file from Ensembl genome browser and htseq-count was used to quantify the gene expression across the samples. The gene expression table was imported to

R software for statistical analyses by DESeq2 R package. Differentially expressed genes (DEGs) were identified by applying DESeq2 using a cutoff of adjusted *P* value <0.01 and -1 > $\log_2$fold change > 1.

In total, 488 genes were found to be differentially expressed in Tam-treated mice compared with vehicle treatment group. Of those, expression of 220 genes were upregulated in mice that received Tam, while 268 genes showed a lower expression. As shown in Figure 3. 21a, the volcano plot exhibits the distribution of 488 DEGs with up- and down-regulated genes represented as red dots and green dots, respectively. The heatmap in Figure 3. 21b indicates the 32 top DEGs (adjusted *P* value <0.001 and -2 > $\log_2$fold change > 2) in Tam-treated mice versus vehicle demonstrating a common gene signature in Tam-treated mice compared with vehicle. To further investigate the biological importance of 488 DEGs, functional categories of each gene was determined by querying the GO database (http://www.geneontology.org/GO.database.shtml). In Figure 13. 22, the heatmap represents GO enrichment analysis of the 488 DEGs. It demonstrates that DEGs were categorized into 22 functional groups and they are enriched in several biological processes mainly in immune system process, inflammatory response, and cell migration. To further comprehend functions of the DEGs, the KEGG pathway analysis of the DEGs was performed by mapping them to terms in the KEGG database (http://www.genome.ad.jp/kegg/). The 488 DEGs were identified in 13 pathways with a KEGG pathway annotation. As illustrated in Figure 3. 23, the DEGs are mostly involved in PI3K/Akt signaling, Janus kinase (JAK)/STAT signaling, and calcium signaling pathways. Based on the published literature, 8 protein-coding genes, *Prr7* [236], *Plaur* [143], *Cyp4f18* [237], *Ccdc88b* [238], *Mmp9* [32], *S100a7a* [239], *Lce3c* [240], and *Cebpd* [241] with the most significantly differential expression were chosen for validation using RT-qPCR analysis.

3.5.2 Tam-induced down-regulation of *S100a7a* is confirmed by RT-qPCR

An RT-qPCR assay was conducted in Tam- and vehicle- treated mice skin tissues to verify RNA-Seq results. Aliquots of the RNA samples which were used for RNA-Seq analysis were served here for the RT-qPCR analysis. Moreover, in order to

enlarge the sample size, RNA was isolated from the remaining part of the ear from Tam- or vehicle-treated mice and utilized for the confirmatory RT-qPCR assay. The gene expression levels from RT-qPCR were calculated relative to 4 reference genes *Actb*, *β2m*, *Casc3*, and *Hprt* using the $2^{-\Delta\Delta CT}$ method. An unpaired t-test or a Mann-Whitney-U test was used to evaluate any statistically significant expression between Tam- and vehicle-treated mice. RT-qPCR results, in accordance with the RNA-Seq results, revealed a lower expression level in 7 genes, *Plaur*, *Cyp4f18*, *Ccdc88b*, *Mmp9*, *S100a7a*, *Lce3c*, *Cebpd* out of 8 in Tam-treated group versus vehicle. Of these, only *S100a7a*, a peptide taking role in the pathogenesis of inflammatory skin diseases [242], showed a statistically significant down-regulation in Tam treatment in relation to vehicle. On the other hand, mRNA expression level of *Prr7* was slightly higher but not significant in Tam treatment group in comparison to vehicle treatment (Figure 3. 24a and b). Taken together, these data imply that *S100a7a* serves as a potential target of Tam.

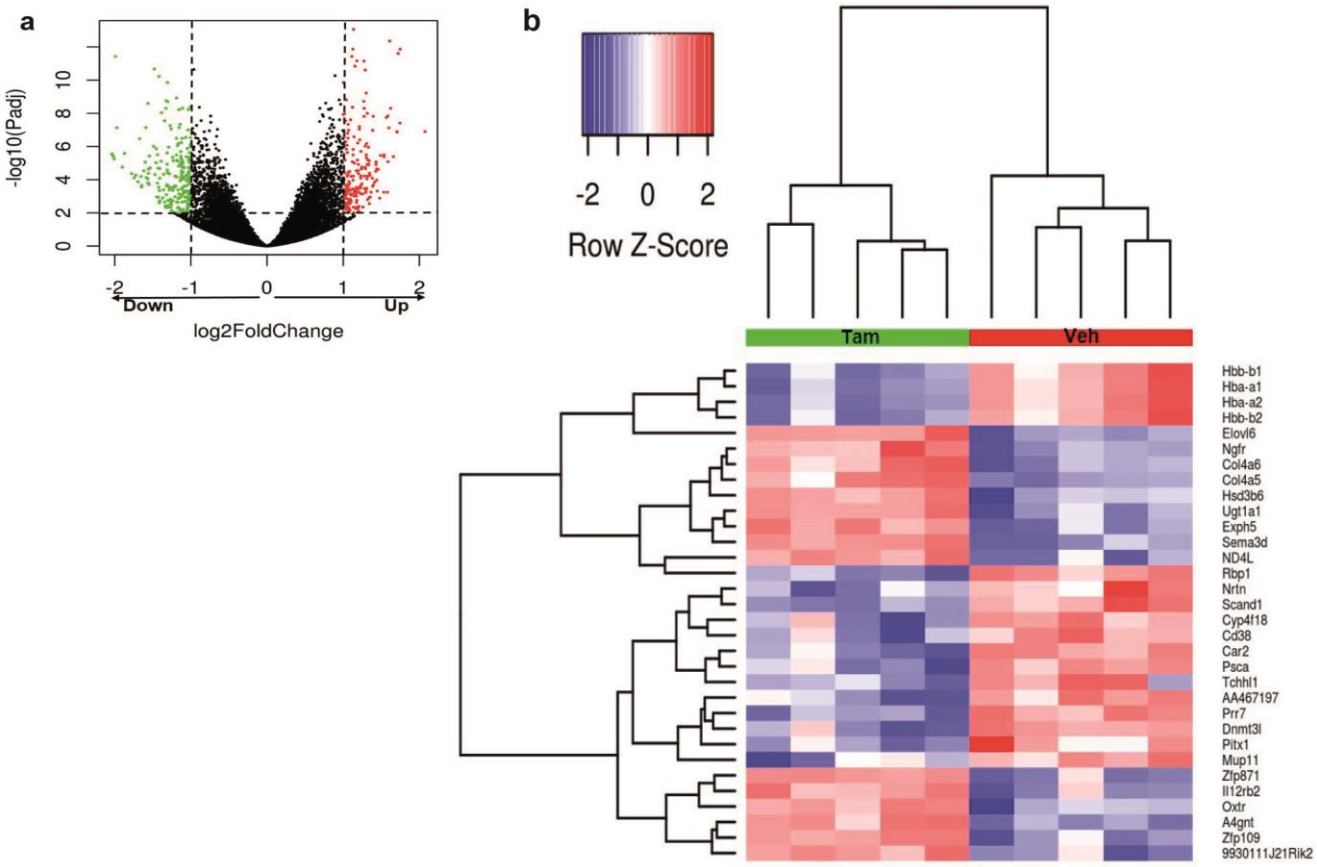

Figure 3. 21: Tam-induced DEGs by RNA-Seq.
a) Visualization of DEGs between Tam-treated and vehicle-treated mice by volcano plot. The colored dots represent DEGs. Green dots indicate down-regulated genes and red dots show up-regulated genes based on the cutoff of adjusted *P* value <0.01 and ≥1-FC. b). Heatmap demonstrates the 32 most differentially expressed genes (adjusted *P* value <0.001 and ≥2 FC) between Tam-treatment and vehicle-treatment. Tam treatment group is designated by green and vehicle by red color. Each row represents one gene transcript, and they were hierarchically clustered. 17 transcripts were downregulated while the 15 transcripts were upregulated in Tam-treated mice compared with vehicle. The red and blue colors on the heatmap indicate over-expressed and under-expressed genes respectively and the color intensity specifies the expression level.

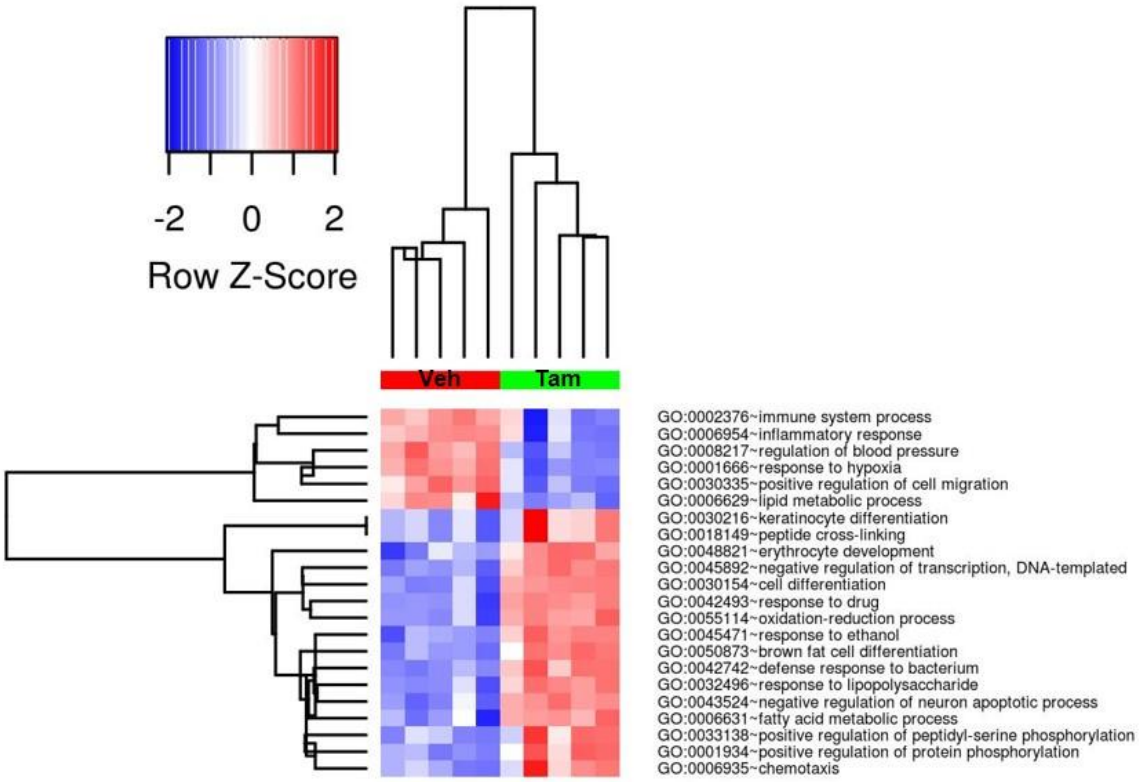

Figure 3. 22: Heatmap of GO enrichment analysis of the 488 DEGs.
Using the GO enrichment analysis of 488 DEGs, a total of 22 functionally enriched GO terms were investigated. Several biological processes such as immune system process, inflammatory response and cell migration are affected by Tam. Tam treatment group is represented by green color and vehicle by red color.

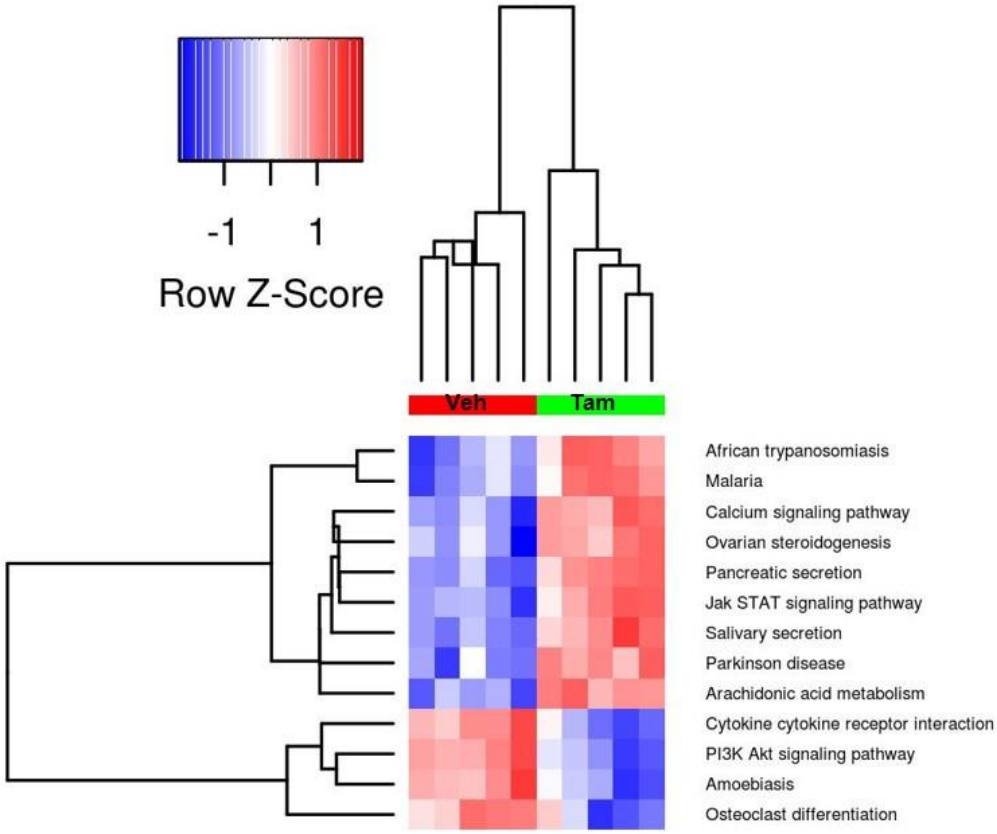

Figure 3. 23: Heatmap of KEGG enrichment analysis of the 488 DEGs.
Applying the KEGG enrichment analysis of 488 DEGs, 13 functionally enriched KEGG pathways were identified. Tam-treatment affects some signaling pathways including PI3K Akt and JAK/STAT signaling pathways. Tam treatment group is denoted by green color and vehicle by red color.

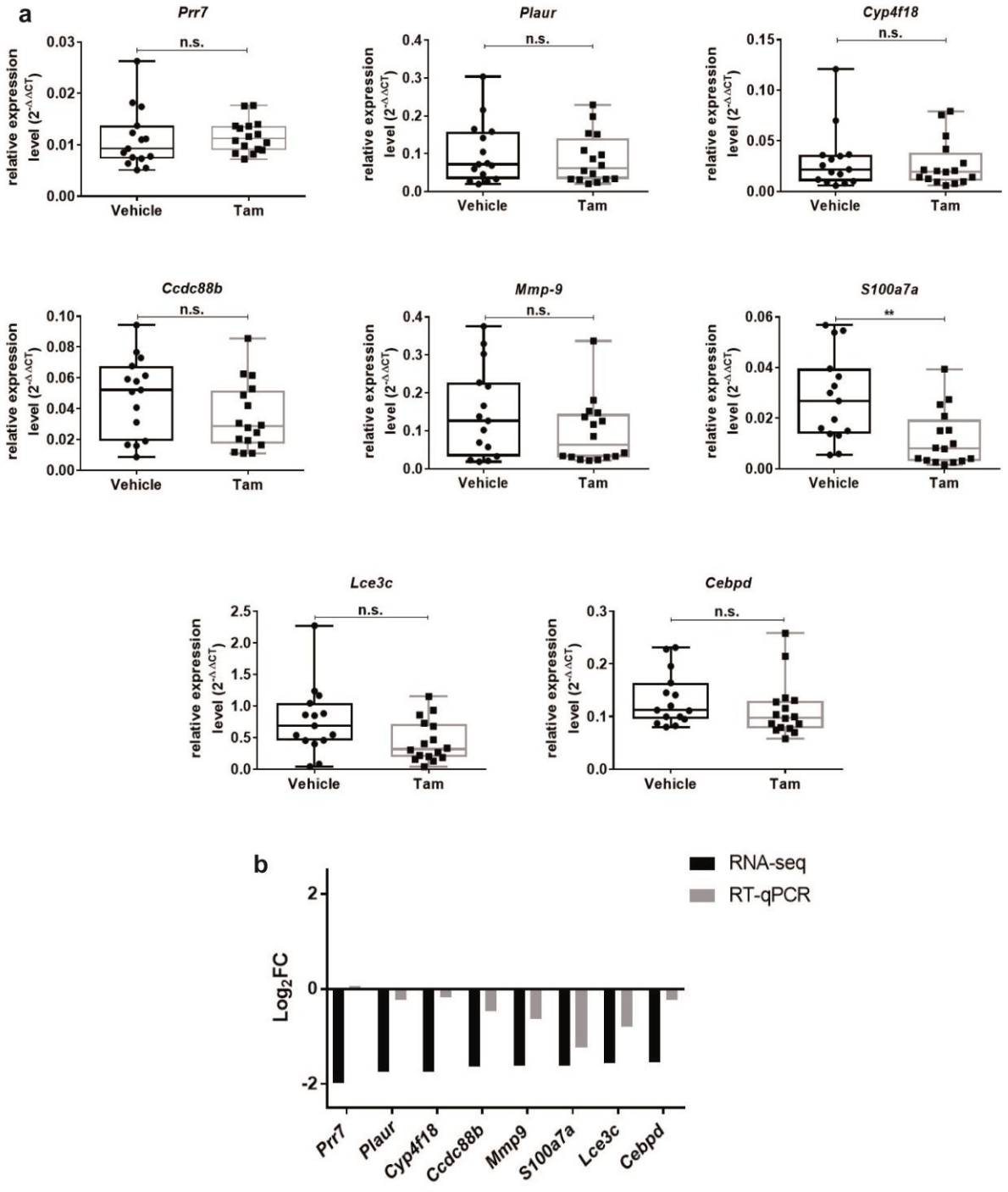

Figure 3. 24: Validation of RNA-Seq results by RT-qPCR.
In order to validate the acquired RNA-Seq results, an RT-qPCR assay was conducted for the 8 selected DEGs using a larger sample size. a) Results of the RT-qPCR for the 8 selected DEGs. b) RNA-Seq results were verified by RT-qPCR analysis. 7 out of 8 top DEGs demonstrated consistent expression levels in both RNA-Seq and RT-qPCR analyses. On the contrary, a differential expression level of *Prr7* was not detectable by RT-qPCR assay while it was amongst the most significantly DEGs in RNA-Seq analysis. Unpaired t-test or Mann-Whitney-U test, **p<0.01, n=16.

3.6 Apo and Tam combination treatment was considerably more efficacious than single treatment in reduction of disease severity in experimental EBA

Since in many diseases multiple signaling pathways are dysregulated, targeting multiple key proteins in different signaling pathways might be more efficacious than a drug targeting a single protein [243]. Drug combination therapy, a combination of two-or-three drugs with different mechanisms of action to treat a disease, is broadly used in clinical practice [243]. Combination therapy can generate a synergistic impact which leads to shorten treatment duration [244], to a reduction of required drug concentrations for each individual drug and/or a reduction of adverse events. Consequently, application of drugs in combination could heighten the success rate of drug repurposing screens [243].

I used Apo and Tam as the most effective candidate drugs in the experimental EBA (results 3.4.3 and 3.4.4), in order to investigate if combined Apo+Tam treatment is more efficient than treatment with either drug alone. To address this, one day before total anti-mCOL7 IgG injection (disease induction) mice were divided into 6 treatment groups:

i) Apo: Mice in this group subcutaneously received 10 mg/kg BW of Apo twice weekly.

ii) Apo vehicle: Mice were subcutaneously given 1X PBS, twice per week.

iii) Tam: 20 mg/kg BW of Tam were subcutaneously administered twice weekly.

iv) Tam vehicle: In this group, mice were treated with a subcutaneous injection of 5% DMSO (v/v) in 95% corn oil, twice a week.

v) Apo+Tam: Mice simultaneously received subcutaneous injections of 10 mg/kg BW of Apo and 20 mg/kg BW of Tam twice weekly.

vi) Apo+Tam vehicle: Mice were concurrently given a subcutaneous injection of 1X PBS and 5% DMSO (v/v) in 95% corn oil twice weekly.

Mice were treated for the entire duration of the experiment (until day 16) and the ABSA and body weight were recorded. Clinical EBA manifestation, presented as %ABSA, significantly declined in all individual and combination treatment groups compared with the corresponding vehicle groups (Figure 3.25 and 3.26a, b and c). However, combination treatment showed a more profound impact on disease reduction beginning from day 12 and reaching to its maximal effectiveness on day 16 (mean %ABSA of 4.1 ± 0.43 in relation to corresponding vehicle with a mean %ABSA of 10.7 ± 1.6) compared with Tam individual treatment (mean %ABSA of 7.0 ± 1.4 in comparison with mean %ABSA of 12.9 ± 1.5 in vehicle group) and Apo single treatment (mean %ABSA of 9.8 ± 1.8 in relation to vehicle group with mean %ABSA of 15.4 ± 1.6) (Figure3. 26a, b and c). Moreover, comparison of the disease magnitude on day 16 indicated that combined treatment markedly ameliorated the disease severity in relation to Tam-single treatment (p=0.037, two-way ANOVA; Figure 3. 26d) and Apo-individual treatment (p<0.0001, two-way ANOVA; Figure 3. 26d). Furthermore, histopathological analysis (Figure 3. 27a, b and c) of the back skin sections revealed that dermal leukocyte infiltration was significantly milder in both Apo single and Tam single treatment groups compared with their corresponding vehicle groups. Whereas, dermal leukocyte infiltration showed a slight but not significant decline in Apo+Tam treatment group in relation to the respective vehicle treated mice (Figure 3. 27a and d). Other histopathological characteristics such as epidermal thickness and blister formation did not differ between single-treatment and combined-treatment groups and the corresponding vehicle groups (data not shown). IF microscopic analysis demonstrated that rabbit IgG and murine C3 depositions at the DEJ were similar in all groups (Figure 3. 25). Of note, circulating mouse anti-rabbit, and rabbit anti-mCOL7C IgG levels were not significantly different between all treatment groups and the respective vehicle groups (data not shown). Relative body weight alterations remained identical between Apo- and Tam-single treatment groups and their corresponding vehicle groups (Figure 3. 28a and b). Even though, mice in Apo+Tam vehicle group gained 10% body weight, Apo+Tam treated mice retained their initial body weight during the entire time of the observation (Figure 3. 28c). Altogether, combination treatment of Apo and Tam attenuated the clinical but not

histological disease substantially more effective than Apo- and Tam-single treatments in experimental EBA.

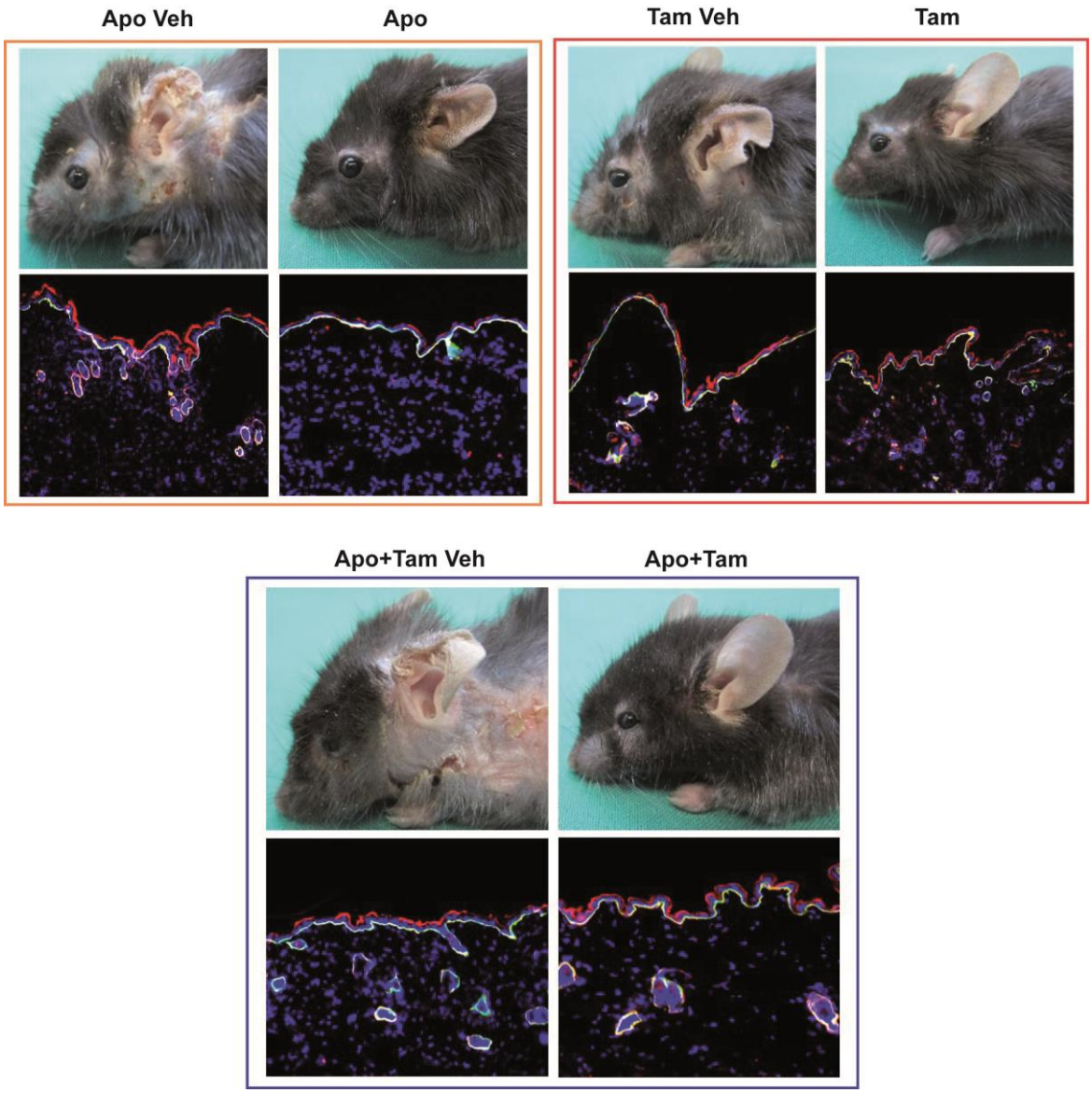

Figure 3. 25: Representative clinical and IF microscopic presentations from indicated treatment groups, on day 16.

One day before disease induction, mice received subcutaneous injections of Apo (10 mg/kg BW) or Tam (20mg/kg BW) or concomitant treatment of Apo (10 mg/kg BW)+Tam (20mg/kg BW) or respective vehicles on a twice weekly basis for the entire time of the experiment (until day 16). The corresponding vehicle groups were given 1X PBS or 5% DMSO (v/v) in 95% corn oil or simultaneous treatment of 1X PBS+5% DMSO (v/v) in 95% corn oil, respectively on the same route and frequencies of administration as drugs treatment groups. Disease was induced in mice using a subcutaneous 6 repetitive injections of 3.5 mg/20g BW of total anti-mCOL7 IgG. C3 (red) and IgG (green) depositions (merged to the yellow emission) were similar in all groups indicating the same disease induction in all mice. NC: negative control section is stained in the absence of anti-rabbit IgG and in the presence of the corresponding isotype control, rat anti-mouse IgG1.

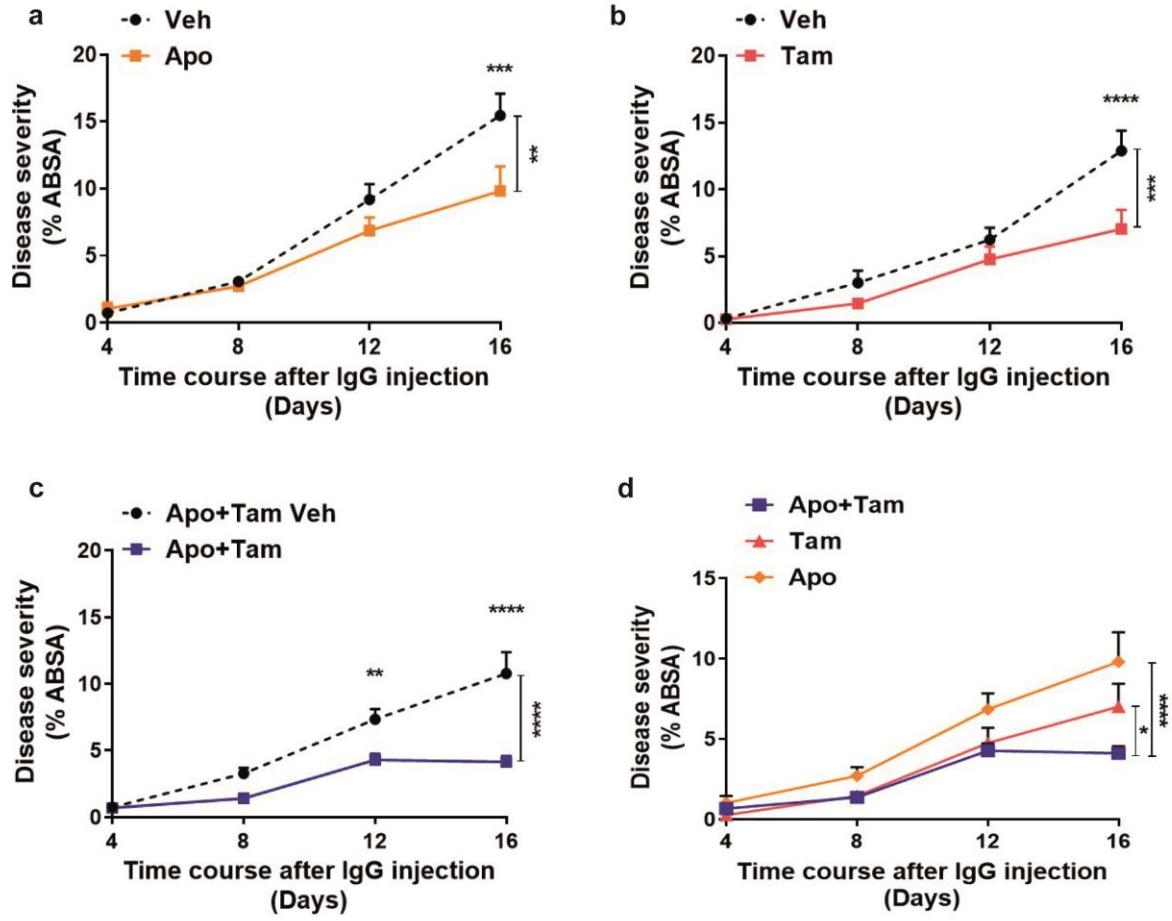

Figure 3. 26: Apo and Tam combination treatment more effectively ameliorated disease symptoms than Apo- and Tam-single treatments in Ab-transfer-induced model of EBA on day 16.

Disease severity represented as %ABSA. a and b) mice receiving a sole treatment of Apo or Tam demonstrated a significant diminished disease severity on day 16. c) While, a substantial alleviating activity of Apo+Tam treatment was started earlier (12 days after total IgG injection) than Apo- and Tam-single treatment. d) Concurrent treatment of Apo+Tam profoundly relieved disease symptoms in comparison with single-treatments on day 16. Two-way ANOVA, Sidak multiple comparison test, (*p < 0.05, **p < 0.01, ***p < 0.001, ****p <0.0001), mean (± SEM), n= minimum of 8 mice/group.

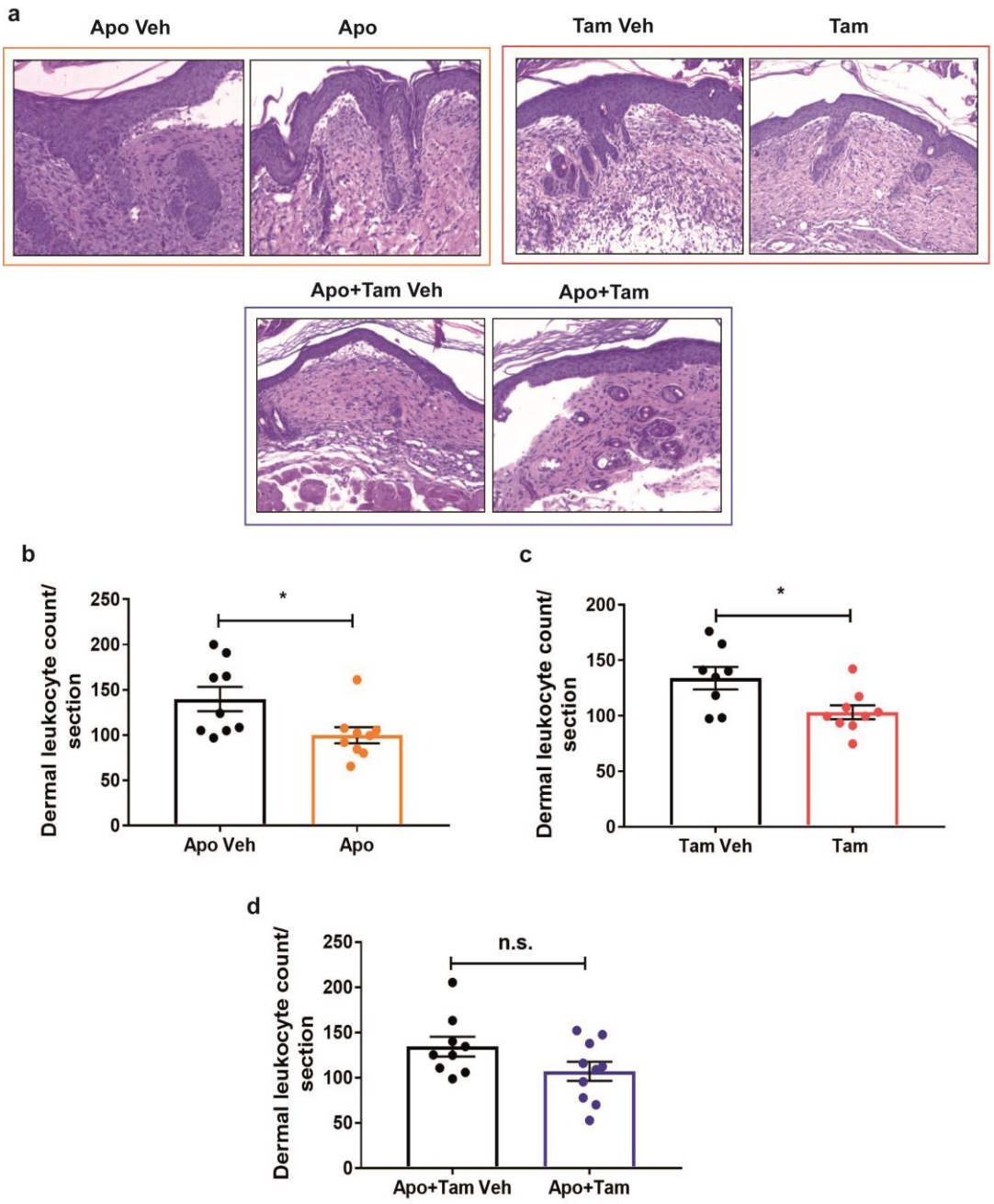

Figure 3. 27: Histological manifestations of the disease did not differ in combined treatment group and the corresponding vehicle.

a) Representative histopathological presentations in indicated treatment groups. Histopathological investigations revealed that no differences exist between drug treatment groups and their corresponding vehicle groups in terms of epidermal thickness and split formation. b and c) Apo- and Tam-single treatments induced a significantly milder dermal infiltration of the leukocytes in relation to their vehicle groups, d) while it was not the case for Apo+Tam treated mice. Unpaired t test (**p < 0.01), mean (± SEM), n= minimum 8 mice/group.

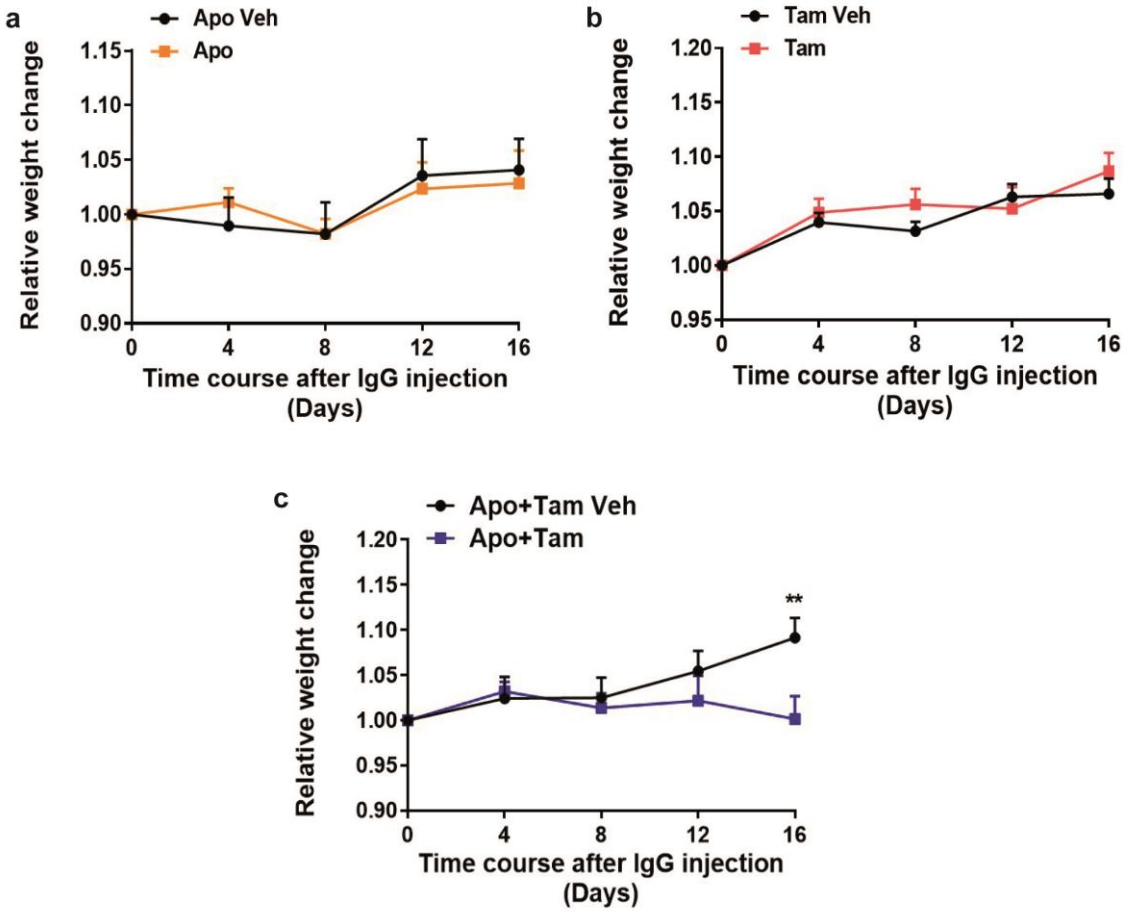

Figure 3. 28: Mice on Apo+Tam treatment did not gain weight during the observational course.

a and b) Mice on sole treatment of Apo and Tam had an identical body weight changes with their vehicle groups. c) Whereas mice in double treatment (Apo+Tam) maintained their initial body weight compared with the mice treated with the corresponding vehicle that significantly gained weight on day 16. Two-way ANOVA, Sidak multiple comparison test, (**p < 0.01, ***p < 0.001, ****p <0.0001), mean (± SEM), n= minimum 8 mice/group.

4 Discussion

Lack of consensus guidelines on the treatment of EBA, coupled with the absence of well-controlled clinical trials due to its rare prevalence, besides significant adverse effects of the current treatments which do not result in long-time remission makes the treatment of EBA a daunting task [40, 107]. Consequently, there is a pressing medical need to develop more effective and safer therapeutics. Despite the growing number of studies in order to find a new therapy for EBA, only some of them have been successfully tested in pre-clinical stages and currently await to move on to the confirmatory stages of clinical trials – such as dimethyl fumarate [245]. Repurposing existing drugs to find new therapeutic applications rather than their original indications will minimize the risk of failure of late-stage clinical trials due to toxicity and thus leads to faster drug approvals [163]. Most drug repurposing efforts are centered on computational approaches with a more focus on target prediction. Computer-aided drug repurposing has been utilized for target prediction for treatments of glioblastoma, lung cancer, breast cancer [246], coronary artery disease [247], neurodegenerative diseases [248], and some immune-based diseases such as RA [249, 250], psoriasis, AD, and alopecia areata [251]. However, only few research on cell-based drug repurposing has been attempted so far to ascertain therapies for prostate cancer [252], retinoblastoma [253], and neurodegenerative diseases such as sporadic amyotrophic lateral sclerosis (ALS) [254], Huntington's disease and Alzheimer's disease [255]. Since, most studies in the field of drug repurposing have focused on computer-aided approaches, one might argue that why here prior to the *in vitro* screens a target prediction was not performed. There are several good reasons for that, first and foremost, all aspects of the pathomechanisms of the autoimmune diseases, in particular, EBA is not well-defined and it can be, therefore, deduced that through computational drug repurposing all promising drugs cannot be captured. In addition, phenotypic drug repurposing may lead to identify novel pathway(s) in the pathogenesis of the disease. Furthermore, disease-based or phenotypic drug repurposing may be preferred to overcome missing knowledge in the pharmacology of a drug (e.g. unknown or additional targets) [256]. No studies have been reportedly conducted a drug repurposing in the context of AIBDs and

this study represents the first cell-based-focused drug repurposing for treatment of AIBDs.

My thesis mainly aimed at repurposing compounds from the PCL in order to identify potential new therapeutics for EBA patients. Evidence in support of my thesis' hypothesis comes from the study in which the same drug library, was utilized for the drug repurposing in search of the new anti-inflammatory agents for treatment of atopic dermatitis (AD). Although in that study, they employed an *in vivo* platform (zebrafish platform) for primary screening of the PCL, subsequently they also used a mouse model of an inflammatory skin disease for further *in vivo* validation. They utilized the ovalbumin-mediated epicutaneous mouse model of AD to reveal the promising anti-inflammatory use of the repurposed drugs for AD [169].

A brief overview of my thesis workflow is illustrated in Figure 4.1. In the first place to evaluate modulatory effects of the drugs (1,200 drugs from PCL) in the correct disease context, an *in vitro* PMN-based screening platform was utilized. Using ROS release assay, activation of the human iIC-stimulated PMNs in the presence of the drugs was assessed. The PCL was screened at 1 µM concentration and a 50% ROS inhibition was selected as cutoff criterion to select compounds with a potential PMN inhibitory effects. Using this approach, 33 (corresponding to a hit-rate of 2.75%) compounds (hits) met this pre-defined cutoff (Figure 3.1). Selection criteria for further *in vitro* validation were, dose dependent suppression of ROS as well as maintenance of ROS inhibition by iIC-stimulated PMNs at the concentration of 1 µM (concentration which had been used for primary screen) and showing no cytotoxic effect on PMNs (Figure 3.2 and 3.3). This step reduced the number of potential novel PMN inhibitory compounds to 6. In order to gain insights into the possible mechanisms underlying the PMN modulatory effects of the 6 candidate drugs, antioxidant capacity (Figure 3.5) and expression of the CD62L (PMN activation marker) on human PMNs (Figure 3.4) were determined. To confirm *in vivo* efficacy of the 6 candidate drugs (Amo, Au, Apo, Dob, Nic, and Tam), the Ab-transfer-induced EBA was used as a model of PD, as well as a prototype model of IC-induced, neutrophil-mediated autoimmune diseases. Here, mice treated with Amo, Apo, and Tam demonstrated a significant improvement of

clinical and histological disease symptoms compared with vehicle receiving mice. Interestingly, Tam (a selective estrogen receptor modulator) exerted its inhibitory activity across a wide dose range (Figure 3.16 and 3.17). Furthermore, by descriptive analysis, the therapeutic effect of Tam at 20 mg/kg, 2X/week was comparable to reference treatment (MP, 20 mg/kg/day). As the pharmacological target of Tam is known, I next evaluated whether the observed disease alleviating effect of Tam, was due to an on- or off-target effect. Tam treatment in both αERKO and βERKO mice failed to reduce disease symptoms compared with vehicle, while it was effective at disease reduction in WT mice in relation to vehicle. Therefore, I clearly demonstrated that the observed disease modifying effect of Tam is due to an interaction with the ER. Furthermore, lower clinical disease score, irrespective of the treatment, was observed in βERKO mice than the corresponding WT littermate controls (Figure 3.20). To obtain further insights into the potential mechanisms of Tam-mediated disease relieving activity, I next determined the Tam-induced gene expression signature in the skin of Tam-treated mice versus vehicle in experimental EBA. Comparison of the mRNA expression in Tam-treated mice with the vehicle group revealed 488 DEGs (cutoff of adjusted *P* value <0.01 and -1 > $\log_2$fold change > 1). By using a cutoff of adjusted *P* value <0.001 and -2 > $\log_2$fold change > 2, 32 genes were identified as the top DEGs, from which 8 genes were chosen for validation using RT-qPCR analysis. Of those, significant down-regulation of *S100a7a* in Tam treatment group versus vehicle was confirmed. Taken together, ameliorative impact of Tam in the Ab-transfer-induced model of EBA was mediated by ER pathway. Likewise, Tam leads to a down regulation of *S100a7a* gene whose overexpression has been previously shown in human psoriatic skin [242, 257] and the mouse model of acute dermatitis [239]. Strong up-regulation of two other proteins from S100 family (S100a8 and S100a9) has been previously reported in experimental EBA as well as EBA patients but their contributions to the EBA pathogenesis have not been shown [258]. I believe that Tam-induced down-regulation of *S100a7a* in the skin of the mice is a key factor in alleviating of the disease symptoms in experimental EBA and reduction of inflammation.

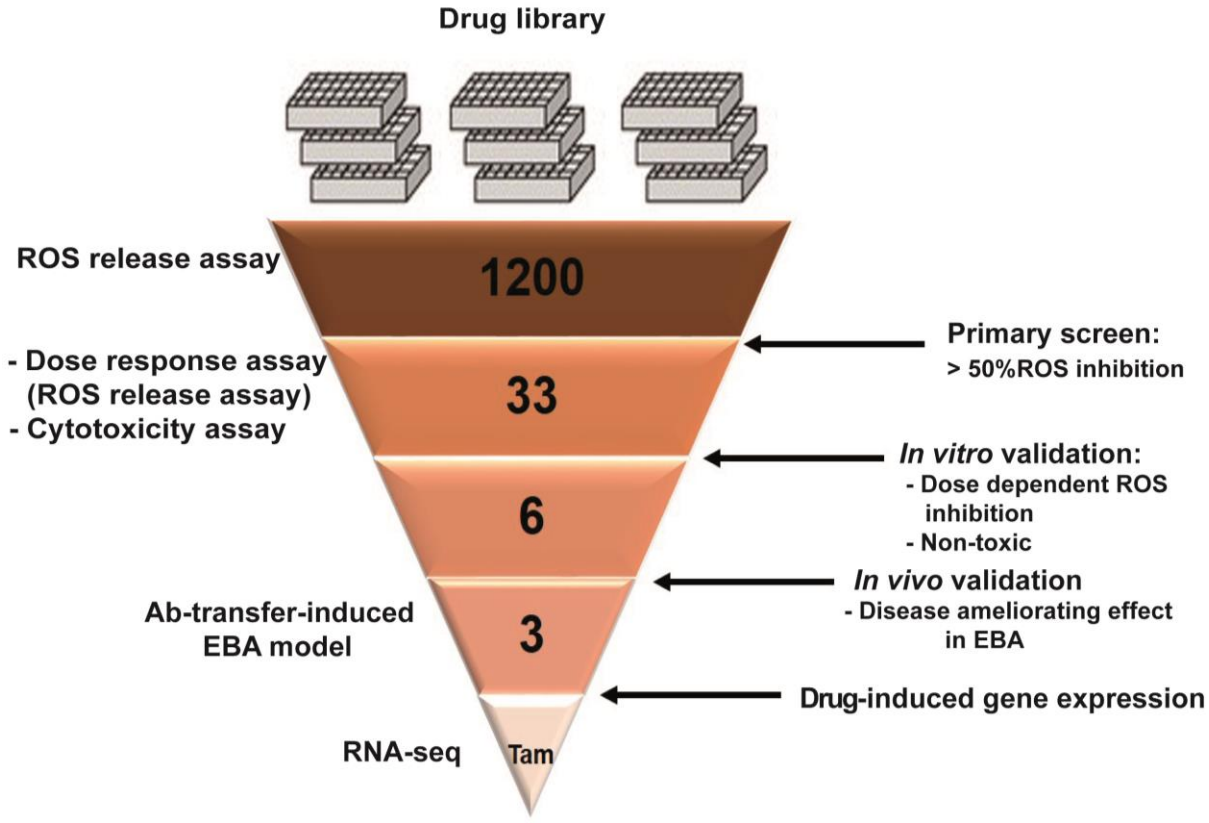

Figure 4. 1: A funnel representing step by step filtering procedures led to the selection of Tam as a potential drug for treatment of EBA.
Through all screening steps Tam was ultimately identified as the most active compound at disease reduction in the experimental EBA. Tam-induced gene expression signature was further revealed using RNA-Seq technology. Numbers indicate the number of drugs at each step.

4.1 Implementation of a primary screen and an *in vitro* validation in order to detect potential EBA therapeutics

In the effector phase of EBA pathogenesis, following binding of PMNs to ICs at the DEJ via their Fc-receptors, a signaling cascade is induced and leads to the stimulation of PMNs and generation of ROS which ultimately causes blister formation. In consequence, I hypothesized that drugs with the effect on PMN's ROS reduction would be potential drugs for the treatment of EBA. In the first part of this work, the PCL containing of 1,200 drugs was screened for its ability to modulate PMN's activity utilizing a relatively straightforward and robust measurable readout, such as ROS release. The PCL was chosen due to its high chemical and pharmacological diversity. Likewise, it encompasses off-patent FDA-approved drugs which decreases low-quality hits and makes it perfectly

appropriate for repurposing-focused screens [169]. The primary screen employing a luminol-enhanced chemiluminescence ROS release assay identified 33 promising drugs (hits) inhibiting iIC-induced PMN activation. None of those, have been previously used for treatment of the autoimmune diseases except for Au which was initially approved by the FDA for treatment of RA [259, 260]. Polymorphprep isolation method was opted here for PMN isolation since it is one of the fastest and the most economic approaches [261] which makes it a suitable method of choice for screening purpose. Notwithstanding, it possesses a variability in PMN purity and is more sensitive to day-to-day variation compared with other commonly-used methods , such as Ficoll density gradient centrifugation and anti-CD15 Ab-conjugated microbeads (positive selection) [261]. In addition, Polymorphprep isolation method used here, requires an erythrocyte lysis step which is considered as a potentially mild cell-activating procedure [261]. More importantly, donor-to-donor variation was also noticed in iIC-stimulated PMN-derived ROS release. Taking all factors mentioned above into account, PMN isolation method can affect screening outcomes meaning that using different method might have led to capture different hits. This can also explain why some drugs such as corticosteroids, that present in the library, with previously known PMN modulatory impacts did not unexpectedly appear in the primary screen.

Most drug screening efforts conducted in the field of PMN modulation, utilized zebrafish as an *in vivo* screening platform. For instance, Loynes and others studied the impact of a group of pharmacological agents (caspase inhibitors) on the resolution of inflammation using a transgenic line of zebrafish which has specifically labeled neutrophils (mpx:GFP) [262]. Another example of that is the study carried out by Wang *et al.* in which a natural product library consisting of 1,040 fungal extracts were screened for their inhibitory effects on PMN migration using the same transgenic zebrafish line (mpx:GFP) [263]. A new high-throughput screening (HTS) approach was exploited in a different study for screening of a library of 32,000 small-molecules to detect neutrophil exocytosis regulators using cell lysates. Twenty selected inhibitors were subsequently tested in a human PMN-based assay using an isoluminol-dependent chemiluminescence assay [264]. However, none of those studies utilized an FDA-approved drug library for

the screen. To date, the drug repurposing approach using an FDA-approved drug library to identify PMN modulatory compounds has only been directed by Hall and colleagues. They screened the PCL for identification of the drugs with inhibitory effects on PMN migration using the transgenic zebrafish (mpx:GFP) system. Thereafter, they suggested a conserved anti-inflammatory activity of their ten repurposed drugs in a mouse model of skin inflammation, AD. Consistent with my results, they also pinpointed Amo as a PMN modulatory agent in the PCL in different model system [169].

In the next step, the 33 promising drugs (hits) were subjected to an *in vitro* validation, which included dose-dependent ROS suppression and confirmation of the inhibitory activity on iIC-induced ROS release from PMN at the 1 μM dose, as well as non-toxic effects. After a two-hour incubation of the PMNs with drugs, the identical exposure time as they had in ROS release assay for primary screen, the cytotoxicity of the drugs was assessed by flow-cytometric analysis of AV and PI staining. At the tested concentration (1 μM), verteporfin showed the highest cytotoxicity amongst the 33 hits (Figure 3.3). It is an FDA-approved photosensitizer for the treatment of age-related macular degeneration [219]. Apoptosis-inducing effect of verteporfin has also been previously demonstrated in hepatocellular carcinoma [265], retinoblastoma [266] and acute lymphoblastic leukemia [267] cell lines. All in all, through *in vitro* validation, 6 compounds among the 33 met the defined criteria (non-toxicity, PMN-derived ROS inhibition in a dose-dependent manner and conserved effect at 1 μM dose) and have been chosen for further study. One possible reason for the low dose-response rate of the drugs could be the variability that exists from donor to donor. It is argued that dose response of a drug depends on several parameters such as high inter-subject variation, donor's state of the health and various number and affinity of the drug receptors on the cells [268, 269]. Low confirmation rate through hit validation process has been already reported in several studies. For instance, in the study performed by Wang *et al.* primary screen of a library of 1,040 crude fungal extracts in search of the PMN migration inhibitory compounds, led to identification of 35 hits. Of those, only two compounds produced consistent inhibitory effects in validation step [263].

To better understand whether the ROS perturbation by the 6 candidate drugs is due to their effect on the PMNs' function, expression level of a PMN's activation marker, CD62L, was evaluated in the exposure to the compounds. Overall, compared with vehicle, none of the 6 candidate drugs influenced the CD62L expression level on PMNs. In order to create a flow cytometric protocol to define human PMN activation state, 3 distinct markers (CD15, CD66b and CD62L) were used. From $CD15^{pos}$ parent population, $CD66b^{pos}CD62L^{neg}$ (activated PMNs) and $CD66b^{pos}CD62L^{pos}$ (resting PMNs) cells were identified. A possible reason for the unchanged PMN function in the presence of the 6 candidate drugs, may be due to the PMN isolation method (Polymorphprep). It has been shown that upon Polymorphprep isolation, expression levels of CD15 and CD66b on PMNs have been decreased compared with other isolation methods- Ficoll density gradient centrifugation and anti-CD15 Ab-conjugated microbeads. While, in the same study authors did not find any changes in the expression level of CD62L [261].

Ultimately, in order to further elucidate the possible mode of action underlying ROS inhibition of the 6 candidate drugs, a cell-free ROS release assay was performed which revealed 4 ROS scavengers amongst the candidate drugs. Taken together, the screening filtering procedures resulted in a list of 6 candidate drugs (0.5% of the PCL) namely Amo, Au, Apo, Dob, Nic and Tam for further *in vivo* interrogation. Of those, Au, a gold compound with an anti-inflammatory activity, was originally approved for treatment of RA [191]. Its use for treatment of psoriatic arthritis is reported as well [270]. Therefore, Au was used for *in vivo* validation as a proof-of-concept and a positive control. In addition, not much research thus far studied the effect of Au on the mouse models of autoimmune diseases.

4.2 *In vivo* validation of candidate drugs using an Ab-transfer induced model of EBA

Animal models are indispensable for translation of drug findings from bench to bedside and their emerged data are essential in predicting the clinical outcome for a specific drug [271]. Hence, on completion of *in vitro* screens, the *in vivo* efficacy of the candidate drug set was performed using the Ab-transfer-induced EBA, a

well-established *in vivo* model of PDs [26, 98, 272]. Of the 6 drugs, two (Dob and Nic) did not demonstrate any disease modifying activity at any time points during the entire course of the experiment.

Au treatment led to a significant improvement of the disease severity only on day 12 of the experiment in relation to the vehicle treatment (Figure 3.8). However, a reduction of the overall disease score (AUC) in mice receiving Au was not statistically profound. This observation might be attributed to Au's side-effects. It has been suggested that in patients on Au treatment, skin rashes account for 30% of all side-effects [273]. Therefore, the potential side effects of the drug which could directly interfere with correct interpretation of the factual drug efficacy in EBA model, can explain the underestimation of Au effectiveness in EBA model. Yet, I did not include a group of healthy mice treated with Au alone. Hence, the impact of Au on skin manifestations in the absence of EBA cannot be fully explained. However, due to the identification of the effective alternatives such as Apo and Tam, I did not further investigate potential skin adverse effect of Au. On the other hand, as expected, the histopathologic results provided evidence for Au's anti-inflammatory impact (Table 4.1, Figure 3.9). This finding was in agreement with those of Fujitsu *et al.* who reported the decreased histological changes in the knee joint of MRL/Mp-lpr/lpr (MRL/lpr) mice (animal model of SLE) treated with Au. In that study, Au was found to inhibit autoantibody production, polyclonal B cell activation and hypergammaglobulinemia [274]. Unexpectedly, Au had little suppressive effect on joint inflammation in an animal model of RA, collagen induced arthritis (CIA) [275]. Several mechanisms of action have been proposed for Au's anti-inflammatory properties such as modulation of MAPK, STAT3 [195] and inhibition of the activation of NF-κB [276] which lead to the reduction of key pro-inflammatory cytokines expressions for instance IL-1β, TNF-α [194].

Three drugs (Amo, Apo and Tam) exhibited a significant reduction in the clinical disease symptoms and in at least two of the parameters (dermal infiltration of leukocytes, epidermal thickness and split formation) used to measure histopathologic features of the disease in EBA model, when compared with vehicle (Table 4.1). Results obtained from Amo treatment is discussed below, while,

results obtained from Apo and Tam treatments will be comprehensively discussed later in this section.

Treatment of mice with Amo, an antimalarial agent, resulted in a clinically prominent amelioration of the disease symptoms on day 16 of the experiment (Figure 3.6) as well as a significant reduction in cumulative disease score throughout the experimental course (Table 4.1). To the best of my knowledge, its effect has not been demonstrated on any mouse models of the autoimmune diseases. Along with the clinical improvement, a significant milder leukocyte infiltration and reduced epidermal thickness were observed in Amo-treated mice in the experimental EBA (Figure 3.7). Amo's beneficial effects have been shown in modulating cancer, via suppression of autophagy [183], and chronic inflammatory diseases such as RA and SLE through its immunosuppressive activity [185, 186].

The mouse model used for the present study, Ab-transfer-induced EBA, is a very convenient tool for examining the impact of drugs in effector phase of the disease [98]. However, as was described earlier, for the disease induction mice received the repetitive injections of rabbit anti-mouse COL7 IgG which triggers an immune response towards the xenogenous antibodies [221]. In patients treated with not fully humanized therapeutic antibodies, production of function-blocking anti-drug antibodies (ADA) may impair the effectiveness of the therapeutic antibodies [277]. It is suggested that ADAs can block or bridge the therapeutic Abs which interfere with the therapy by inducing adverse events such as infusion reactions and may neutralize the effects of the therapeutic antibodies [278]. Based on aforementioned aspect, the murine anti-rabbit Abs may also interfere with the disease process in two ways: (a) An enhancement of the disease severity by binding to the rabbit anti-mouse COL7 IgG at the DEJ which leads to a strong recruitment of PMNs to the DEJ due to their murine nature. (b) Amelioration of the disease by neutralizing the rabbit anti-mouse COL7 IgG before binding to its target at the DEJ. Both assumptions are debatable, since B cell deficient JHT mice that lacked both circulating and tissue deposited murine anti-rabbit IgG, developed the similar skin lesions as WT mice in Ab-transfer-induced model of EBA and the difference in disease severity became visible only at later time point (day 19 of the experiment) [221]. To rule out the plausible interference of the mouse anti-rabbit

IgG in the Ab transfer-induced EBA mouse model, with the therapeutic effects of the candidate drugs, I evaluated the levels of both mouse anti-rabbit IgG and rabbit anti-mouse COL7 IgG in sera. In all experiments and for both antibodies, no significant differences were found between drug-treatment group and vehicle-receiving mice (excluding βERKO mice). Thus, the compounds did not mediate their impact through affecting the rabbit IgG half-life, or through modulation of the anti-rabbit IgG immune response in the mouse.

In order to check the toxicity of the candidate drug set in mice, weight of the mice was monitored throughout the experiments and results demonstrated that drug-treated mice in almost all groups either sustained their initial body weight or gained weight. In addition, it is demonstrated that experimental EBA is associated with either body weight loss or failure of gaining weight in mice [220]. Hence, body weight change was checked as a well-being factor of the mice throughout the course of the experiment. If the mice lost over 25% body weight and thus suffered from disease, they would be euthanized.

Ranking the candidate drugs by significance of effect on clinical and histological disease improvement, Apo and Tam (Table 4.1) were selected for further scrutiny with more focus on their effectiveness.

Table 4. 1: Summary of statistical analysis of the disease scores (AUC) and histopathologic parameters in treated mice with 4 candidate drugs relative to vehicle-treated controls.

	Disease severity (AUC)	**Leukocyte infiltration**	**Epidermal thickness**	**%Split**
	(*P*-value)	**(*P*-value)**	**(*P*-value)**	**(*P*-value)**
Apo	0.0045**	0.0231*	0.2109	0.0464*
Tam	0.0125 *	0.0019**	0.0126*	0.0008***
Amo	0.0346*	0.0094**	0.0161*	0.156
Au	0.1067	0.0088**	0.0644	0.0253*

After checking for data normality using Shapiro-Wilk test, either Mann-Whitney test or unpaired two-tailed t-test were utilized for calculation of *P*-values.

Through the *in vivo* validation, Apo was revealed as one of the two most potent drugs at alleviating clinical and histological disease in experimental EBA (Figure 3.10 and 3.11). Its prominent disease-ameliorating effect started on day 12 of the

experiment and reached to its maximal impact on day 16. In order to establish a probable dose dependent relationship of Apo's effect at improvement of EBA, 3 different dosing regimens were scheduled. Apo was given to the mice at a concentration of 10 mg/kg BW, once (Apo 1X/w) or twice (Apo 2X/w) or three times (Apo 3X/w) a week. Surprisingly, administration of Apo on twice-weekly basis was the solely effective dosing at both the clinical and histological levels (Figure 3.12 and 3.13). The observed lack of response at Apo 3X/w regimen could be interpreted as being a result of drug tolerance. Drug tolerance is defined as the phenomenon whereby the effect of a drug decreases following repeated administration, requiring an increase in dose to maintain the original level of efficacy [279]. In my view, testing the higher concentration of Apo than 10 mg/kg BW with the same frequency of administration (2X/week) could be a means of proving this assumption. What was more interesting regarding Apo's effect was the significant decrease of infiltrated leukocytes into the dermis of the mice in all groups of treatment regimens in comparison with vehicle (Figure 3.13). These results suggests that Apo may abate leukocyte migration into the dermis, though, mice on Apo 1X/w and Apo 3X/w treatment regimens showed severe disease symptoms despite the reduced inflammatory profile. It is difficult to explain this result, but it seems that even few number of the recruited leukocytes into the dermis are capable of inducing blister in skin of the mice treated with Apo (1x/w) and Apo (3x/w). It may be explained in this way that the infiltrated leukocytes have an activated phenotype and release contributing factors to blister formation such as ROS and proteases. Although ROS is suppressed by Apo, proteases are not blocked and they seem to be sufficient for induction of blister in the mice. Other histopathologic aspects (epidermal thickness and split formation) remained unchanged in all groups of treatment regimens in relation to the vehicle group. Apo is a dopamine-receptor agonist with high affinity for all known dopamine receptors (D1, D2, D3, D4, and D5). It has been used for treatment of different diseases including Parkinson's disease [188], erectile dysfunction [189], and alcohol dependency [190]. Since, expressions of dopamine receptors have been suggested on leukocytes [280], it is conceivable that the action of Apo contributes to its immunomodulatory effect. What has not yet studied is the impact of Apo on treatment of autoimmune diseases and its anti-inflammatory characteristics. The

present study seems to be the first report on the effect of Apo in the autoimmunity and in particular EBA as a paradigm of autoimmune diseases.

Tam, as a well-known SERM, is an estrogen agonist in some tissues, while in others the drug has antagonistic effects [204]. Tam has been used for adjuvant therapy of early-stage, estrogen-positive breast cancer for decades [281]. In the present study, Tam was identified as one of the two drugs with the most robust activity at mitigating clinical and histological disease in EBA. Profound alleviating effect of Tam treatment compared with vehicle was observable from day 12 of the experiment and reached to its highest effect on day 16 (Figure 3.14). Tam treatment was as effective as reference treatment control (MP) on day 16 of the experiment. Tam was the only compound among the 3 effective drugs that reduced all histologic features of the disease including leukocyte infiltration, epidermal thickness and DEJ separation (Figure 3.15). These results concur well with previous findings on the effects of Tam in ameliorating disease manifestations in several animal models of immune-mediated diseases such as SLE, contact dermatitis, ovalbumin-induced dermatitis and experimental autoimmune encephalomyelitis (EAE) [230-232, 282-286]. To confirm the efficacy of Tam in relieving disease symptoms in experimental EBA, three different concentrations (10 mg/kg BW or 20 mg/kg BW or 40 mg/kg BW, 2X/week) of the drug were used. A significant decline of the disease severity was demonstrated across all tested doses (Figure 3.16). Histopathologic examination of the H&E stained skin sections demonstrated that in mice receiving the highest dose of Tam, there was a prominent reduction in dermal leukocyte infiltration, epidermal thickness and split formation, which are all hallmarks of the disease. In the case of mice treated with 20 mg/kg BW of Tam, two histopathologic features (inflammation and epidermal thickness) were significantly decreased in comparison with vehicle-treated mice (Figure 3.17). On the other hand, compared with vehicle treatment group, mice on 10 mg/kg BW of Tam treatment did not show any improvement in histological features of the disease despite the significant reduction at clinical level (Figure 3.17). Extensive research has been carried out on Tam's effect in various mouse models of SLE. Sthoeger *et al*. showed that Tam (40 mg/kg BW, 2X/week) increased survival rate of the mice in experimental SLE (NZBxNZW F1 mice).

Furthermore, they demonstrated diminished proteinuria and production of IgG3 autoantibodies against nuclear extracts and DNA in mice on Tam-treatment [232]. In NZB/W F1 mice, that spontaneously develop a lupus-like disease, treatment with Tam (40 mg/kg BW, every 2 weeks) improved survival rate, reduced histopathological renal disease and decreased proteinuria [283]. In another study using 16/6 idiotype-induced model of SLE, no IC deposits in kidney sections of the mice treated with 40 mg/kg BW of Tam (2X/week) were seen and Tam delayed disease onset. Tam has been also shown to induce a reduction in numbers of splenic B-cells and serum levels of TNF receptors in these mice [231]. Using the same model of SLE (16/6 idiotype-induced model), Dayan *et al.* have suggested a beneficial effect of Tam treatment (40 mg/kg BW, 2X/week) on the clinical manifestation of the disease (decreased level of proteinuria, IC deposits in the kidney sections). They also reported diminished levels of IL-1 and TNF-α and elevated levels of IL-2, IL-4 and IFN-γ in mice that received Tam [230]. In other lupus-prone mice, MRL-lpr/lpr mice, Tam treatment at 2 different doses (10 or 40 mg/kg BW, every 2 weeks) improved survival rate and declined disease severity in both groups demonstrated by decreased proteinuria, aAbs (anti-double stranded DNA) and lymphadenopathy [284]. In another mouse model of chronic autoimmune disease, Bebo *et al.* examined the effects of Tam on EAE, the mouse model of MS. They observed a reduction in disease symptoms and degree of demyelination in mice treated with Tam. Furthermore, a suppressed myelin antigen specific T-cell proliferation in Tam-treated mice was observed. They also demonstrated that Tam impaired the ability of dendritic cells to stimulate myelin-specific T-cells and noted a shift in the T cell polarization towards a Th2 response in Tam treated animals [285]. In this study mice received a subcutaneous implantation of Tam at doses of 25 or 50 mg/mouse over a course of 14 or 20 days. Taken together, my findings on *in vivo* efficacy of Tam support those of the previous studies that have examined its effect on other animal models of autoimmune diseases. Accordingly, it strengthened the confidence that this drug is a potent treatment at mitigating several autoimmune diseases, now including experimental EBA.

Since Tam is a SERM, it is noteworthy to shortly describe the function and signaling pathways of ERs. Two types of ERs have been described in mammals, ERα and ERβ which are expressed in cells either as classic nuclear ERs, membrane-localized nuclear ERs, and/or membrane-bound G protein-coupled ER (GPER, also known as GPR30) [287]. After binding of estrogen to the ERs in the cytosol, a dimerization of ERs is induced leading to their translocation into the nucleus. Subsequently, they recruit coactivator/corepressor molecules and bind to their respective estrogen response elements (ERE) in the promoter of target genes and function as nuclear transcription factors, to alter transcription and expression of specific target hormone responsive genes [287]. Besides nuclear-initiated genomic signaling via ERα and ERβ localized inside nuclei, membrane-initiated non-genomic estrogenic signaling via membrane-bound ERs also occurs. These membrane-localized ERs are GPER or membrane isoforms of nuclear ERs [287]. The non-genomic ER signaling starts at membrane, activates several kinase cascade pathways and triggers intracellular signaling, and subsequently induces multiple actions such as gene transcriptions. Binding of estrogens to non-nuclear ERs may induce several intracellular signaling kinase cascade pathways, including stimulation of adenylyl cyclase activity and cAMP-dependent protein kinase (PKA) pathway, mobilization of intracellular Ca^{2+}-dependent protein kinase (PK) C pathway, activation of ERK/ MAPK pathway, and activation of receptor tyrosine kinase (RTK) and PI3K/Akt signaling pathway [287]. An alternative ER signaling pathway is ligand-independent signaling in which ERs can be activated in the absence of estrogen. Phosphorylation of the ERs or their associated co-regulators can cause ligand-independent ER activation. Signaling pathways responsible for this modulation include regulators of general cellular phosphorylation state, such as PKA or PKC, extracellular signals such as peptide growth factors, cytokines or neurotransmitters and cell cycle regulators [288]. The expression of ERs on both the lymphoid and myeloid cells has been shown. Estrogen influences immune cells as a growth and differentiation factor with impacts on hemopoiesis, lymphocyte activation, Th polarization, and cytokine production [289]. SERMs, ER-binding compounds, can compete with estrogen and act as either agonists or antagonists of ER function in a tissue-dependent manner [289]. Interestingly, in some studies, the immunomodulatory effects of Tam has

been attributed to the ER-independent pathways as its immunomodulation was not fully reversed by concomitant treatment of 17beta-estradiol [285, 290]. In the present study, in order to address the question whether the ameliorative effect of Tam in experimental EBA is mediated by either ER-dependent or ER-independent pathway, ER-deficient (αERKO or βERKO) mice were utilized. KO mice and their wildtype (WT) littermate controls received either Tam or vehicle. Indeed, significantly alleviated disease symptoms were observed in WT mice treated with Tam in relation to vehicle. Nevertheless, the disease severity in KO mice were unaffected upon treatment with Tam compared with vehicle suggesting that Tam requires the ER-mediated signaling pathway to attenuate the disease severity in the experimental EBA (Figure 3.18). This is in line with previous findings by Dayan *et al.* who showed an ER-dependent mechanism of action for disease alleviating activity of Tam in mice afflicted with experimental SLE. They treated mice with either Tam or a monoclonal anti-estradiol Ab (anti-E2) and they found an equal beneficial effect in clinical manifestation of experimental SLE in both treatment groups. They therefore proposed that the ameliorative impact of Tam on the clinical disease is mediated via its ER-mediated mechanism of action [230]. Moreover, an *in vitro* study on development of murine bone-marrow derived dendritic cells (BMDCs), has indicated that differentiation of BMDC from GM-CSF-stimulated precursors was promoted by the presence of E2 in the culture medium. This effect was counteracted by Tam demonstrating that Tam impairs murine BMDC differentiation and activation in an ER-dependent mechanism [291]. Taken together, on the basis of previous findings and the result of the present study, this conclusion can be supported that Tam exerts its immunomodulation activity in experimental EBA through a ligand (ER)-dependent pathway. Interestingly, comparison of the disease magnitude between WT and ERKO mice, irrespective of the treatment, revealed a significantly decreased disease severity in βERKO mice. Whereas, αERKO mice developed identical disease severity to the WT littermates (Figure 3.20). This result appears to provide evidence for possible involvement of βER in disease induction in experimental EBA. An independent experiment excluding Tam treatment is required to test this hypothesis. There is no studies to show a protective effect of ERβ deficiency in induction of any mouse models of autoimmune diseases.

4.3 Identification of Tam-induced gene expression signature

In order to obtain insights into the mechanism underlying the disease-alleviating activity of Tam, drug-induced gene expression profile was contrasted between vehicle and Tam treated mice with experimental EBA. Following treatment of mice with either Tam or vehicle, skin specimens (ear) were harvested, RNA was purified and RNA-Seq was conducted. The results revealed the 488 DEGs (cutoff of adjusted *P* value <0.01 and ≥1 FC) in Tam-treatment group compared with the vehicle-treatment (Figure 3.21). The DEGs were mostly contributed to the immune system, inflammatory response, and cell migration processes and they were also involved in PI3K Akt, JAK/STAT, and calcium signaling pathways (Figure 3.22 and 3.23). Amongst the 32 most differentially expressed genes (cutoff of adjusted *P* value <0.001 and ≥2 FC), eight genes, *Prr7*, *Plaur*, *Cyp4f18*, *Ccdc88b*, *Mmp9*, *S100a7a*, *Lce3c* and *Cebpd* selected for further interrogation using RT-qPCR analysis, a significant down-regulation of *S100a7a* was confirmed by RT-qPCR analysis in Tam treatment in comparison with vehicle (Figure 3.24). S100 proteins, the small calcium-binding proteins, comprise the largest multi-genic family of calcium-binding EF-hand proteins [242]. Besides their importance in intracellular calcium-signaling cascade, they take roles as chemo-attractants and antimicrobials which make them the putative players in keratinocyte differentiation, inflammation, pathogen defense and thus to be pivotal in the pathogenesis of inflammatory skin diseases [242]. When released to the extracellular space, S100 proteins have crucial activities in the regulation of immune homeostasis, post-traumatic injury, and inflammation [292]. S100 proteins trigger inflammation through interacting with receptor for advanced glycation end products (RAGE) and TLR4. Upon binding to TLR4, an NF-κB-dependent signaling pathway initiates and regulates inflammation, cell proliferation, differentiation [292]. By interacting with RAGE, S100 proteins activate NF-κB, induce the production of pro-inflammatory cytokines leading to the migration of neutrophils, monocytes, and macrophages. In addition to the NF-κB pathway, MAP kinase-mediated signaling is also induced by S100 proteins (Figure 4.2) [292]. Elevated levels of two members of S100 protein family, S100a8 and S100a9, in sera of the EBA and BP patients as well as mouse models of these diseases have been previously demonstrated. Their increased

expressions in skin of the experimental AIBD were also observed, however, gene-specific KO mice showed equal disease to that of WT. These findings suggested that S100a8 and S100a9 proteins do not contribute to the pathogenesis in the effector phase of experimental EBA and BP [258].

S100a7a (S100A15 or Koebnerisin), another member of S100 protein family, was identified here as a target gene whose expression was significantly down-regulated by Tam treatment compared with vehicle. This result correlates favorably well with previous findings demonstrating an overexpression of S100a7a in psoriasis and chronic atopic eczema patients [242]. S100a7a was first identified in psoriatic skin [293]. Its expression in cultured human keratinocytes is strongly induced upon treatment with pro-inflammatory cytokines such as TNF-α, IFN-γ and IL-1β suggesting that the pro-inflammatory milieu in inflamed skin contributes to S100a7a overexpression [242]. In experimental EBA, in addition to a strong Th1-like cytokine profile in dLN [71], the importance of several pro-inflammatory cytokines, including GM-CSF [126], TNF-α [135] and IL-1β [136], at initiation of leukocyte extravasation has been previously pointed out. On the other hand, several possible mechanisms of Tam's action have been thus far suggested [294]. One of those is perturbation of non-genomic pathway of ER signaling. Through binding to the ERs, Tam inhibits protein kinase-C (PKC) which leads to the suppression of PKC/MEK/ERK and PKC/PI3K/Akt pathways [295]. Activation of some of aforementioned signal transduction factors (PI3K β and δ [145, 147], AKT, ERK1/2 [148]) in PMNs in the EBA pathogenesis have been previously shown. Based on all these findings, as well as the capability of Tam at induction of a Th2-polarized immune response [285, 290], the immunomodulatory effect of Tam in experimental EBA can be proposed as follows. Binding of the anti-COL7 Abs to their target at the DEJ in the skin, is followed by a deposition of the complement and release of lipid mediators and pro-inflammatory cytokines (Th1-cytokine profile). The pro-inflammatory milieu leads to the overexpression of *S100a7a* from keratinocytes and leukocytes [296] amplifying the infiltration of leukocytes, particularly PMNs [137] to the inflamed skin which leads to the exacerbation of the disease. On the other hand, Tam treatment via suppression of PI3K β and δ, AKT, ERK1/2 [295] in leukocytes (PMNs) and skewing immunity towards a Th2-

dominated response [285, 290] leads to a decreased production of pro-inflammatory cytokines. Subsequently, it leads to a reduced expression of *S100a7a* diminishing migration of leukocytes into the skin which was evident in the skin of the mice treated with Tam (Figures 3.15 and 3.17).

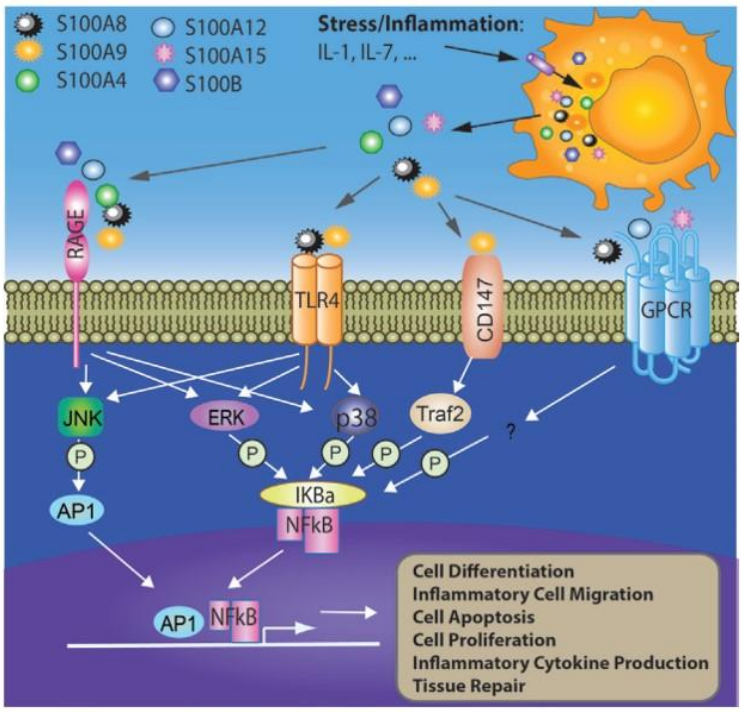

Figure 4. 2: S100 proteins are contributed to the stress and inflammation-mediated responses.
For details see the text above. From [292]

4.4 Combination treatment with Apo and Tam more significantly attenuated experimental EBA in relation to single-treatments

Combined treatment with two or more compounds possessing different mechanisms of action is an alternative approach to enhance the success rate of drug repurposing. If each of the drugs perturbs a different target or signaling pathway, their combination can exert a synergistic effect which results in reduction of required drug amount for each individual drug [243] or reduction of treatment duration [244]. Moreover, recognition of the effective synergistic drug combination enables us to better understanding of the complicated disease pathophysiology and to find better treatment options for the disease [243]. For all above-mentioned reasons, combination treatment of Apo and Tam (Apo+Tam) or their respective

vehicle were performed in mice one day prior to induction of the experimental EBA. Treatment of the mice with single drugs and their corresponding vehicles were concurrently conducted. Dual treatment of Apo+Tam more effectively attenuated the clinical disease than single treatments of Apo and Tam (Figure 3.25 and 3.26). Contrary to expectations, dermal leukocyte infiltration in the skin sections of the mice receiving combined treatment did not show any significant difference compared with the vehicle. Even though, in mice on single treatments a significantly milder infiltration of leukocytes into the dermis was found in comparison with vehicle. Collectively, these findings imply that concomitant treatment of Apo with Tam had a synergistic/additive impact at amelioration of clinical symptoms of the experimental EBA, however, histological examination showed no significant changes when compared with vehicle. Table 4.2 summarizes all clinical and histological findings in combined- and single-treated mice compared with the corresponding vehicle groups in experimental EBA. Combination therapy have been reportedly used for treatment of EBA patients. The most commonly used first line combination treatment for EBA is prednisolone (1.0-2.0 mg/kg/d) tapering + azathioprine or mycophenolate mofetil (MMF) [107]. Treatment of EBA patients with combination of rituximab (RTX) and immunoadsorption (IA) might provide an effective treatment protocol in EBA [297-299]. Combination of IVIG with dapsone or colchicine have achieved clinical improvement in several studies [153]. In a retrospective study of 30 EBA patients who were primarily treated with a combination of methylprednisolone, dapsone and colchicine (6 patients who did not respond, were subsequently treated with other immunosuppressants), 8 among 24 patients (33%) achieved complete remission and 5 amongst 24 (21%) achieved partial remission within 1 year [108].

Table 4. 2: Effects of concomitant treatment of Apo with Tam and their single treatments on clinical and histological disease severity in Ab-transfer-induced EBA.

	Disease score (Mean at peak)	Cumulative disease score (AUC)	Infiltration (Leukocyte count)	%Split	Epidermal thickness (µm)
Apo+Tam	4.13 ± 0.43	46.6 ± 3.6	107.1 ± 10.56	19.22 ± 3.99	93.48 ± 10.44
Apo+Tam Veh	10.78 ± 1.6	89.62 ± 8.16	134.3 ± 11	36.52 ± 7.86	139.4 ± 19.85
Apo	9.82 ± 1.84	83.48 ± 10.57	99.78 ± 8.92	21.37 ± 4.68	126.2 ± 18.98
Apo Veh	15.46 ± 1.63	108.9 ± 9.53	139.8 ± 13.41	37.62 ± 6.58	146.2 ± 18.52
Tam	7.03 ± 1.43	53.2 ± 9.13	103.2 ± 6.24	25.13 ± 6.6	122.1 ± 26.63
Tam Veh	12.9 ± 1.51	83.47 ± 9.75	133.9 ± 10.06	27.64 ± 7.78	113.6 ± 11.6

Data are represented as mean ± SEM and are from 9 mice per group.

4.5 Summary

Having screened the Prestwick chemical library (PCL) in search of the new therapeutics for Epidermolysis bullosa acquisita (EBA), six compounds (amodiaquine (Amo), apomorphine (Apo), auranofin (Au), dobutamin (Dob), niclosamide (Nic) and tamoxifen (Tam)) were identified through a PMN-based screening approach. These compounds inhibited IIC induced ROS release from PMNs, key drivers of tissue injury and inflammation in EBA. Subsequently, an *in vivo* validation of the candidate drugs (Amo, Apo, Au, Dob, Nic and Tam) using the Ab-transfer-induced model of EBA, revealed three drugs (Amo, Apo and Tam) with the clinical and histological disease-relieving impacts on the experimental EBA. Additional *in vivo* validation of Apo and Tam, as the more effective drugs at ameliorating clinical outcomes and disease-associated histopathological features, suggested that their combination exerted a synergistic or additive effects on diminution of clinical disease symptoms. Due to the most potent impact of Tam in the *in vivo* validation coupled with its known pharmacological target (selective estrogen receptor modulator, SERM) along with its unclear immunomodulatory effect in inflammatory diseases, I next evaluated the mechanisms of Tam-mediated alleviation of clinical disease in experimental EBA. First, I here show that in estrogen-receptor deficient mice (αERKO and βERKO) mice, Tam had no effect on the clinical manifestation of EBA. Furthermore, ERβ deficient mice show a reduced clinical phenotype when compared with wild type littermate controls. Taken together this suggests that the effects of Tam in EBA are mediated by ER signaling pathway. Second, when contrasting Tam-induced gene expression profile with vehicle, PI3K/Akt signaling pathway whose contributing role to EBA pathogenesis has been previously described, was revealed as the most significantly down-regulated pathway. Moreover, the results showed that Tam treatment leads to a substantial down-regulation of *S100a7a*, whose over-expression has been found in the skin inflammatory diseases. Collectively, I here identified Tam as a potential therapeutic that could be used in the treatment of EBA, and possibly also other diseases with a similar pathogenesis, such as bullous pemphigoid.

5 References

1. Griffiths, C., et al., *Rook's Textbook of Dermatology, 4 Volume Set*. 2016: John Wiley & Sons.
2. Pasparakis, M., I. Haase, and F.O. Nestle, *Mechanisms regulating skin immunity and inflammation.* Nature Reviews Immunology, 2014. **14**(5): p. 289-301.
3. Nestle, F.O., et al., *Skin immune sentinels in health and disease.* Nature Reviews Immunology, 2009. **9**(10): p. 679-691.
4. Eckhart, L., et al., *Cell death by cornification.* Biochimica et Biophysica Acta (BBA)-Molecular Cell Research, 2013. **1833**(12): p. 3471-3480.
5. Woodley, D.T. and S. McNutt, *The Basement Membrane Zone at the Dermal—Epidermal Junction of Human Skin*, in *Epidermolysis Bullosa*. 1992, Springer. p. 19-36.
6. Bruckner-Tuderman, L. and C. Has, *Disorders of the cutaneous basement membrane zone—The paradigm of epidermolysis bullosa.* Matrix Biology, 2014. **33**: p. 29-34.
7. Villone, D., et al., *Supramolecular Interactions in the Dermo-epidermal Junction Zone ANCHORING FIBRIL-COLLAGEN VII TIGHTLY BINDS TO BANDED COLLAGEN FIBRILS.* Journal of Biological Chemistry, 2008. **283**(36): p. 24506-24513.
8. Burgeson, R.E. and A.M. Christiano, *The dermal—epidermal junction.* Current opinion in cell biology, 1997. **9**(5): p. 651-658.
9. Woodley. Available from: https://www.uptodate.com/contents/epidermolysis-bullosa-acquisita.
10. Freinkel, R.K. and D.T. Woodley, *The biology of the skin*. 2001: CRC Press.
11. Streilein, J.W., *Skin-associated lymphoid tissues (SALT): origins and functions.* Journal of Investigative Dermatology, 1983. **80**.
12. Di Meglio, P., G.K. Perera, and F.O. Nestle, *The multitasking organ: recent insights into skin immune function.* Immunity, 2011. **35**(6): p. 857-869.
13. Schmidt, E. and D. Zillikens, *The diagnosis and treatment of autoimmune blistering skin diseases.* Deutsches Ärzteblatt International, 2011. **108**(23): p. 399.
14. Hammers, C.M. and J.R. Stanley, *Mechanisms of disease: pemphigus and bullous pemphigoid.* Annual Review of Pathology: Mechanisms of Disease, 2016. **11**: p. 175-197.
15. Iwata, H., et al., *Animal models to investigate pathomechanisms and evaluate novel treatments for autoimmune bullous dermatoses.* Current pharmaceutical design, 2015. **21**(18): p. 2422-2439.
16. Stanley, J.R., *Pemphigus and pemphigoid as paradigms of organ-specific, autoantibody-mediated diseases.* The Journal of clinical investigation, 1989. **83**(5): p. 1443-1448.
17. Chiorean, R., M. Mahler, and C. Sitaru, *Molecular diagnosis of autoimmune skin diseases.* Rom J Morphol Embryol, 2014. **55**(3 Suppl): p. 1019-1033.
18. Witebsky, E., et al., *Chronic thyroiditis and autoimmunization.* Journal of the American Medical Association, 1957. **164**(13): p. 1439-1447.
19. Rose, N.R. and C. Bona, *Defining criteria for autoimmune diseases (Witebsky's postulates revisited).* Immunology today, 1993. **14**(9): p. 426-430.
20. Anhalt, G.J., et al., *Induction of pemphigus in neonatal mice by passive transfer of IgG from patients with the disease.* New England Journal of Medicine, 1982. **306**(20): p. 1189-1196.
21. Ujiie, H. and H. Shimizu, *Evidence for pathogenicity of autoreactive T cells in autoimmune bullous diseases shown by animal disease models.* Experimental dermatology, 2012. **21**(12): p. 901-905.
22. Takahashi, H., et al., *Desmoglein 3–specific CD4+ T cells induce pemphigus vulgaris and interface dermatitis in mice.* The Journal of clinical investigation, 2011. **121**(9).
23. Amagai, M., et al., *Antibodies against desmoglein 3 (pemphigus vulgaris antigen) are present in sera from patients with paraneoplastic pemphigus and cause acantholysis in vivo in neonatal mice.* The Journal of clinical investigation, 1998. **102**(4): p. 775-782.

24. Zillikens, D., et al., *Antibodies to desmogleins 1 and 3, but not to BP180, induce blisters in human skin grafted onto SCID mice.* The Journal of pathology, 2001. **193**(1): p. 117-124.
25. Chiriac, M.T., et al., *Passive transfer of collagen XVII-specific antibodies induces sustained blistering disease in adult mice.* Orphanet journal of rare diseases, 2013. **8**(1): p. 17.
26. Sitaru, C., et al., *Induction of dermal-epidermal separation in mice by passive transfer of antibodies specific to type VII collagen.* The Journal of clinical investigation, 2005. **115**(4): p. 870-878.
27. Woodley, D.T., et al., *Induction of epidermolysis bullosa acquisita in mice by passive transfer of autoantibodies from patients.* Journal of Investigative Dermatology, 2006. **126**(6): p. 1323-1330.
28. Heppe, E.N., et al., *Experimental laminin 332 mucous membrane pemphigoid critically involves C5aR1 and reflects clinical and Immunopathological characteristics of the human disease.* Journal of Investigative Dermatology, 2017. **137**(8): p. 1709-1718.
29. Marietta, E., et al., *A new model for dermatitis herpetiformis that uses HLA-DQ8 transgenic NOD mice.* The Journal of clinical investigation, 2004. **114**(8): p. 1090-1097.
30. Hirose, M., et al., *Repetitive immunization breaks tolerance to type XVII collagen and leads to bullous pemphigoid in mice.* The Journal of Immunology, 2011. **187**(3): p. 1176-1183.
31. Sitaru, C., et al., *Induction of complement-fixing autoantibodies against type VII collagen results in subepidermal blistering in mice.* The Journal of Immunology, 2006. **177**(5): p. 3461-3468.
32. Yancey, K.B., *The pathophysiology of autoimmune blistering diseases.* Journal of Clinical Investigation, 2005. **115**(4): p. 825.
33. Vorobyev, A., R.J. Ludwig, and E. Schmidt, *Clinical features and diagnosis of epidermolysis bullosa acquisita.* Expert review of clinical immunology, 2017. **13**(2): p. 157-169.
34. MBL. Available from: https://www.mblintl.com/products/skin-blistering-diseases.
35. Chen, M., et al., *Epidermolysis bullosa acquisita: autoimmunity to anchoring fibril collagen.* Autoimmunity, 2012. **45**(1): p. 91-101.
36. Elliott, G., *Two cases of epidermolysis bullosa.* J Cutan Genitourin Dis, 1895. **13**: p. 10.
37. Kablitz, R., *Ein Beitrag Zur Frage der Epidermolysis bullosa (hereditaria et acquisita).* Dissertation, 1904.
38. Gupta, R., D.T. Woodley, and M. Chen, *Epidermolysis bullosa acquisita.* Clinics in dermatology, 2012. **30**(1): p. 60-69.
39. Kasperkiewicz, M., et al., *Epidermolysis bullosa acquisita: From pathophysiology to novel therapeutic options.* Journal of Investigative Dermatology, 2016. **136**(1): p. 24-33.
40. Ludwig, R.J., *Clinical presentation, pathogenesis, diagnosis, and treatment of epidermolysis bullosa acquisita.* ISRN dermatology, 2013. **2013**.
41. Hübner, F., et al., *Prevalence and age distribution of pemphigus and pemphigoid diseases in Germany.* Journal of Investigative Dermatology, 2016. **136**(12): p. 2495-2498.
42. Guerra, L., et al., *Childhood epidermolysis bullosa acquisita during squaric acid dibutyl ester immunotherapy for alopecia areata.* British Journal of Dermatology, 2017. **176**(2): p. 491-494.
43. Woodley, D.T., et al., *Identification of the skin basement-membrane autoantigen in epidermolysis bullosa acquisita.* New England Journal of Medicine, 1984. **310**(16): p. 1007-1013.
44. Woodley, D., et al., *Epidermolysis bullosa acquisita antigen is the globular carboxyl terminus of type VII procollagen.* The Journal of clinical investigation, 1988. **81**(3): p. 683-687.
45. Chung, H.J. and J. Uitto, *Type VII collagen: the anchoring fibril protein at fault in dystrophic epidermolysis bullosa.* Dermatologic clinics, 2010. **28**(1): p. 93-105.
46. Sakai, L.Y., et al., *Type VII collagen is a major structural component of anchoring fibrils.* The Journal of cell biology, 1986. **103**(4): p. 1577-1586.

47. Ryynänen, J., et al., *Type VII collagen gene expression by cultured human cells and in fetal skin. Abundant mRNA and protein levels in epidermal keratinocytes.* The Journal of clinical investigation, 1992. **89**(1): p. 163-168.
48. Keene, D.R., et al., *Type VII collagen forms an extended network of anchoring fibrils.* The Journal of cell biology, 1987. **104**(3): p. 611-621.
49. Christiano, A.M., et al., *Cloning of human type VII collagen. Complete primary sequence of the alpha 1 (VII) chain and identification of intragenic polymorphisms.* Journal of Biological Chemistry, 1994. **269**(32): p. 20256-20262.
50. Chen, M., et al., *Interactions of the Amino-terminal Noncollagenous (NC1) Domain of Type VII Collagen with Extracellular Matrix Components A POTENTIAL ROLE IN EPIDERMAL-DERMAL ADHERENCE IN HUMAN SKIN.* Journal of Biological Chemistry, 1997. **272**(23): p. 14516-14522.
51. Lapiere, J.-C., et al., *Epitope mapping of type VII collagen. Identification of discrete peptide sequences recognized by sera from patients with acquired epidermolysis bullosa.* The Journal of clinical investigation, 1993. **92**(4): p. 1831-1839.
52. Chen, M., et al., *The carboxyl terminus of type VII collagen mediates antiparallel dimer formation and constitutes a new antigenic epitope for epidermolysis bullosa acquisita autoantibodies.* Journal of Biological Chemistry, 2001. **276**(24): p. 21649-21655.
53. Tanaka, H., et al., *A novel variant of acquired epidermolysis bullosa with autoantibodies against the central triple-helical domain of type VII collagen.* Laboratory investigation; a journal of technical methods and pathology, 1997. **77**(6): p. 623-632.
54. Ishii, N., et al., *Epidermolysis bullosa acquisita sera react with distinct epitopes on the NC1 and NC2 domains of type VII collagen: study using immunoblotting of domain-specific recombinant proteins and postembedding immunoelectron microscopy.* British Journal of Dermatology, 2004. **150**(5): p. 843-851.
55. Gammon, W.R., et al., *Evidence that anti-basement membrane zone antibodies in bullous eruption of systemic lupus erythematosus recognize epidermolysis bullosa acquisita autoantigen.* Journal of investigative dermatology, 1985. **84**(6): p. 472-476.
56. TROMOVITCH, T.A. and A.B. HYMAN, *Systemic Lupus Erythematosus with Hemorrhagic Bullae: A Case with LE Cells Recovered from the Bullae.* Archives of dermatology, 1961. **83**(6): p. 910-914.
57. Kim, J. and S.C. Kim, *Epidermolysis bullosa acquisita.* Journal of the European Academy of Dermatology and Venereology, 2013. **27**(10): p. 1204-1213.
58. Invernizzi, P. and M.E. Gershwin, *The genetics of human autoimmune disease.* Journal of autoimmunity, 2009. **33**(3-4): p. 290-299.
59. Rosenblum, M.D., K.A. Remedios, and A.K. Abbas, *Mechanisms of human autoimmunity.* The Journal of clinical investigation, 2015. **125**(6): p. 2228-2233.
60. Ludwig, R.J., *Signaling and targeted-therapy of inflammatory cells in epidermolysis bullosa acquisita.* Experimental Dermatology, 2017.
61. Gammon, W.R., et al., *Increased frequency of HLA-DR2 in patients with autoantibodies to epidermolysis bullosa acquisita antigen: evidence that the expression of autoimmunity to type VII collagen is HLA class II allele associated.* Journal of investigative dermatology, 1988. **91**(3): p. 228-232.
62. Zumelzu, C., et al., *Black patients of African descent and HLA-DRB1* 15: 03 frequency overrepresented in epidermolysis bullosa acquisita.* Journal of Investigative Dermatology, 2011. **131**(12): p. 2386-2393.
63. Noe, M.H., et al., *Familial epidermolysis bullosa acquisita.* Dermatology online journal, 2008. **14**(12).
64. Ludwig, R.J., et al., *Generation of antibodies of distinct subclasses and specificity is linked to H2s in an active mouse model of epidermolysis bullosa acquisita.* Journal of Investigative Dermatology, 2011. **131**(1): p. 167-176.

65. Ludwig, R.J., et al., *Identification of quantitative trait loci in experimental epidermolysis bullosa acquisita.* Journal of Investigative Dermatology, 2012. **132**(5): p. 1409-1415.
66. Srinivas, G., et al., *Genome-wide mapping of gene–microbiota interactions in susceptibility to autoimmune skin blistering.* Nature communications, 2013. **4**: p. 2462.
67. Ellebrecht, C.T., et al., *Skin microbiota-associated inflammation precedes autoantibody induced tissue damage in experimental epidermolysis bullosa acquisita.* Journal of autoimmunity, 2016. **68**: p. 14-22.
68. Müller, R., et al., *T and B cells target identical regions of the non-collagenous domain 1 of type VII collagen in epidermolysis bullosa acquisita.* Clinical Immunology, 2010. **135**(1): p. 99-107.
69. Sitaru, A.G., et al., *T cells are required for the production of blister-inducing autoantibodies in experimental epidermolysis bullosa acquisita.* The journal of immunology, 2010. **184**(3): p. 1596-1603.
70. Iwata, H., et al., *B cells, dendritic cells, and macrophages are required to induce an autoreactive CD4 helper T cell response in experimental epidermolysis bullosa acquisita.* The Journal of Immunology, 2013. **191**(6): p. 2978-2988.
71. Hammers, C.M., et al., *Complement-fixing anti-type VII collagen antibodies are induced in Th1-polarized lymph nodes of epidermolysis bullosa acquisita-susceptible mice.* The Journal of Immunology, 2011. **187**(10): p. 5043-5050.
72. Tukaj, S., et al., *Immunomodulatory effects of heat shock protein 90 inhibition on humoral immune responses.* Experimental dermatology, 2014. **23**(8): p. 585-590.
73. Iwata, Y., et al., *Characterization of a rare IL-10–competent B-cell subset in humans that parallels mouse regulatory B10 cells.* Blood, 2011. **117**(2): p. 530-541.
74. Abrams, M.L., et al., *Congenital epidermolysis bullosa acquisita: vertical transfer of maternal autoantibody from mother to infant.* Archives of dermatology, 2011. **147**(3): p. 337-341.
75. Kim, J., et al., *Serum levels of anti-type VII collagen antibodies detected by enzyme-linked immunosorbent assay in patients with epidermolysis bullosa acquisita are correlated with the severity of skin lesions.* Journal of the European Academy of Dermatology and Venereology, 2013. **27**(2).
76. Marzano, A.V., et al., *Diagnosis and disease severity assessment of epidermolysis bullosa acquisita by ELISA for anti-type VII collagen autoantibodies: an Italian multicentre study.* British Journal of Dermatology, 2013. **168**(1): p. 80-84.
77. Sitaru, C., et al., *Autoantibodies to type VII collagen mediate Fcγ-dependent neutrophil activation and induce dermal-epidermal separation in cryosections of human skin.* The American journal of pathology, 2002. **161**(1): p. 301-311.
78. Recke, A., et al., *Recombinant human IgA1 and IgA2 autoantibodies to type VII collagen induce subepidermal blistering ex vivo.* The Journal of Immunology, 2014. **193**(4): p. 1600-1608.
79. Woodley, D.T., et al., *Evidence that anti-type VII collagen antibodies are pathogenic and responsible for the clinical, histological, and immunological features of epidermolysis bullosa acquisita.* Journal of Investigative Dermatology, 2005. **124**(5): p. 958-964.
80. Manz, R.A., et al., *Maintenance of serum antibody levels.* Annu. Rev. Immunol., 2005. **23**: p. 367-386.
81. Kasperkiewicz, M., et al., *Heat-shock protein 90 inhibition in autoimmunity to type VII collagen: evidence that nonmalignant plasma cells are not therapeutic targets.* Blood, 2011. **117**(23): p. 6135-6142.
82. Tiburzy, B., et al., *Persistent autoantibody-production by intermediates between short-and long-lived plasma cells in inflamed lymph nodes of experimental epidermolysis bullosa acquisita.* PloS one, 2013. **8**(12): p. e83631.

83. Sesarman, A., G. Vidarsson, and C. Sitaru, *The neonatal Fc receptor as therapeutic target in IgG-mediated autoimmune diseases.* Cellular and molecular life sciences, 2010. **67**(15): p. 2533-2550.
84. Sesarman, A., et al., *Neonatal Fc receptor deficiency protects from tissue injury in experimental epidermolysis bullosa acquisita.* Journal of molecular medicine, 2008. **86**(8): p. 951-959.
85. Mooney, E., R.J. Falk, and W.R. Gammon, *Studies on complement deposits in epidermolysis bullosa acquisita and bullous pemphigoid.* Archives of dermatology, 1992. **128**(1): p. 58-60.
86. Recke, A., et al., *Pathogenicity of IgG subclass autoantibodies to type VII collagen: Induction of dermal–epidermal separation.* Journal of autoimmunity, 2010. **34**(4): p. 435-444.
87. Mihai, S., et al., *specific inhibition of complement activation significantly ameliorates autoimmune Blistering Disease in Mice.* Frontiers in immunology, 2018. **9**: p. 535.
88. Mihai, S., et al., *The alternative pathway of complement activation is critical for blister induction in experimental epidermolysis bullosa acquisita.* The Journal of Immunology, 2007. **178**(10): p. 6514-6521.
89. Jackson, J.E., et al., *Flii neutralizing antibodies improve wound healing in porcine preclinical studies.* Wound Repair and Regeneration, 2012. **20**(4): p. 523-536.
90. Cowin, A.J., et al., *Flightless I deficiency enhances wound repair by increasing cell migration and proliferation.* The Journal of pathology, 2007. **211**(5): p. 572-581.
91. Kopecki, Z. and A.J. Cowin, *Flightless I: an actin-remodelling protein and an important negative regulator of wound repair.* The international journal of biochemistry & cell biology, 2008. **40**(8): p. 1415-1419.
92. Chong, H., et al., *Reducing Flightless I expression decreases severity of psoriasis in an imiquimod-induced murine model of psoriasiform dermatitis.* British Journal of Dermatology, 2017. **176**(3): p. 705-712.
93. Kopecki, Z., et al., *Flightless I regulates hemidesmosome formation and integrin-mediated cellular adhesion and migration during wound repair.* Journal of Investigative Dermatology, 2009. **129**(8): p. 2031-2045.
94. Kopecki, Z., et al., *Topically applied flightless I neutralizing antibodies improve healing of blistered skin in a murine model of epidermolysis bullosa acquisita.* Journal of Investigative Dermatology, 2013. **133**(4): p. 1008-1016.
95. Kopecki, Z., et al., *Overexpression of the Flii gene increases dermal–epidermal blistering in an autoimmune ColVII mouse model of epidermolysis bullosa acquisita.* The Journal of pathology, 2011. **225**(3): p. 401-413.
96. Kopecki, Z., et al., *Regulation of focal adhesions by flightless i involves inhibition of paxillin phosphorylation via a Rac1-dependent pathway.* Journal of Investigative Dermatology, 2011. **131**(7): p. 1450-1459.
97. Yu, X. and F. Petersen, *A methodological review of induced animal models of autoimmune diseases.* Autoimmunity reviews, 2018.
98. Bieber, K., H. Koga, and W. Nishie, *In vitro and in vivo models to investigate the pathomechanisms and novel treatments for pemphigoid diseases.* Experimental dermatology, 2017. **26**(12): p. 1163-1170.
99. Bieber, K., et al., *Animal models for autoimmune bullous dermatoses.* Experimental dermatology, 2010. **19**(1): p. 2-11.
100. Chen, M., et al., *The cartilage matrix protein subdomain of type VII collagen is pathogenic for epidermolysis bullosa acquisita.* The American journal of pathology, 2007. **170**(6): p. 2009-2018.
101. Csorba, K., et al., *Blister-inducing antibodies target multiple epitopes on collagen VII in mice.* Journal of cellular and molecular medicine, 2014. **18**(9): p. 1727-1739.

102. Vorobyev, A., et al., *Autoantibodies to multiple epitopes on the non-collagenous-1 domain of type VII collagen induce blisters.* Journal of Investigative Dermatology, 2015. **135**(6): p. 1565-1573.
103. Sadeghi, H., et al., *The retinoid-related orphan receptor alpha is essential for the end-stage effector phase of experimental epidermolysis bullosa acquisita.* The Journal of pathology, 2015. **237**(1): p. 111-122.
104. Yaoita, H., et al., *Epidermolysis bullosa acquisita: ultrastructural and immunological studies.* Journal of Investigative Dermatology, 1981. **76**(4): p. 288-292.
105. Otten, J.V., et al., *Molecular diagnosis in autoimmune skin blistering conditions.* Current molecular medicine, 2014. **14**(1): p. 69-95.
106. Mutasim, D.F., *Therapy of autoimmune bullous diseases.* Therapeutics and clinical risk management, 2007. **3**(1): p. 29.
107. Kasperkiewicz, M. and E. Schmidt, *Current treatment of autoimmune blistering diseases.* Current drug discovery technologies, 2009. **6**(4): p. 270-280.
108. Kim, J.H., Y.H. Kim, and S.-C. Kim, *Epidermolysis bullosa acquisita: a retrospective clinical analysis of 30 cases.* Acta dermato-venereologica, 2011. **91**(3): p. 307-312.
109. Gürcan, H.M. and A.R. Ahmed, *Current concepts in the treatment of epidermolysis bullosa acquisita.* Expert opinion on pharmacotherapy, 2011. **12**(8): p. 1259-1268.
110. Piette, E.W. and V.P. Werth, *Dapsone in the management of the autoimmune bullous diseases.* Dermatologic clinics, 2011. **29**(4): p. 561.
111. Schmidt, E., et al., *Successful adjuvant treatment of recalcitrant epidermolysis bullosa acquisita with anti-CD20 antibody rituximab.* Archives of dermatology, 2006. **142**(2): p. 147-150.
112. Mehren, C.R. and R. Gniadecki, *Epidermolysis bullosa acquisita: current diagnosis and therapy.* Dermatology reports, 2011. **3**(3).
113. Kawase, K., et al., *Inflammatory epidermolysis bullosa acquisita effectively treated with minocycline.* Acta dermato-venereologica, 2014. **94**(5): p. 615-616.
114. Egan, C., et al., *Treatment of epidermolysis bullosa acquisita with the humanized anti-Tac mAb daclizumab.* Clinical Immunology, 2001. **101**(2): p. 146-151.
115. Ludwig, R.J., et al., *Emerging treatments for pemphigoid diseases.* Trends in molecular medicine, 2013. **19**(8): p. 501-512.
116. Witte, M., et al., *Discovering potential drug-targets for personalized treatment of autoimmune disorders-what we learn from epidermolysis bullosa acquisita.* Expert opinion on therapeutic targets, 2016. **20**(8): p. 985-998.
117. Lehman, J.S., M.J. Camilleri, and L.E. Gibson, *Epidermolysis bullosa acquisita: concise review and practical considerations.* International journal of dermatology, 2009. **48**(3): p. 227-236.
118. Amber, K.T., et al., *Autoimmune subepidermal bullous diseases of the skin and mucosae: clinical features, diagnosis, and management.* Clinical reviews in allergy & immunology, 2017: p. 1-26.
119. Callot-Mellot, C., et al., *Epidermolysis bullosa acquisita in childhood.* Archives of dermatology, 1997. **133**(9): p. 1122-1126.
120. Németh, T. and A. Mócsai, *The role of neutrophils in autoimmune diseases.* Immunology letters, 2012. **143**(1): p. 9-19.
121. Wright, H.L., et al., *Neutrophil function in inflammation and inflammatory diseases.* Rheumatology, 2010. **49**(9): p. 1618-1631.
122. Abbas, A.K., A.H. Lichtman, and S. Pillai, *Cellular and molecular immunology E-book*. 2014: Elsevier Health Sciences.
123. Németh, T. and A. Mócsai, *Feedback amplification of neutrophil function.* Trends in immunology, 2016. **37**(6): p. 412-424.

124. Woodfin, A., et al., *Endothelial cell activation leads to neutrophil transmigration as supported by the sequential roles of ICAM-2, JAM-A, and PECAM-1.* Blood, 2009. **113**(24): p. 6246-6257.
125. Yang, L., et al., *ICAM-1 regulates neutrophil adhesion and transcellular migration of TNF-α-activated vascular endothelium under flow.* Blood, 2005. **106**(2): p. 584-592.
126. Samavedam, U.K.S., et al., *GM-CSF modulates autoantibody production and skin blistering in experimental epidermolysis bullosa acquisita.* The Journal of Immunology, 2014. **192**(2): p. 559-571.
127. Holden, N., et al., *ANCA-stimulated neutrophils release BLyS and promote B cell survival: a clinically relevant cellular process.* Annals of the rheumatic diseases, 2011: p. annrheumdis153890.
128. Palanichamy, A., et al., *Neutrophil-mediated IFN activation in the bone marrow alters B cell development in human and murine systemic lupus erythematosus.* The Journal of Immunology, 2014. **192**(3): p. 906-918.
129. Ludwig, R.J., et al., *Mechanisms of autoantibody-induced pathology.* Frontiers in immunology, 2017. **8**: p. 603.
130. Chiriac, M., et al., *NADPH oxidase is required for neutrophil-dependent autoantibody-induced tissue damage.* The Journal of pathology, 2007. **212**(1): p. 56-65.
131. Kasperkiewicz, M., et al., *Genetic identification and functional validation of FcγRIV as key molecule in autoantibody-induced tissue injury.* The Journal of pathology, 2012. **228**(1): p. 8-19.
132. Yu, X., et al., *Neutrophil adhesion is a prerequisite for antibody-mediated proteolytic tissue damage in experimental epidermolysis bullosa acquisita.* Journal of Investigative Dermatology, 2018.
133. Karsten, C.M., et al., *Anti-inflammatory activity of IgG1 mediated by Fc galactosylation and association of FcγRIIB and dectin-1.* Nature medicine, 2012. **18**(9): p. 1401.
134. Hirose, M., et al., *The allosteric CXCR1/2 inhibitor DF2156A improves experimental epidermolysis bullosa acquisita.* J Genet Syndr Gene Ther S, 2013. **3**: p. 2.
135. Hirose, M., et al., *Reduced skin blistering in experimental epidermolysis bullosa acquisita after anti-TNF treatment.* Molecular Medicine, 2016. **22**: p. 918.
136. Sadeghi, H., et al., *Caspase-1–Independent IL-1 Release Mediates Blister Formation in Autoantibody-Induced Tissue Injury through Modulation of Endothelial Adhesion Molecules.* The Journal of Immunology, 2015. **194**(8): p. 3656-3663.
137. Sezin, T., et al., *The leukotriene B4 and its receptor BLT1 act as critical drivers of neutrophil recruitment in murine bullous pemphigoid-like epidermolysis bullosa acquisita.* Journal of Investigative Dermatology, 2017. **137**(5): p. 1104-1113.
138. Samavedam, U.K.S., et al., *Recombinant IL-6 treatment protects mice from organ specific autoimmune disease by IL-6 classical signalling-dependent IL-1ra induction.* Journal of autoimmunity, 2013. **40**: p. 74-85.
139. Trastoy, B., et al., *Structural basis for the recognition of complex-type N-glycans by Endoglycosidase S.* Nature communications, 2018. **9**(1): p. 1874.
140. Hirose, M., et al., *Enzymatic autoantibody glycan hydrolysis alleviates autoimmunity against type VII collagen.* Journal of autoimmunity, 2012. **39**(4): p. 304-314.
141. Mihai, S., et al., *In vivo enzymatic modulation of IgG antibodies prevents immune complex-dependent skin injury.* Experimental dermatology, 2017. **26**(8): p. 691-696.
142. Kovács, M., et al., *The Src family kinases Hck, Fgr, and Lyn are critical for the generation of the in vivo inflammatory environment without a direct role in leukocyte recruitment.* Journal of Experimental Medicine, 2014: p. jem. 20132496.
143. Samavedam, U.K., et al., *Whole-genome expression Profiling in skin reveals sYK as a Key regulator of inflammation in experimental epidermolysis Bullosa acquisita.* Frontiers in immunology, 2018. **9**: p. 249.

144. Németh, T., et al., *The Syk tyrosine kinase is required for skin inflammation in an in vivo mouse model of epidermolysis bullosa acquisita.* Journal of Investigative Dermatology, 2017. **137**(10): p. 2131-2139.
145. Kulkarni, S., et al., *PI3Kβ plays a critical role in neutrophil activation by immune complexes.* Sci. Signal., 2011. **4**(168): p. ra23-ra23.
146. Koga, H., et al., *PDE4 inhibition as potential treatment of epidermolysis bullosa acquisita.* Journal of Investigative Dermatology, 2016. **136**(11): p. 2211-2220.
147. Koga, H., et al., *Therapeutic effect of a novel Phosphatidylinositol-3-Kinase δ inhibitor in experimental epidermolysis Bullosa acquisita.* Frontiers in immunology, 2018. **9**.
148. Hellberg, L., et al., *Methylprednisolone blocks autoantibody-induced tissue damage in experimental models of bullous pemphigoid and epidermolysis bullosa acquisita through inhibition of neutrophil activation.* Journal of Investigative Dermatology, 2013. **133**(10): p. 2390-2399.
149. Shimanovich, I., et al., *Granulocyte-derived elastase and gelatinase B are required for dermal–epidermal separation induced by autoantibodies from patients with epidermolysis bullosa acquisita and bullous pemphigoid.* The Journal of pathology, 2004. **204**(5): p. 519-527.
150. Bieber, K., et al., *T cells mediate autoantibody-induced cutaneous inflammation and blistering in epidermolysis bullosa acquisita.* Scientific reports, 2016. **6**.
151. Bieber, K., et al., *regulatory T cells suppress inflammation and Blistering in Pemphigoid Diseases.* Frontiers in immunology, 2017. **8**: p. 1628.
152. Deng, F., et al., *CD11b-deficient mice exhibit an increased severity in the late phase of antibody transfer-induced experimental epidermolysis bullosa acquisita.* Experimental dermatology, 2017. **26**(12): p. 1175-1178.
153. Koga, H., et al., *Epidermolysis bullosa acquisita: The 2018 update.* Frontiers in Medicine, 2018. **5**: p. 362.
154. Li, J. and Z. Lu, *Pathway-based drug repositioning using causal inference.* BMC bioinformatics, 2013. **14**(16): p. S3.
155. Amantea, D. and G. Bagetta, *Drug repurposing for immune modulation in acute ischemic stroke.* Current opinion in pharmacology, 2016. **26**: p. 124-130.
156. Xue, H., et al., *Review of drug repositioning approaches and resources.* International journal of biological sciences, 2018. **14**(10): p. 1232.
157. Strittmatter, S.M., *Overcoming drug development bottlenecks with repurposing: old drugs learn new tricks.* Nature medicine, 2014. **20**(6): p. 590-591.
158. Hernandez, J.J., et al., *Giving Drugs a Second Chance: Overcoming Regulatory and Financial Hurdles in Repurposing Approved Drugs As Cancer Therapeutics.* Frontiers in oncology, 2017. **7**: p. 273.
159. Qu, X.A., et al., *Inferring novel disease indications for known drugs by semantically linking drug action and disease mechanism relationships.* BMC bioinformatics, 2009. **10**(5): p. S4.
160. Sheskin, J., *Thalidomide in the treatment of lepra reactions.* Clinical Pharmacology & Therapeutics, 1965. **6**(3): p. 303-306.
161. Ashburn, T.T. and K.B. Thor, *Drug repositioning: identifying and developing new uses for existing drugs.* Nature reviews Drug discovery, 2004. **3**(8): p. 673-683.
162. Su, E.W. and T.M. Sanger, *Systematic drug repositioning through mining adverse event data in ClinicalTrials. gov.* PeerJ, 2017. **5**: p. e3154.
163. Li, Y.Y. and S.J. Jones, *Drug repositioning for personalized medicine.* Genome medicine, 2012. **4**(3): p. 27.
164. Novac, N., *Challenges and opportunities of drug repositioning.* Trends in pharmacological sciences, 2013. **34**(5): p. 267-272.
165. Dudley, J.T., et al., *Computational repositioning of the anticonvulsant topiramate for inflammatory bowel disease.* Science translational medicine, 2011. **3**(96): p. 96ra76-96ra76.

166. Clark, P.M., et al., *Bioinformatics analysis reveals transcriptome and microRNA signatures and drug repositioning targets for IBD and other autoimmune diseases.* Inflammatory bowel diseases, 2012. **18**(12): p. 2315-2333.
167. Vesterinen, H.M., et al., *Drug repurposing: a systematic approach to evaluate candidate oral neuroprotective interventions for secondary progressive multiple sclerosis.* PloS one, 2015. **10**(4): p. e0117705.
168. Xu, X. and H.-Y. Zhang, *The Immunogenetics of Psoriasis and Implications for Drug Repositioning.* International journal of molecular sciences, 2017. **18**(12): p. 2650.
169. Hall, C.J., et al., *Repositioning drugs for inflammatory disease–fishing for new anti-inflammatory agents.* Disease models & mechanisms, 2014. **7**(9): p. 1069-1081.
170. Cooper, G.S. and B.C. Stroehla, *The epidemiology of autoimmune diseases.* Autoimmunity reviews, 2003. **2**(3): p. 119-125.
171. PCL. Available from: http://www.prestwickchemical.com/libraries-screening-lib-pcl.html.
172. Siles, S.A., et al., *High-throughput screening of a collection of known pharmacologically active small compounds for identification of Candida albicans biofilm inhibitors.* Antimicrobial agents and chemotherapy, 2013. **57**(8): p. 3681-3687.
173. Yu, X., et al., *FcγRIIA and FcγRIIIB are required for autoantibody-induced tissue damage in experimental human models of bullous pemphigoid.* The Journal of investigative dermatology, 2010. **130**(12): p. 2841.
174. Bedouhène, S., et al., *Luminol-amplified chemiluminescence detects mainly superoxide anion produced by human neutrophils.* American journal of blood research, 2017. **7**(4): p. 41.
175. Mütze, S., et al., *Myeloperoxidase-derived hypochlorous acid antagonizes the oxidative stress-mediated activation of iron regulatory protein 1.* Journal of Biological Chemistry, 2003. **278**(42): p. 40542-40549.
176. Iwakami, S., et al., *Concentration-dependent dual effects of hydrogen peroxide on insulin signal transduction in H4IIEC hepatocytes.* PloS one, 2011. **6**(11): p. e27401.
177. Biosciences, B., *Detection of Apoptosis Using the BD Annexin V FITC Assay on the BD FACSVerse™ System*. 2011.
178. Boer, K., et al., *CD62L on neutrophil granulocytes, a useful, complementary marker for the prediction of ventriculitis in blood-containing CSF.* Clinical biochemistry, 2010. **43**(16-17): p. 1351-1355.
179. Gustafson, M.P., et al., *A method for identification and analysis of non-overlapping myeloid immunophenotypes in humans.* PloS one, 2015. **10**(3): p. e0121546.
180. Lakschevitz, F.S., et al., *Identification of neutrophil surface marker changes in health and inflammation using high-throughput screening flow cytometry.* Experimental cell research, 2016. **342**(2): p. 200-209.
181. Leineweber, S., S. Schönig, and K. Seeger, *Insight into interactions of the von-Willebrand-factor-A-like domain 2 with the FNIII-like domain 9 of collagen VII by NMR and SPR.* FEBS letters, 2011. **585**(12): p. 1748-1752.
182. Achan, J., et al., *Quinine, an old anti-malarial drug in a modern world: role in the treatment of malaria.* Malaria journal, 2011. **10**(1): p. 144.
183. Qiao, S., et al., *The antimalarial amodiaquine causes autophagic-lysosomal and proliferative blockade sensitizing human melanoma cells to starvation-and chemotherapy-induced cell death.* Autophagy, 2013. **9**(12): p. 2087-2102.
184. He, Y., et al., *Identification of a lysosomal pathway that modulates glucocorticoid signaling and the inflammatory response.* Sci. Signal., 2011. **4**(180): p. ra44-ra44.
185. Augustijns, P., P. Geusens, and N. Verbeke, *Chloroquine levels in blood during chronic treatment of patients with rheumatoid arthritis.* European journal of clinical pharmacology, 1992. **42**(4): p. 429-433.
186. Meinao, I., et al., *Controlled trial with chloroquine diphosphate in systemic lupus erythematosus.* Lupus, 1996. **5**(3): p. 237-241.

187. Millan, M.J., et al., *Differential actions of antiparkinson agents at multiple classes of monoaminergic receptor. I. A multivariate analysis of the binding profiles of 14 drugs at 21 native and cloned human receptor subtypes.* Journal of Pharmacology and Experimental Therapeutics, 2002. **303**(2): p. 791-804.
188. Jenner, P. and R. Katzenschlager, *Apomorphine-pharmacological properties and clinical trials in Parkinson's disease.* Parkinsonism & related disorders, 2016. **33**: p. S13-S21.
189. Albersen, M., H. Orabi, and T.F. Lue, *Evaluation and treatment of erectile dysfunction in the aging male: a mini-review.* Gerontology, 2012. **58**(1): p. 3-14.
190. Van der Kam, E., et al., *The effects of stress on alcohol consumption: mild acute and sub-chronic stressors differentially affect apomorphine susceptible and unsusceptible rats.* Life sciences, 2005. **76**(15): p. 1759-1770.
191. Zhang, H., et al., *In vitro antineoplastic effects of auranofin in canine lymphoma cells.* BMC cancer, 2018. **18**(1): p. 522.
192. Liu, C., et al., *Enhancement of auranofin-induced apoptosis in MCF-7 human breast cells by selenocystine, a synergistic inhibitor of thioredoxin reductase.* PloS one, 2013. **8**(1): p. e53945.
193. Sobhakumari, A., et al., *Susceptibility of human head and neck cancer cells to combined inhibition of glutathione and thioredoxin metabolism.* PLoS One, 2012. **7**(10): p. e48175.
194. Han, S., et al., *Auranofin inhibits overproduction of pro-inflammatory cytokines, cyclooxygenase expression and PGE 2 production in macrophages.* Archives of pharmacal research, 2008. **31**(1): p. 67-74.
195. Nakaya, A., et al., *The gold compound auranofin induces apoptosis of human multiple myeloma cells through both down-regulation of STAT3 and inhibition of NF-κB activity.* Leukemia research, 2011. **35**(2): p. 243-249.
196. Palmer, O.R., et al., *In vivo characterization of the murine venous system before and during dobutamine stimulation: implications for preclinical models of venous disease.* Annals of Anatomy-Anatomischer Anzeiger, 2017. **214**: p. 43-52.
197. Sloka, J. and M. Stefanelli, *The mechanism of action of methylprednisolone in the treatment of multiple sclerosis.* Multiple Sclerosis Journal, 2005. **11**(4): p. 425-432.
198. Sack, U., et al., *Novel effect of antihelminthic Niclosamide on S100A4-mediated metastatic progression in colon cancer.* Journal of the National Cancer Institute, 2011. **103**(13): p. 1018-1036.
199. Wieland, A., et al., *Anticancer effects of niclosamide in human glioblastoma.* Clinical Cancer Research, 2013. **19**(15): p. 4124-4136.
200. Xu, M., et al., *Identification of small-molecule inhibitors of Zika virus infection and induced neural cell death via a drug repurposing screen.* Nature medicine, 2016. **22**(10): p. 1101-1107.
201. Wu, C.-S., et al., *Antihelminthic niclosamide modulates dendritic cells activation and function.* Cellular immunology, 2014. **288**(1-2): p. 15-23.
202. Liang, L., et al., *Inhibitory effects of niclosamide on inflammation and migration of fibroblast-like synoviocytes from patients with rheumatoid arthritis.* Inflammation Research, 2015. **64**(3-4): p. 225-233.
203. Wang, X., et al., *Tamoxifen provides structural and functional rescue in murine models of photoreceptor degeneration.* Journal of Neuroscience, 2017. **37**(12): p. 3294-3310.
204. Lonard, D.M. and C.L. Smith, *Molecular perspectives on selective estrogen receptor modulators (SERMs): progress in understanding their tissue-specific agonist and antagonist actions.* Steroids, 2002. **67**(1): p. 15-24.
205. Feil, S., N. Valtcheva, and R. Feil, *Inducible cre mice*, in *Gene knockout protocols*. 2009, Springer. p. 343-363.
206. Al-Refu, K., *General Methods in Preparation of Skin Biopsies for Haematoxylin & Eosin Stain and Immunohistochemistry*, in *Skin Biopsy-Perspectives*. 2011, InTech.

207. Griffith, M., et al., *Informatics for RNA sequencing: a web resource for analysis on the cloud.* PLoS computational biology, 2015. **11**(8): p. e1004393.
208. NextSeq. *NextSeq* Available from: http://omegabioservices.com/index.php/next-gen-sequencing/rna-seq/.
209. mouse, C.-B.; Available from: https://radiantrecovery.com/learn/resource-center/radiant-reports/c57-story/images/.
210. Mueller, O., S. Lightfoot, and A. Schroeder, *RNA integrity number (RIN)–standardization of RNA quality control.* Agilent application note, publication, 2004: p. 1-8.
211. Dobin, A., et al., *STAR: ultrafast universal RNA-seq aligner.* Bioinformatics, 2013. **29**(1): p. 15-21.
212. Huang, D.W., B.T. Sherman, and R.A. Lempicki, *Bioinformatics enrichment tools: paths toward the comprehensive functional analysis of large gene lists.* Nucleic acids research, 2008. **37**(1): p. 1-13.
213. Huang, D.W., B.T. Sherman, and R.A. Lempicki, *Systematic and integrative analysis of large gene lists using DAVID bioinformatics resources.* Nature protocols, 2008. **4**(1): p. 44.
214. Oturai, D.B., et al., *Identification of suitable reference genes for peripheral blood mononuclear cell subset studies in multiple sclerosis.* Scandinavian journal of immunology, 2016. **83**(1): p. 72-80.
215. Ledderose, C., et al., *Selection of reliable reference genes for quantitative real-time PCR in human T cells and neutrophils.* BMC research notes, 2011. **4**(1): p. 427.
216. Zhang, X., L. Ding, and A.J. Sandford, *Selection of reference genes for gene expression studies in human neutrophils by real-time PCR.* BMC molecular biology, 2005. **6**(1): p. 4.
217. Livak, K.J. and T.D. Schmittgen, *Analysis of relative gene expression data using real-time quantitative PCR and the 2− ΔΔCT method.* methods, 2001. **25**(4): p. 402-408.
218. Hughes, J.P., et al., *Principles of early drug discovery.* British journal of pharmacology, 2011. **162**(6): p. 1239-1249.
219. Wang, C., et al., *Verteporfin inhibits YAP function through up-regulating 14-3-3σ sequestering YAP in the cytoplasm.* American journal of cancer research, 2016. **6**(1): p. 27.
220. Ishii, N., et al., *Autoantibody-induced intestinal inflammation and weight loss in experimental epidermolysis bullosa acquisita.* The Journal of pathology, 2011. **224**(2): p. 234-244.
221. Niebuhr, M., et al., *Evidence for a contributory role of a xenogeneic immune response in experimental epidermolysis bullosa acquisita.* Experimental dermatology, 2017. **26**(12): p. 1207-1213.
222. Olalubi, O.A., O.E. Ogunlana, and O.B. Fagbemi, *In-Vivo Evaluation of the Antiplasmodial Effect of Amodiaquine and Amodiaquine-Promethazine Combination in Plasmodium berghei Infected Mice.* International Journal of Health Research, 2011. **4**(2): p. 83-89.
223. Simon, T.M., et al., *Screening trial with the coordinated gold compound auranofin using mouse lymphocytic leukemia P388.* Cancer Research, 1981. **41**(1): p. 94-97.
224. Reid, J.M., et al., *Pharmacokinetics of endoxifen and tamoxifen in female mice: implications for comparative in vivo activity studies.* Cancer chemotherapy and pharmacology, 2014. **74**(6): p. 1271-1278.
225. Marín, F. and M.C. Barbancho, *Action of selective estrogen receptor modulators (SERMs) through the classical mechanism of estrogen action*, in *Selective Estrogen Receptor Modulators*. 2006, Springer. p. 71-77.
226. Farooq, A., *Structural and functional diversity of estrogen receptor ligands.* Current topics in medicinal chemistry, 2015. **15**(14): p. 1372-1384.
227. McDonnell, D.P. and J.D. Norris, *Connections and regulation of the human estrogen receptor.* Science, 2002. **296**(5573): p. 1642-1644.
228. Nalbandian, G. and S. Kovats, *Understanding sex biases in immunity.* Immunologic research, 2005. **31**(2): p. 91-106.

229. Cowell, L., et al., *Tamoxifen treatment promotes phosphorylation of the adhesion molecules, p130Cas/BCAR1, FAK and Src, via an adhesion-dependent pathway.* Oncogene, 2006. **25**(58): p. 7597.
230. Dayan, M., et al., *The beneficial effects of treatment with tamoxifen and anti-oestradiol antibody on experimental systemic lupus erythematosus are associated with cytokine modulations.* Immunology, 1997. **90**(1): p. 101-108.
231. Sthoeger, Z., et al., *The beneficial effect of the estrogen antagonist, tamoxifen, on experimental systemic lupus erythematosus.* The Journal of rheumatology, 1994. **21**(12): p. 2231-2238.
232. Sthoeger, Z., H. Zinger, and E. Mozes, *Beneficial effects of the anti-oestrogen tamoxifen on systemic lupus erythematosus of (NZB× NZW) F1 female mice are associated with specific reduction of IgG3 autoantibodies.* Annals of the rheumatic diseases, 2003. **62**(4): p. 341-346.
233. Morad, S.A. and M.C. Cabot, *Tamoxifen regulation of sphingolipid metabolism—therapeutic implications.* Biochimica et Biophysica Acta (BBA)-Molecular and Cell Biology of Lipids, 2015. **1851**(9): p. 1134-1145.
234. Corriden, R., et al., *Tamoxifen augments the innate immune function of neutrophils through modulation of intracellular ceramide.* Nature communications, 2015. **6**: p. 8369.
235. Chen, Y., A.T. Lun, and G.K. Smyth, *From reads to genes to pathways: differential expression analysis of RNA-Seq experiments using Rsubread and the edgeR quasi-likelihood pipeline.* F1000Research, 2016. **5**.
236. Hrdinka, M., et al., *PRR7 is a transmembrane adaptor protein expressed in activated T cells involved in regulation of T cell receptor (TCR) signaling and apoptosis.* Journal of Biological Chemistry, 2011: p. jbc. M110. 175117.
237. Vaivoda, R., et al., *CYP4F18-deficient neutrophils exhibit increased chemotaxis to complement component C5a.* Journal of immunology research, 2015. **2015**.
238. Fodil, N., et al., *CCDC88B is required for pathogenesis of inflammatory bowel disease.* Nature communications, 2017. **8**(1): p. 932.
239. Webb, M., et al., *Expression analysis of the mouse S100A7/psoriasin gene in skin inflammation and mammary tumorigenesis.* BMC cancer, 2005. **5**(1): p. 17.
240. Riveira-Munoz, E., et al., *Meta-analysis confirms the LCE3C_LCE3B deletion as a risk factor for psoriasis in several ethnic groups and finds interaction with HLA-Cw6.* Journal of Investigative Dermatology, 2011. **131**(5): p. 1105-1109.
241. Balamurugan, K. and E. Sterneck, *The many faces of C/EBPδ and their relevance for inflammation and cancer.* International journal of biological sciences, 2013. **9**(9): p. 917.
242. Wolf, R., et al., *Human S100A15 splice variants are differentially expressed in inflammatory skin diseases and regulated through Th1 cytokines and calcium.* Experimental dermatology, 2007. **16**(8): p. 685-691.
243. Sun, W., P.E. Sanderson, and W. Zheng, *Drug combination therapy increases successful drug repositioning.* Drug discovery today, 2016. **21**(7): p. 1189-1195.
244. Lee, B.-Y., et al., *Drug regimens identified and optimized by output-driven platform markedly reduce tuberculosis treatment time.* Nature communications, 2017. **8**: p. 14183.
245. Müller, S., et al., *Dimethylfumarate impairs neutrophil functions.* Journal of Investigative Dermatology, 2016. **136**(1): p. 117-126.
246. Lee, H., S. Kang, and W. Kim, *Drug repositioning for cancer therapy based on large-scale drug-induced transcriptional signatures.* PloS one, 2016. **11**(3): p. e0150460.
247. Grover, M.P., et al., *Novel therapeutics for coronary artery disease from genome-wide association study data.* BMC medical genomics, 2015. **8**(2): p. S1.
248. Durães, F., M. Pinto, and E. Sousa, *Old drugs as new treatments for neurodegenerative diseases.* Pharmaceuticals, 2018. **11**(2): p. 44.

249. Grammer, A.C. and P.E. Lipsky, *Drug repositioning strategies for the identification of novel therapies for rheumatic autoimmune inflammatory diseases.* Rheumatic Disease Clinics, 2017. **43**(3): p. 467-480.
250. Xu, R. and Q. Wang, *A genomics-based systems approach towards drug repositioning for rheumatoid arthritis.* BMC genomics, 2016. **17**(7): p. 518.
251. Patrick, M.T., et al., *Drug Repurposing Prediction for Immune-Mediated Cutaneous Diseases using a Word-Embedding–Based Machine Learning Approach.* Journal of Investigative Dermatology, 2018.
252. Iljin, K., et al., *High-throughput cell-based screening of 4910 known drugs and drug-like small molecules identifies disulfiram as an inhibitor of prostate cancer cell growth.* Clinical Cancer Research, 2009. **15**(19): p. 6070-6078.
253. Antczak, C., et al., *Revisiting old drugs as novel agents for retinoblastoma: in vitro and in vivo antitumor activity of cardenolides.* Investigative ophthalmology & visual science, 2009. **50**(7): p. 3065-3073.
254. Burkhardt, M.F., et al., *A cellular model for sporadic ALS using patient-derived induced pluripotent stem cells.* Molecular and Cellular Neuroscience, 2013. **56**: p. 355-364.
255. Zhang, L., et al., *Small molecule regulators of autophagy identified by an image-based high-throughput screen.* Proceedings of the National Academy of Sciences, 2007. **104**(48): p. 19023-19028.
256. Dudley, J.T., T. Deshpande, and A.J. Butte, *Exploiting drug–disease relationships for computational drug repositioning.* Briefings in bioinformatics, 2011. **12**(4): p. 303-311.
257. Madsen, P., et al., *Molecular cloning, occurrence, and expression of a novel partially secreted protein "psoriasin" that is highly up-regulated in psoriatic skin.* Journal of Investigative Dermatology, 1991. **97**(4): p. 701-712.
258. Akbarzadeh, R., et al., *Myeloid-related proteins-8 and-14 are expressed but dispensable in the pathogenesis of experimental epidermolysis bullosa acquisita and bullous pemphigoid.* Journal of dermatological science, 2016. **81**(3): p. 165-172.
259. Giannini, E.H., E.J. Brewer, and D.A. Person, *Auranofin in the treatment of juvenile rheumatoid arthritis.* The Journal of pediatrics, 1983. **102**(1): p. 138-141.
260. Finkelstein, A., et al., *Auranofin. New oral gold compound for treatment of rheumatoid arthritis.* Annals of the rheumatic diseases, 1976. **35**(3): p. 251.
261. Zhou, L., et al., *Impact of human granulocyte and monocyte isolation procedures on functional studies.* Clinical and Vaccine Immunology, 2012. **19**(7): p. 1065-1074.
262. Loynes, C.A., et al., *Pivotal Advance: Pharmacological manipulation of inflammation resolution during spontaneously resolving tissue neutrophilia in the zebrafish.* Journal of leukocyte biology, 2010. **87**(2): p. 203-212.
263. Wang, X., et al., *Inhibitors of neutrophil recruitment identified using transgenic zebrafish to screen a natural product library.* Disease models & mechanisms, 2014. **7**(1): p. 163-169.
264. Johnson, J.L., et al., *Identification of Nexinhibs, small-molecule inhibitors of neutrophil exocytosis and inflammation. Druggability of the small GTPase Rab27a.* Journal of Biological Chemistry, 2016: p. jbc. M116. 741884.
265. Liu-Chittenden, Y., et al., *Genetic and pharmacological disruption of the TEAD–YAP complex suppresses the oncogenic activity of YAP.* Genes & development, 2012. **26**(12): p. 1300-1305.
266. Brodowska, K., et al., *The clinically used photosensitizer Verteporfin (VP) inhibits YAP-TEAD and human retinoblastoma cell growth in vitro without light activation.* Experimental eye research, 2014. **124**: p. 67-73.
267. Morishita, T., et al., *The photosensitizer verteporfin has light-independent anti-leukemic activity for Ph-positive acute lymphoblastic leukemia and synergistically works with dasatinib.* Oncotarget, 2016. **7**(35): p. 56241.
268. Ziemssen, F. and M. Zierhut, *Principles of therapy*, in *Clinical Ocular Toxicology*. 2008, Elsevier. p. 1-7.

269. Peper, A., *Aspects of the relationship between drug dose and drug effect.* Dose-Response, 2009. **7**(2): p. dose-response. 08-019. Peper.
270. Dorwart, B.B., et al., *Chrysotherapy in psoriatic arthritis.* Arthritis & Rheumatism: Official Journal of the American College of Rheumatology, 1978. **21**(5): p. 513-515.
271. Denayer, T., T. Stöhr, and M. Van Roy, *Animal models in translational medicine: Validation and prediction.* New Horizons in Translational Medicine, 2014. **2**(1): p. 5-11.
272. Sitaru, C., *Experimental models of epidermolysis bullosa acquisita.* Experimental dermatology, 2007. **16**(6): p. 520-531.
273. Kean, W. and I. Kean, *Clinical pharmacology of gold.* Inflammopharmacology, 2008. **16**(3): p. 112-125.
274. Fujitsu, T., et al., *Effect of auranofin on autoimmune disease in a mouse model.* International journal of immunopharmacology, 1986. **8**(8): p. 897-910.
275. Kato, F., M. Nomura, and K. Nakamura, *Arthritis in mice induced by a single immunisation with collagen.* Annals of the rheumatic diseases, 1996. **55**(8): p. 535-539.
276. Jeon, K.-I., J.-Y. Jeong, and D.-M. Jue, *Thiol-reactive metal compounds inhibit NF-κB activation by blocking IκB kinase.* The Journal of Immunology, 2000. **164**(11): p. 5981-5989.
277. Krishna, M. and S.G. Nadler, *Immunogenicity to biotherapeutics–the role of anti-drug immune complexes.* Frontiers in immunology, 2016. **7**: p. 21.
278. Goto, M., et al., *High prevalence of human anti-mouse antibodies in the serum of colorectal cancer patients.* Anticancer research, 2010. **30**(10): p. 4353-4356.
279. Bespalov, A., et al., *Drug tolerance: a known unknown in translational neuroscience.* Trends in pharmacological sciences, 2016. **37**(5): p. 364-378.
280. Arreola, R., et al., *Immunomodulatory effects mediated by dopamine.* Journal of immunology research, 2016. **2016**.
281. Behjati, S. and M. Frank, *The effects of tamoxifen on immunity.* Current medicinal chemistry, 2009. **16**(24): p. 3076-3080.
282. Nagy, E. and I. Berczi, *Immunomodulation by tamoxifen and pergolide.* Immunopharmacology, 1986. **12**(2): p. 145-153.
283. Wu, W.M., et al., *Tamoxifen decreases renal inflammation and alleviates disease severity in autoimmune NZB/W F1 mice.* Scandinavian journal of immunology, 2000. **52**(4): p. 393-400.
284. Wu, W.M., et al., *Tamoxifen alleviates disease severity and decreases double negative T cells in autoimmune MRL-lpr/lpr mice.* Immunology, 2000. **100**(1): p. 110-118.
285. Bebo Jr, B.F., et al., *Treatment with selective estrogen receptor modulators regulates myelin specific T-cells and suppresses experimental autoimmune encephalomyelitis.* Glia, 2009. **57**(7): p. 777-790.
286. Babina, M., et al., *Tamoxifen counteracts the allergic immune response and improves allergen-induced dermatitis in mice.* Clinical & Experimental Allergy, 2010. **40**(8): p. 1256-1265.
287. Liu, X. and H. Shi, *Regulation of estrogen receptor α expression in the hypothalamus by sex steroids: implication in the regulation of energy homeostasis.* International journal of endocrinology, 2015. **2015**.
288. Vrtačnik, P., et al., *The many faces of estrogen signaling.* Biochemia medica: Biochemia medica, 2014. **24**(3): p. 329-342.
289. Nalbandian, G., et al., *The selective estrogen receptor modulators, tamoxifen and raloxifene, impair dendritic cell differentiation and activation.* The Journal of Immunology, 2005. **175**(4): p. 2666-2675.
290. de Kozak, Y., et al., *Intraocular injection of tamoxifen-loaded nanoparticles: a new treatment of experimental autoimmune uveoretinitis.* European journal of immunology, 2004. **34**(12): p. 3702-3712.

291. Paharkova-Vatchkova, V., R. Maldonado, and S. Kovats, *Estrogen preferentially promotes the differentiation of CD11c+ CD11bintermediate dendritic cells from bone marrow precursors.* The Journal of Immunology, 2004. **172**(3): p. 1426-1436.
292. Xia, C., et al., *S100 proteins as an important regulator of macrophage inflammation.* Frontiers in immunology, 2018. **8**: p. 1908.
293. Wolf, R., et al., *Molecular cloning and characterization of alternatively spliced mRNA isoforms from psoriatic skin encoding a novel member of the S100 family.* The FASEB journal, 2003. **17**(13): p. 1969-1971.
294. Ribeiro, M.P., A.E. Santos, and J.B. Custódio, *Rethinking tamoxifen in the management of melanoma: New answers for an old question.* European journal of pharmacology, 2015. **764**: p. 372-378.
295. Matsuoka, H., et al., *Tamoxifen inhibits tumor cell invasion and metastasis in mouse melanoma through suppression of PKC/MEK/ERK and PKC/PI3K/Akt pathways.* Experimental cell research, 2009. **315**(12): p. 2022-2032.
296. Batycka-Baran, A., et al., *Leukocyte-derived koebnerisin (S100A15) and psoriasin (S100A7) are systemic mediators of inflammation in psoriasis.* Journal of dermatological science, 2015. **79**(3): p. 214-221.
297. Kolesnik, M., et al., *Treatment of severe autoimmune blistering skin diseases with combination of protein A immunoadsorption and rituximab: a protocol without initial high dose or pulse steroid medication.* Journal of the European Academy of Dermatology and Venereology, 2014. **28**(6): p. 771-780.
298. Niedermeier, A., et al., *Clinical response of severe mechanobullous epidermolysis bullosa acquisita to combined treatment with immunoadsorption and rituximab (anti-CD20 monoclonal antibodies).* Archives of dermatology, 2007. **143**(2): p. 192-198.
299. Kubisch, I., et al., *Premonitory Epidermolysis Bullosa Acquisita Mimicking Eyelid Dermatitis.* American journal of clinical dermatology, 2010. **11**(4): p. 289-293.

6 Appendix

6.1 List of tables

6.2 List of figures

6.3 List of abbreviations

aAb	autoantibody
Ab	antibody
ABSA	affected body surface area
AD	atopic dermatitis
ADA	Anti-drug antibody
AF	anchoring fibrils
AIBD	autoimmune bullous disease
Amo	amodiaquin dihydrochloride dihydrate
ANOVA	analysis of variance
anti-mCOL7-IgG	IgG fractions against vWFA2 subdomain
APC	antigen-presenting cell
Apo	R(-) apomorphine hydrochloride hemihydrate
Au	auranofin
AUC	area under the curve
AV	annexin V
BAFF	B cell activating factor
BMZ	basement membrane zone
BP	bullous pemphigoid
Breg	regulatory B cell
BSLE	bullous variant of systemic lupus erythematosus
C3	complement component 3
CAT	catalase
CD62L	L-selectin
CFA	complete Freund’s adjuvant
CMP	cartilage matrix protein
COL7	type VII collagen
DAVID	Database for Annotation, Visualization and Intergrated Discovery
DC	dendritic cell
DEB	dystrophic epidermolysis bullosa
DEGs	differentially expressed genes
DEJ	dermal-epidermal junction
DIF	direct immunofluorescence
dLN	draining lymph node
Dob	dobutamine hydrochloride
EAE	experimental autoimmune encephalomyelitis
EB	epidermolysis bullosa
EBA	epidermolysis bullosa acquisita
ELISA	enzyme-linked immunosorbent assay
EMA	European Medicines Agency
ER	estrogen receptor

ERK	extracellular signal-regulated kinase
ERK	extracellular-signal regulated kinases
FC	fold change
FcγR	Fcγ receptor
FDA	United States Food and Drug Administration
Flii	flightless I
FNIII	fibronectin III-like
Glc	glucose
GlyCAM	glycosylation dependent cell adhesion molecule
GM-CSF	granulocyte-monocyte colony-stimulating factor
GOX	glucose oxidase
GPA	Granulomatosis with polyangiitis
Gr-1	granulocyte receptor-1 antigen
GST	glutathione S-transferase
h	hour
HBSS	Hank's Balanced Salt Solution
HClO	hypochlorous acid
HEK	human embryonic kidney
HIV	human immunodeficiency virus
HKGs	housekeeping genes
HLA	human leukocyte antigen
HTS	high-throughput screening
IA	immunoadsorption
i.p.	intraperitoneal
IBD	inflammatory bowel disease
IC	immune complex
ICAM	intercellular adhesion molecule
IF	immunofluorescence
IFN-γ	interferon-γ
Ig	immunoglobulin
iIC	immobalized immune complex
IIF	Indirect immunofluorescence
IL	interleukin
ImmGen	Immunological Genome Project
IVIG	intravenous immunoglobulin
JAM	junctional adhesion molecule
KEGG	Kyoto Encyclopedia of Genes and Genomes
LAD	linear IgA disease
LC	langerhans cell
LFA	lymphocyte function-associated antigen-1
LIED	Lübeck Institute of Experimental Dermatology
LN	lymph node
LTB4	leukotriene B4

MAC	membrane attack complex
MAC-1	macrophage antigen-1
MAdCAM	mucosal vascular addressin cell adhesion molecule
MAPK	Mitogen-activated protein kinase
MAPK	mitogen-activated protein kinase
mCOL7	murine COL7
MHC	major histocompatibility complex
min	minute
MMP	mucous membrane pemphigoid
MMP-9	matrix metalloproteinase-9
MOA	Mechanism of action
MP	methylprednisolone
MPO	myeloperoxidase
MS	multiple sclerosis
NAC	*N*-acetyl-l-cysteine
NADPH	nicotinamide adenine dinucleotide phosphate
NC1	non-collagenous 1
NC2	non-collagenous 2
NF-kB	nuclear factor kappa-light-chain-enhancer of activated B cells
Nic	niclosamide
NK-T	natural killer-T
O.C.T.	optimum cutting temperature
PCL	Prestwick chemical library
PD	pemphigoid diseases
pDC	plasmacytoid dendritic cell
PDE-4	phosphodiesterase-4
PECAM	platelet endothelial-cell adhesion molecule
PI	propidium iodide
PI3K	phosphatidylinositol 3-kinase
PI3K	phosphoinositide 3-kinase
PK	protein kinase
PMA	phorbol-myristate-acetate
PMN	polymorphonuclear leukocyte
PS	phosphatidylserine
RA	rheumatoid arthritis
RAGE	receptor for advanced glycation end products
RIN	RNA integrity number
RNA-Seq	RNA sequencing
RORα	RAR-related orphan receptor alpha
ROS	reactive oxygen species
RT	room temperature
RTK	receptor tyrosine kinase
SALT	skin-associated lymphoid tissue

SEM	standard error of the mean
SERM	selective estrogen receptor modulator
SLE	systemic lupus erythematosus
STAR	spliced transcripts alignment to a reference
STAT	signal transducer and activator of transcription
Syk	spleen tyrosine kinase
Tac	T cell activation
Tam	tamoxifen
TH1	T helper 1
TH17	T helper 17
TH2	T helper 2
TNF-α	tumor necrosis factor-α
Treg	regulatory T cell
VCAM	vascular cell-adhesion molecule-1
VLA-4	very late antigen-4
vWFA	Willebrand factor A-like

6.4 Materials and buffers

6.4.1 Laboratory equipment

Equipment	Source
Agilent 2100 Bioanalyzer system	Agilent Technologies, Waldbronn, Germany
Bio-photometer 8,5 mm	Eppendorf AG, Hamburg, Germany
Cell incubator containing 5% CO2	Memmert, Schwabach, Germany
Centrifuge, 5804R	Eppendorf, Hamburg
Centrifuge, BIOFUGE Fresco	Haereus Instruments GmbH, Hanau, Germany
Centrifuge, Varifuge 3.0 R	Haereus Instruments GmbH, Hanau, Germany
Cold room (4°C)	Viessmann GmbH & Co. KG, Allendorf, Germany
Cryostat, Leica CM 3050S	Leica Mikrosysteme Vertrieb GmbH, Wetzlar, Germany
Deep freezer, C660 (-80°C)	New Brunswick Scientific (UK) Ltd, England
Dry heat sterilizer	Binder GmbH, Tuttlingen, Germany
FACSCalibur flow Cytometer	BD Bioscience, Heidelberg, Germany
GloMax® Discover System	Promega GmbH, Mannheim, Germany
Laminar flow hood, Biowizard	Kojair Tech Oy, Vilppula, Finnland
Light/Fluorescence Microscope BZ-9000	Keyence Deutschland GmbH, Neu-Isenburg, Germany
Magnetic stirrer MR3002	Heidolph Instruments, Schwabach
Mastercycler ep realplex	Eppendorf AG, Hamburg, Germany
Micro centrifuge Micro Star 17R	VWR International GmbH, Darmstadt, Germany
Microscopy, Olympus BX40	Olympus Deutschland GmbH, Hamburg, Germany
Microtome	Leica Mikrosysteme Vertrieb GmbH, Wetzlar, Germany
NanoDrop 2000c spectrophotometer	Thermo Fisher Scientific GmbH, Dreieich, Germany
Neubauer chamber	Paul Marienfeld, Lauda Königshofen
NextSeq® 500	Illumina, San Diego, USA
pH-meter, ph526	WTW GmbH, Weilheim, Germany
Pipettes	Eppendorf AG, Hamburg
Plate reader, VICTOR3 Wallac 1420 Multilabel Counter	Perkin Elmer, Inc., CA, USA
Refrigerator (4°C)/freezer (-20°C)	Liebherr International AG, Bulle, Switzerland
S1000TM Thermal Cycler	Bio-Rad Laboratories GmbH, Munich, Germany
Shaker, Duomax 1030	Heidolph Instruments, Schwabach
Vortex	Scientific Industries, Inc., Bohemia, New York, USA

6.4.2 Consumable materials

Name of item	Source
1.5ml/2.0ml tubes	Sarstedt AG&Co., Nuembrecht, Germany
96-well microtiter plates (Maxisorb®)	Nunc, Roskilde, Denmark
96-well white CELLSTAR plate	Greiner Bio-One, Germany
Amicon Ultra-15 (30KDa)Centrifugal Filter Units	Merck Millipore, Darmstadt, Germany
Applied Biosystems™ MicroAmp™ EnduraPlate™ Optical 96-Well Clear Reaction Plates	Thermo Scientific, Germany
Barrier pen (Dako-pen)	Dako Deutschland GmbH, Hamburg, Germany
Cell strainer 70 µm	Becton Dickinson GmbH, Heidelberg, Germany
Cover glasses (24x60mm)	Gerhard Menzel, Glasbearbeitungswerk GmbH&Co. KG, Braunchweig, Germany
Dark chamber	Werner Hassa GmbH, Lübeck, Germany
Dialysis tubing visking cellulose type 36/32 inch 0.020 mm thick	Carl Roth GmbH & Co. KG, Karlsruhe, Germany
Disposable cuvettes	BRAND GmbH, Wertheim, Germany
Disposable needle (BD Microlance 3, 26Gx1/2)	Becton Dickinson GmbH, Heidelberg, Germany
Disposable syringe-1ml (BD PlastipakTM)	Becton Dickinson GmbH, Heidelberg, Germany
Disposable syringe-20ml (BD DiscarditTM II)	Becton Dickinson GmbH, Heidelberg, Germany
Sarstedt S-Monovette 9-ml K3 EDTA	Sarstedt AG&Co., Nuembrecht, Germany
ELISA plate seal	Sarstedt AG&Co., Nuembrecht, Germany
Falcon tubes (15 ml; 50 ml)	Sarstedt AG&Co., Nuembrecht, Germany
Fliter Minisart-Sterile (0.20µm)	Sarstedt AG&Co., Nuembrecht, Germany
Microplate, 96 well, clear, non-binding	Greiner Bio-One, Germany
Microtubes (1.5 ml; 2 ml)	Sarstedt AG&Co., Nuembrecht, Germany
Osmotic pumps (ALZET model 1002)	Durect Corporation, Cupertino, California, USA
Parafilm	Th. Geyer GmbH & Co. KG, Renningen, Germany
Pipette tips (10 µl; 100 µl; 1000 µl)	Sarstedt AG&Co., Nuembrecht, Germany
Protein G sepharose columns	Amersham Biosciences, Heidelberg, Germany
Protein G sepharose columns	Amersham Biosciences, Heidelberg, Germany
Serological pipettes (5 ml; 10 ml; 25 ml)	Sarstedt AG&Co., Nuembrecht, Germany
Skin closure thread (SERALON USP 3/0)	SERAG-WIESSNER GmbH & Co. KG, Naila, Germany
SuperFrost/Plus- slide glasses	Gerhard Menzel, Glasbearbeitungswerk GmbH&Co. KG, Braunchweig, Germany

SuperFrost/Plus-slide glasses	Gerhard Menzel, Glasbearbeitungswerk, GmbH&Co. KG, Germany
Syringe (5 ml; 20 ml)	Becton Dickinson GmbH, Heidelberg, Germany
Syringe 1 ml	Becton Dickinson GmbH, Heidelberg, Germany
Tissue-Tek® Cryomold	Sakura Finetek Europe B.V. Alphen aan den Rijn, Netherland

6.4.3 Chemicals, antibodies and kits

Name	Source
2N NaOH solution	Carl Roth, Karlsruhe, Germany
4% histofix solution	Roth, Karlsruhe, Germany
Acetone	Sigma-Aldrich, Darmstadt, Germany
Agilent DNA 7500 Kit	Agilent Technologies, Waldbronn, Germany
Agilent RNA 6000 Nano Kit	Agilent Technologies, Waldbronn, Germany
Amo	Sigma-Aldrich, Steinheim, Germany
AMPure XP beads	Beckman Coulter, Krefeld, Germany
APC-anti-CD15	BD GmbH, Heidelberg, Germany
Apo	Sigma-Aldrich, Steinheim, Germany
Au	Sigma-Aldrich, Steinheim, Germany
AV-binding buffer	BioLegend GmbH, Fell, Germany
AV-FITC	BioLegend GmbH, Fell, Germany
BSA	Carl Roth GmbH & Co. KG, Karlsruhe, Germany
CAT	Sigma-Aldrich, St. Louis, MO, USA
Corn oil	Sigma-Aldrich, Steinheim, Germany
Cremophore	Sigma-Aldrich, Steinheim, Germany
DAPI	Life Technologies GmbH, Germany
DMSO	Sigma-Aldrich, Hamburg, Germany
Dob	Sigma-Aldrich, Steinheim, Germany
DPBS	Invitrogen GmbH, Darmstadt, Germany
EDTA	Carl Roth, Karlsruhe, Germany
FCS	Biochron GmbH, Berlin, Germany
FITC-anti-CD66b	BD GmbH, Heidelberg, Germany
Fluoromount-G®	Southern Biotech, USA
Glucose	Sigma-Aldrich, Darmstadt, Germany
Goat serum	Dako, Glostrup, Denmark
GOX	Sigma-Aldrich, St. Louis, MO, USA
H&E	Merck KgaA, Darmstadt, Germany
HBSS	Life Technologies GmbH, Germany
HEPES	PAN Biotech, Aidenbach, Germnay
HRP-conjugated goat anti-mouse IgG	Bethyl laboratories, Inc., Montgomery, Texas, USA
HRP-conjugated goat anti-rabbit IgG (HRP-Goat polyclonal anti-rabbit IgG)	Dako, Glostrup, Denmark
Isotype control antibody, purified rat anti-mouse IgG1	BD Pharmingen™
Ketamine	Sigma-Aldrich, Hamburg, Germany
Luminol	Sigma-Aldrich, Darmstadt, Germany
Mouse anti-rabbit IgG	Novus Biologicals, Germany
MPO	Enzo Life Sciences, Lörrach, Germany

Na2CO3	Merck, Darmstadt, Germany
Na2HPO4	Carl Roth, Karlsruhe, Germany
N-acetyl-l-cysteine (NAC)	Sigma-Aldrich, Steinheim, Germany
NaCl	Carl Roth, Karlsruhe, Germany
NaH2PO4	Carl Roth, Karlsruhe, Germany
NaHCO3	Merck, Darmstadt, Germany
NextSeq 500 High Output Kit, 150 cycles	Illumina, San Diego, CA, USA
Nic	Sigma-Aldrich, Steinheim, Germany
PE-anti-CD62L	BD Pharmingen™
PI	Miltenyi Biotec GmbH, Gemany
PMA	Sigma-Aldrich, Darmstadt, Germany
PolymorohprepTM	Axis-Shield, Heidelberg, Germany
Prestwick chemical Library®	Prestwick Chemical, Illkirch-Graffenstaden, France
Primary Ab, anti-murine C3 (C3b/iC3b/C3c, Mouse, mAb (clone 2/11)	Hycultec GmbH, Beutelsbach, Germany
Protein G sepharose	GE Healthcare Europe GmbH, Freiburg, Germany
QIAamp RNA Blood Mini Kit	Qiagen GmbH, Germany
RevertAid™ First Strand cDNA Synthesis Kit	Thermo Scientific™, Germany
RNase-Free Dnase Set	Qiagen GmbH, Germany
RPMI1640	Lonza, Verviers, Belgium
RPMI1640 W/O phenol red medium	Genaxxon Bioscience GmbH, Ulm, Germany
Secondary Ab, Alexa Fluor 594-Goat anti-rat IgG	BioLegend GmbH, Fell, Germany
Secondary Ab, FITC-Donkey anti-rabbit IgG	Jackson ImmunoResearch, UK
SYBR® Green PCR Master Mix	Life Technologies (ABI)
Tam	Sigma-Aldrich, Steinheim, Germany
Tissue-Tek® O.C.T. Compound	Sakura Finetek Europe B.V. Alphen aan den Rijn, Netherland
TMB chromogen substrate	Thermo Scientific, Germany
Triton X100	Sigmal-Aldrich, Germany
TruSeq® Stranded mRNA Sample Preparation Kits	Illumina, San Diego, CA, USA
Tween20®	Sigma-Aldrich, Hamburg, Germany
Xylazine	Sigma-Aldrich, Hamburg, Germany
Xylene	Sigma-Aldrich, Germany
β-mercaptoethanol	Sigma-Aldrich, Darmstadt, Germany

6.4.4 Buffers

Name	Chemical composition
10x posphate buffer saline (PBS)	80.0 g NaCl (MW: 58 g/mol) 2.0 g KCl (MW: 75 g/mol) 14.4 g Na2HPO4 (MW: 142 g/mol) 2.4 g KH2PO4 (MW: 136 g/mol) Adjust volume to 1L with distilled water
0.1 M glycin pH 2.9	7.52g of glycine in 1L of distilled water Adjust pH to 2.8 with 1N HCl
Phoshphate buffered saline-Tween 20 (PBST)	0.05% Tween 20 in 1X PBS with pH 7.2
TRIS-buffer	181.71g of TRIS base in 1L of distilled water Adjust pH to 8.8 with 1N HCl
Carbonate-bicarbonate buffer (coating buffer)	5.3g of Na2CO3 5.04g of NaHCO3 in 1L of distilled water Adjust pH to 9.6 with 1N HCl
FACS buffer	1% BSA in 1X PBS pH 7.2
TBS-T 5X (tris-buffered saline-Tween 20)	12 g Tris base (MW: 121.1 g) 44 g NaCl (MW: 58.4 g) in 1L of distilled water pH to 7.6 with 12 N HCl
half medium	1 volume of RPMI1640:1 volume of dH2O
lysis buffer	4 volume of dH2O: 1 volume of DPBS (Dulbecco's phosphate buffered saline)
1 M Tris-HCl pH 9.0	121.10 gr Tris Dissolved in 1 L DDW. Adjusted pH to 9.0

6.5 Acknowledgment

I wish to take this opportunity to thank many people who provided their invaluable help, support, love, guidance and mentorship over the years, during which I was carrying out my PhD project in Lübeck.

First and foremost, I would like to express my sincere gratitude to my supervisor, motivator, leader, Prof. Ralf J. Ludwig, for giving me the opportunity to accomplish my PhD project in his lab, for his constant support and encouragement during the ups and downs of the project and for his wisdom, guidance and compassion throughout my doctoral journey. I would also like to express my heartfelt gratitude to Prof. Wolfgang Müller-Ruchholtz who believed in me, supported me to find what I truly intended to do in my scientific career and helped me to had the honor of getting to know Prof. Ludwig. I am genuinely grateful to Prof. Detlef Zillikens for providing me with the opportunity to conduct my thesis project at the Department of Dermatology, Lübeck. I would also like to thank my mentors Prof. Markus Schwaninger and PD Dr. Kathrin Kalies for their excellent advice and critical discussions during my thesis.

I would especially like to thank Wendelien Veldkamp for her engagement in performing some parts of the preliminary screen experiments. A special thanks goes to Dr. Yask Gupta, Dr. Katja Bieber and Dr. Unni Samavedam for their help and useful advice. I would also like to give a big thank to Claudia Kauderer, Rebecca Cames and Sadegh Mousavi for their excellent technical assistance.

It was the greatest pleasure to work together with so many great colleagues and fellow PhD students during these years. I want to say thanks to all. My stay in Lübeck would have not been so great without the great friends I made here. I warmly thank Aida Abadpour for all her care and help when I first arrived in Lübeck. I would also offer my deep appreciation to Shirin Emtenani, Kazuko Matsumoto, Lenche Chakievska and Fahimeh Khorsand for being always there for me.

I would like to express my sincere appreciation to my aunts and their families for their tremendous support and for helping me to live without homesickness in Germany. I would like to especially express my gratitude to Mr. Hamid Sharifzadeh for being wholeheartedly supportive and for his generous help during my doctoral journey.

Last but not least, I would express my profoundest gratitude to my parents, my brother and my sister for their unconditional love, considerable encouragement and wholehearted support. The last word goes to my loving husband for his overwhelming love, for his endless patience, for understanding me best, for being supportive and being my best friend.

6.6 Declarations and Copyright Statement

No part of the work referred to in this dissertation has been submitted in support of an application for any degree or qualification of The University of Lübeck or any other University or Institute of learning.

Copyright for the text of this dissertation rests with the author. Copies of this work by any process, either in full, or as extracts, may be made only in accordance with instructions given by and the express permission of the author. Further details may be obtained from the appropriate Graduate Office. This page must form part of any such copies made. Further copies (by any process) made in accordance with such instructions should only be made with the permission (in writing) of the author.

The ownership of any intellectual property rights arising from this dissertation is vested with the University of Lübeck, subject to any prior agreement to the contrary, and may not be made available for use by third parties without the written permission of the University, which will prescribe the terms and conditions of any such agreement.

Further information on the conditions under which disclosures and use may be permitted is available from the Dean of the Department of Technology and Science.